The Effect of Mechanical Strain on Non-enzymatic Cross-linking of Collagen type II fibrils in Artilcular Cartilage

J.G. Lagrand

Master's thesis

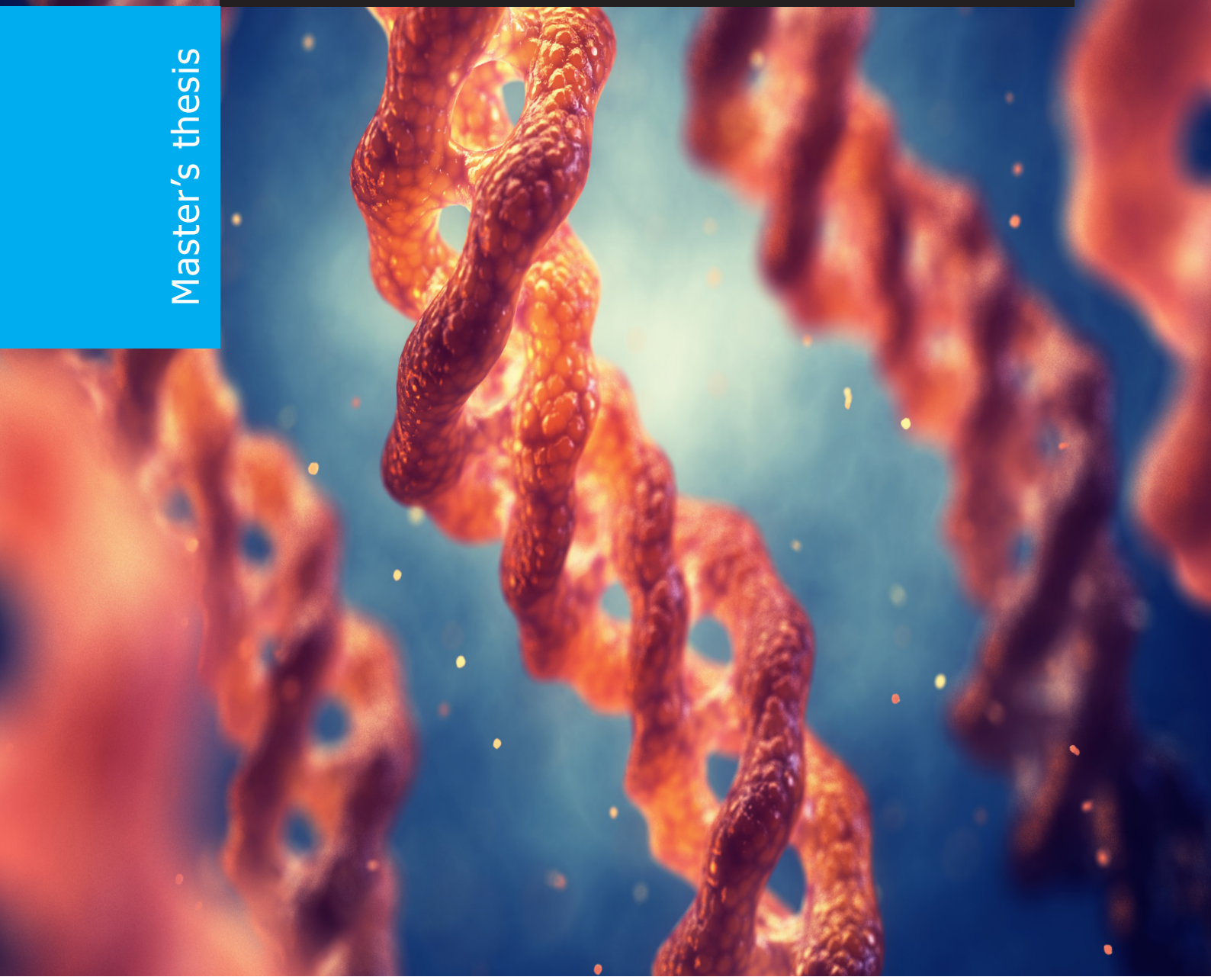

TU Delft Delft University of Technology

Challenge the future

DELFT UNIVERSITY OF TECHNOLOGY

MASTER'S THESIS

The Effect of Mechanical Strain on Non-enzymatic Cross-linking of Collagen type II Fibrils in Articular Cartilage

Author:
Jaap LAGRAND

Supervisors:
Dr. ir. Behdad POURAN
Prof. dr. ir. Harrie WEINANS

A thesis submitted in fulfillment of the requirements for the degree of Master of Science

in the field of

Biomedical Engineering
Biomaterials and Tissue Biomechanics

Department of Biomechanical Engineering
Faculty of Mechanical, Maritime and Materials Engineering

August 8, 2019

TU Delft

DELFT UNIVERSITY OF TECHNOLOGY

Abstract

Faculty of Mechanical, Maritime and Materials Engineering
Department of Biomechanical Engineering

Master of Science

The Effect of Mechanical Strain on Non-enzymatic Cross-linking of Collagen type II Fibrils in Articular Cartilage

by Jaap LAGRAND

Investigations into mechanotransduction in connective tissue extracellular matrix (ECM) have demonstrated that collagen networks show cell-independent mechanosensitive behavior. It has been suggested that mechanical strain could lead to conformational changes in the molecular structure of collagen, thereby influencing the susceptibility to other molecules. In the process of normal aging, the collagen fibrils in cartilage undergo a non-enzymatic process known as glycation. It involves the accumulation of advanced glycation end products (AGEs) after exposure to sugars, resulting in the formation of cross-links between the collagen fibrils. This process is correlated with increased stiffness and brittleness of the cartilage, making it more prone to mechanical damage. The goal of this thesis was to assess whether mechanical compression has any effects on the formation of non-enzymatic cross-links during the aging of articular cartilage.

Two different models have been developed to mimic aging knees that undergo static and dynamic compression. Healthy cartilage explants were exposed to L-threose sugar to induce artificial aging. During incubation, these explants were submitted to either static or dynamic unconfined compression. Treatment with static compression consisted of a 5, 10 or 15% strain throughout the whole incubation period, using a custom-made bioreactor. Treatment with dynamic compression consisted of multiple loading cycles at a frequency of either 0.01 Hertz (Hz) or 1 Hz, using a Dynamic Mechanical Analyzer (DMA). We conducted cartilage surface color analyses, micro-indentation tests, dynamic mechanical analyses and biochemical measurements of pentosidine cross-links to assess the effects of advanced glycation cross-linking under these different conditions.

Dynamic compression at a frequency of 1 Hz was found to affect the formation of non-enzymatic cross-links. Biomechanical and biochemical data showed a similar trend, namely, the average values for equilibrium modulus, dynamic moduli, phase shifts and pentosidine per collagen level were noticeably higher (or lower in case of phase shift) for the 1 Hz treated samples compared to samples of other treatment groups.

The results of these studies suggest that compression at the physiological frequency of walking does affect the formation of cross-links in the articular cartilage during aging. These findings contribute to a better understanding of the mechanochemistry of collagen fibrils, which is necessary to develop future strategies against cartilage aging and deterioration.

Acknowledgements

I would like to express my gratitude to all those who actively contributed to the realization of this thesis. Foremost, I would like to thank my direct supervisor Behdad Pouran, for the guidance he has provided me throughout my time in Utrecht. Thanks for showing me the relevance of this research and for stimulating my interest in literature. Working together was very inspiring and fun. I would also like to thank my other supervisor, Harrie Weinans, for his feedback and his academic interest in my work.

Furthermore, I would like to acknowledge with much appreciation Ambika Bajpayee, for offering me the opportunity to conduct experiments in her lab, at Northeastern University. Her insightful guidance was invaluable during my stay in Boston. I would like to extend my thanks to all the members of the Bajpayee lab as well, for welcoming me with open arms. A special thanks goes to Shikhar and Armin for their daily support and for making me feel at home in Boston and to Matt and Sumayyah, for their exceptional help with the dynamic mechanical analyzer.

Finally, I want to thank Mies Steenbergen, for his crucial assistance with the HPLC measurements in the Pharmaceutics lab.

I am thankful for the great opportunity to work on this research and I hope you enjoy reading this thesis.

Contents

List of Abbreviations

ACN	**A**ceto**n**itrile
AGE	**A**dvanced **G**lycation **E**ndproduct
ANOVA	**An**alysis **o**f **va**riance
AU	**A**rbitrary **u**nit
DMA	**D**ynamic **M**echanical **A**nalysis
DMA	**D**ynamic **M**echanical **A**nalyzer
ECM	**E**xtra**c**ellular **m**atrix
GAG	**G**lycos**a**mino**g**lycans
HFBA	**H**epta**f**luoro**b**utyric **a**cid
HPLC	**H**igh-**P**erformance **L**iquid **C**hromatography
Hyp	**Hy**droxy**p**roline
MMP	**M**atrix **M**etallo**p**roteinase
OA	**O**steo**a**rthritis
PBS	**P**hosphate **b**uffered **s**aline
PG	**P**roteo**g**lycan
RPC	**R**eversed-**P**hase **C**hromatography

Chapter 1

Background

1.1 The Knee joint

A synovial joint, also known as a diarthrosis, is the most mobile type of joint in a mammal's body. This type of joint has an articular capsule, consisting of an outer fibrous layer and an inner synovial membrane, which surrounds a fluid-filled synovial cavity. Multiple types of synovial joints exist in the human body, including hinge joints, ball and socket joints, saddle joints, pivot joints and gliding joints [1]. The knee joint is the largest and most heavily loaded joint in the human body [2]. It is a hinge joint that permits flexion and extension and a limited amount of medial and lateral rotation. It consists of four bones (see Figure 1.1): the femur (thigh bone), the tibia (shin bone), the patella (knee cap) and the fibula.

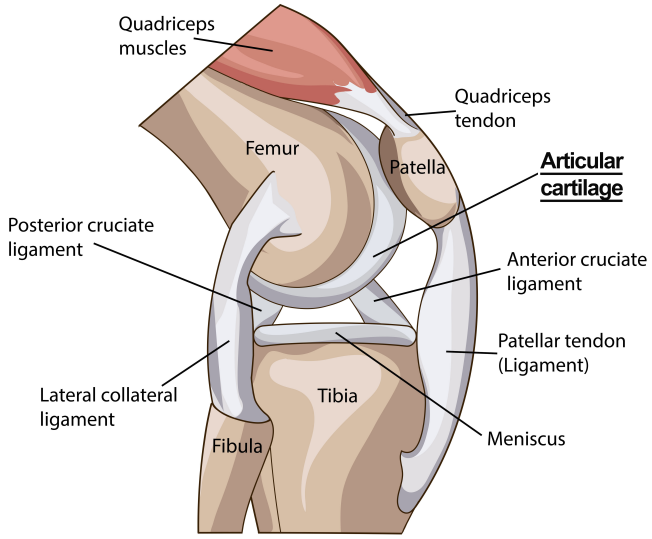

FIGURE 1.1: Anatomy of the human knee joint.
[shutterstock.com]

The joint structure of the knee can be divided into two parts: the tibiofemoral joint, where the medial and lateral condyles of the femur articulate with the tibial condyles, and the patellofemoral joint, where an aspect of the distal femur articulates with the patella [3]. The tibiofemoral joint is the weight-bearing joint of the knee [4]. The knee bone surfaces of the femur, tibia, and patella are covered with a thin (1-6 mm), dense, translucent, white connective tissue, called hyaline articular cartilage, which represents the weight-bearing surface. Articular cartilage is precisely suited to withstand the high cyclic loading experienced during daily activities

without failure for an average individual's lifetime [5]. One of the two primary functions of articular cartilage is to support and distribute applied joint loads to dissipate the produced energy and reduce localized stress concentrations in underlying bone [6, 7]. Its second function is to provide a lubricated and smooth surface, to allow movement of opposing joint surfaces with minimal friction and wear [8]. Physiologically, it is devoid of blood vessels, lymphatics, and nerves. Nutrition of the articular cartilage occurs by diffusion from the synovial fluid [9]. Moreover, cartilage has the lowest cellular density of any tissue in the body [10]. This limits its capacity for intrinsic healing and repair, making the health and preservation of the articular cartilage essential for joint health [11]. Its unique mechanical behavior and poor regenerative capacities make it a highly specialized material.

1.2 Composition of Articular Cartilage

Articular cartilage is a biphasic material, consisting of a solid matrix phase and an interstitial fluid phase [12]. The composition of articular cartilage is summarized in Table 1.1.

The solid phase consists of an extracellular matrix (ECM) with a small number of fibroblast-like cells, called chondrocytes. Chondrocytes are the only type of cells that reside in healthy cartilage. These chondrocytes do not directly contribute to the mechanical properties of cartilage, but they can sense and respond to mechanical stimuli [13, 14]. Regardless of their sparse distribution, they build, secrete, organize and maintain the macromolecules of the ECM, a dense network of collagen fibrils that are enmeshed in a concentrated solution of proteoglycans [15]. These main constituents and their functions will be discussed separately.

TABLE 1.1: The composition of articular cartilage [16].

Phase	**Component**	**% wet weight**	**% dry weight**
Solid phase (ECM)	*Collagen*		
	Type II	15-20%	50-75%
	Type V,VI,IX,XI	< 2%	-
	Proteoglycans		
	Aggrecan	4-7%	20-25%
	Biglycan, Decorin and Fibromodulin	< 1%	-
Solid Phase (Cells)	Chondrocytes	2%	-
Fluid phase	Interstitial water and electrolytes	60-80%	-

1.2.1 Collagen

Collagen is the most abundant protein in the human body and a predominant structural macromolecule of cartilage [15]. The majority of the collagen in cartilage is of type II. Additionally, an array of other types of collagen is present in lesser amounts

(types V, VI, IX, and XI). The basic biologic unit of collagen is tropocollagen, a structure composed of three procollagen polypeptide chains (alpha chains) coiled into left-handed helices which are further coiled about each other into right-handed triple helices. The sequence follows the pattern Glycine-X-Y, where X is usually proline and Y is usually either proline or hydroxyproline [17]. These rod-like tropocollagen molecules are polymerized extracellularly into larger collagen fibrils that are often arranged in bundles called fibers [18] (see Figure 1.2). Its hierarchical structure in combination with the alignment of fibrils, make collagen a component with an exceptional tensile strength along its primary axis [19]. Collagen fibrils are stiff and relatively immobile not only individually, but also when they are entwined and bonded with other structural macromolecules, such as proteoglycans. Moreover, the collagen in the cartilage tissue is cross-linked, which is thought to add stability to the network. The collagen fiber network does not offer significant resistance to compression, but it is stiff and strong in tension, providing resistance to swelling and tensile strain [19].

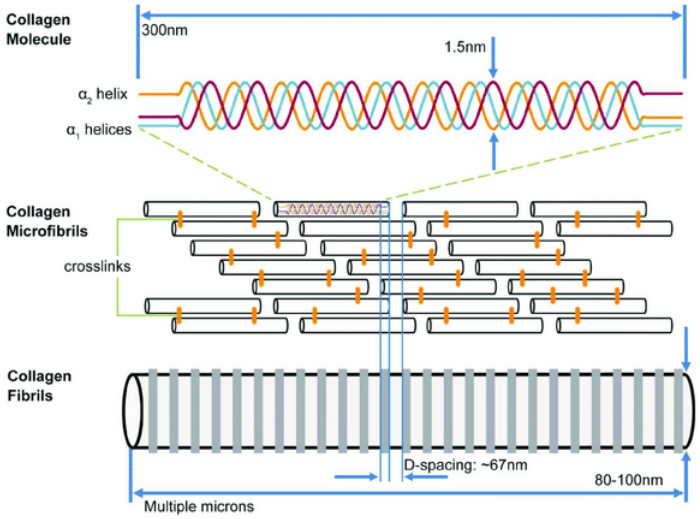

FIGURE 1.2: Collagen molecules self-assemble in a quarter-staggered array into microfibrils to form collagen fibrils with characteristic periodic D-spacing [20].

1.2.2 Proteoglycans

Proteoglycans are heavy and complex macromolecules that consist of a protein core to which one or more glycosaminoglycans (GAGs) are covalently bound [21]. Most of the proteoglycans found in cartilage are organized in aggregates (aggrecan). Aggrecan is a large proteoglycan with long and unbranched GAG chains that, because of their negative charge, spread out like tubular brushes. These structures consist of chondroitin sulfate and keratin sulfate molecules attached to a protein core [22]. The N-terminal of this protein core is able to bind to hyaluronate. When many aggrecan molecules bind to a chain of hyaluronate, a macromolecular complex is formed. Since aggrecan has many carboxyl (COO^-) and sulfate (SO_3^-) groups, it is highly negatively charged. This makes the aggrecan very attracted to the mobile cations in the fluid phase of the ECM. The collagen network immobilizes the aggrecan, resulting in what is termed the "Donnan osmotic pressure". This osmotic pressure manages the water amount within the tissue and causes the cartilage to swell [23, 24]. This

swelling is restrained by the collagen network and contributes to the compressive stiffness of tissue.

1.2.3 Interstitial fluid

Generally, the fluid phase contributes to 60-80% of the tissues total wet weight [25]. This viscous fluid consists of water with many free mobile cations (e.g., Na^+ , K^+ and Ca^{2+}) The flow of water through the matrix and across the articular surface contributes greatly to the nutrition and lubrication processes in the tissue [26, 27]. Most of the interstitial fluid may be moved through the ECM when a pressure gradient is applied across the tissue or by compressing the solid matrix [12]. This incompressible interstitial fluid phase encounters friction as it flows out of the porous collagen-proteoglycan solid matrix. The resulting frictional drag counterbalances the applied compressive forces. This forms the damping mechanism by which articular cartilage derives its ability to withstand significant loads [11].

1.2.4 Depth dependency

The way these constituents are arranged and distributed varies throughout the tissue's depth, making it a heterogeneous material [28, 29]. Four different zones can be identified: the superficial (or tangential) zone, the middle (or transitional) zone, the deep (or radial) zone, and the calcified zone [30].

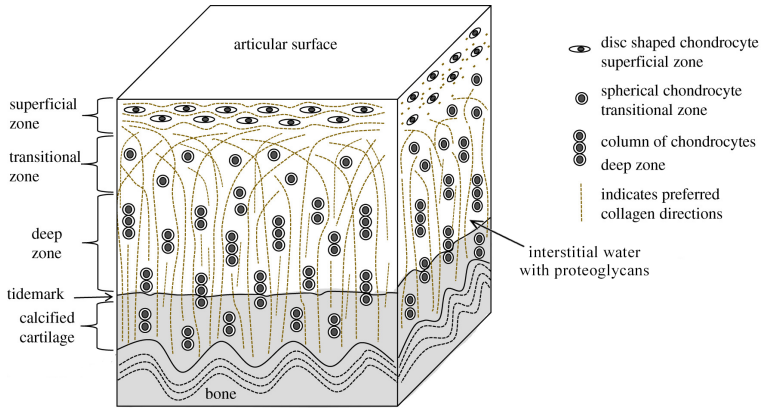

FIGURE 1.3: Zonal organization of healthy articular cartilage [31].

The superficial zone, which represents 10-20% of the total thickness, is the gliding surface of the cartilage and has a protective role for the deeper layers. Relatively thin collagen fibers are densely packed in sheets that are aligned in planes parallel to the articular surface. It has the highest water content and the lowest proteoglycan content. A relatively small number of chondrocytes with few organelles is flattened and oriented parallel to the surface [32].

In the middle zone, the largest zone in cartilage, the collagen fibrils are thicker and arranged randomly. When they traverse deeper in the cartilage, collagen fibers start bending towards the vertical direction. Furthermore, chondrocytes are at lower density than in the superficial zone and have a more spherical shape. The proteoglycan content increases towards the deep zone where its content is highest [18].

The deep zone provides resistance to compressive forces as the collagen fibrils and chondrocytes are aligned perpendicularly to the articular surface. The diameter

of the collagen fibers is the largest. In this zone, the lowest water content (65%) and the highest concentration of proteoglycans is found.

The calcified zone forms the transition where the soft hyaline cartilage is secured to the stiffer subchondral bone, by collagen fibrils that are anchored to the underlying bone. This tide mark consists of small cells which are distributed in a cartilaginous matrix [11].

All off the components described above have important roles and are indispensable in the ability of articular cartilage to resist compressive forces and protect the bone and joint. Each should be present in the right amount and structure. The chondrocytes play a crucial role in the generation and maintenance of the zonal architecture and regulate the equilibrium between synthesis and degradation. The collagen network is responsible for tensile integrity, while the proteoglycans contribute to compressive strength. The remarkable mechanical properties of articular cartilage depend on each of these components and are sensitive to disruption [33].

1.3 Biomechanical properties of articular cartilage

To understand how articular cartilage responds under physiological loading conditions, its biomechanical behavior must be reviewed. The biomechanical behavior of articular cartilage can best be explained with the biphasic theory, which models the tissue as a binary mixture of two phases: an incompressible fluid phase and an elastic porous solid phase (i.e., the ECM) [12]. The interaction between these two phases gives the material viscoelastic properties. The frictional resistance associated with the interstitial fluid flow through the porous permeable solid matrix is responsible for the compressive viscoelastic behavior of the tissue.

Viscoelastic materials exhibit both viscous and elastic characteristics when undergoing deformation. When a load is applied to a viscoelastic material, it stores part of the energy (like an elastic material) and it dissipates part of the energy (like a viscous material). Hysteresis is observed in the stress-strain curve, with the area of the hysteresis loop being equal to the energy loss during the loading cycle. Applying stress results in an instantaneous elastic strain, followed by a viscous, time-dependent strain.

Characterizing the mechanical properties of viscoelastic materials is important for understanding their response in specific mechanical conditions. Since articular cartilage has as main function to support and distribute applied joint loads, its biomechanical behavior is mainly determined through compression tests. A specific set of different characterization methods and loading protocols exist to assess the biomechanical behavior through these compression tests.

1.3.1 Mechanical testing methods

The three methods that are commonly used to determine the biomechanical properties of cartilage are confined compression, unconfined compression, and indentation. During confined compression, the specimen is placed in a confining chamber and compressed with a permeable piston. This way, the fluid is only able to flow through the piston and transverse expansion is restrained by the confining chamber. In unconfined compression the specimen is placed between two smooth plates, allowing a transverse flow of the fluid. During indentation, only a part of the specimen is compressed, while fluid can flow any way, by using a hemispherical or plane-ended indenter (Figure 1.4).

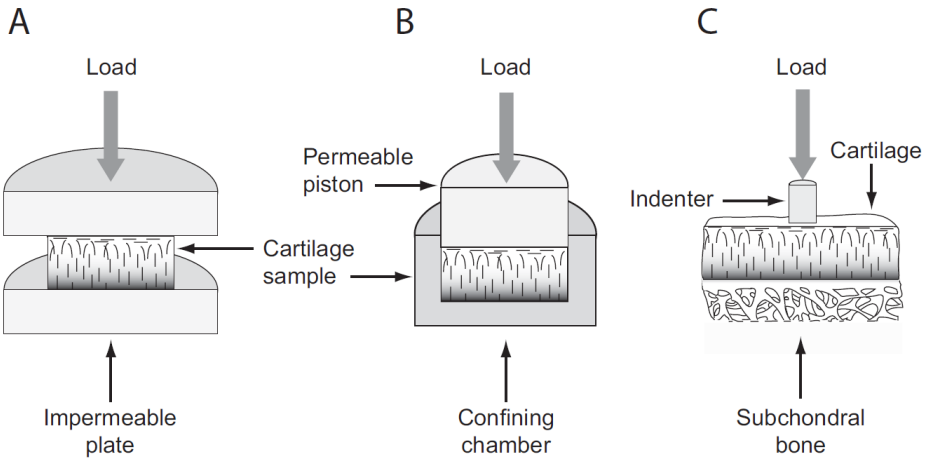

FIGURE 1.4: Unconfined compression, confined compression and indentation loading methods for determination of cartilage mechanical properties [34].

1.3.2 Loading methods

The main loading methods that are used with these configurations are stress-relaxation, creep and dynamic loading.

Stress relaxation

When cartilage is in compression, the fixed charged proteoglycans (PGs) in the ECM are forced in closer proximity, thereby increasing the electrostatic repulsive forces. Once the fluid is not anymore pressurized and flow has ceased, the tissue is at steady-state and PGs mainly regulate the equilibrium modulus [35].

Stress-relaxation is the time-dependent decrease in stress under a constant strain. At the beginning of a stress relaxation test, the strain is applied to the specimen at a constant rate to achieve the desired elongation. Once the specimen reaches the desired elongation, the strain is held constant for a predetermined amount of time. The stress decay, which occurs because of stress relaxation, is observed as a function of time. The magnitude of stress is recorded at certain time intervals and the results are plotted to obtain a stress versus time curve. Stress-relaxation protocols aim to determine the viscoelastic properties by means of strain-controlled loading [12, 36].

Creep

Similarly, creep protocols too aim to determine the viscoelastic properties, but through stress-controlled loading. When constant compressive stress is applied to the tissue, its deformation increases with time. It will deform, or creep until an equilibrium value is reached (i.e. there is no fluid flow). The resulting time-data plots of such tests are used to derive simple estimations for the viscoelastic parameters of materials [12, 36]. Viscoelastic materials also behave strain-rate dependent, as their stiffness increases with increasing strain. At the same time the part of the energy that dissipates, decreases with an increasing strain rate. So, at high strain rates, viscoelastic materials behave more elastic, while at low strain rates, they behave more viscous [37]. When analyzing the experimental data from stress-relaxation or

creep measurements, often the instantaneous and equilibrium (Young's) moduli are used to express the viscoelastic behavior of the specimen. Hooke's law can be used to define these moduli:

$$E_{eq} = \frac{\sigma}{\epsilon} \tag{1.1}$$

Where E_{eq} is the Young's modulus, σ the stress and ϵ the strain at equilibrium. However, for indentation, analysis of the data requires a mathematical model, because cartilage is not isotropic. Frequently, Hayes' method is used to determine the specimen's stiffness [38]. The equilibrium modulus is defined from Hayes' method as follows:

$$E_{eq} = \frac{(1-v^2)\pi\alpha}{2\kappa h} F \tag{1.2}$$

where F is the indentation force, v is the Poisson's ratio of the soft tissue, a is the radius of the indenter, h is the tissue thickness, d is the indentation depth, and k is a scaling factor, which depends on aspect ratio a/h and Poisson's ratio v.

Dynamic loading

Repeated loading and unloading cycles can be applied to study the viscoelastic response to dynamic loading, like the subjected loading during daily activity. Sinusoidal stress or strain is applied while the resulting displacement or force is measured as a function of time [39]. Its viscoelastic nature results in a strain rate-dependent behavior. Because of its viscoelastic behavior, the sinusoidal stress is out of phase with the applied strain, by a phase angle δ. For a Newtonian liquid (viscous), this phase angle would be 90 degrees and for a Hookean solid (elastic), it would be 0 degrees. The phase angle of viscoelastic material falls in between these two extremes.

With dynamic loading tests, viscoelastic materials can be characterized in terms of a storage ($E^{'}$) and a loss ($E^{''}$) modulus. $E^{'}$ represents the ability to store energy, whereas $E^{''}$ represents the ability to dissipate energy in the form of heat [40]. The storage and loss moduli are defined as follows:

$$E^{'} = \frac{\sigma_0}{\epsilon_0} cos\delta \tag{1.3}$$

$$E^{''} = \frac{\sigma_0}{\epsilon_0} sin\delta \tag{1.4}$$

where δ is the phase angle. σ_0 is calculated from the peak-to-peak value of the measured stress and ϵ_0 from the peak-to-peak value of the measured strain. Subsequently, the dynamic modulus, E^{*}, can be calculated as follows:

$$E^{*} = \sqrt{(E^{'})^2 + (E^{''})^2} \tag{1.5}$$

The correlation between the moduli and phase angle is shown in Figure 1.5.

1.4 Strain dependent enzymatic degradation of collagen

As described in Section 1.2, fibrillar collagen is the most abundant structural molecule in the ECM and plays a crucial load-bearing role in articular cartilage.

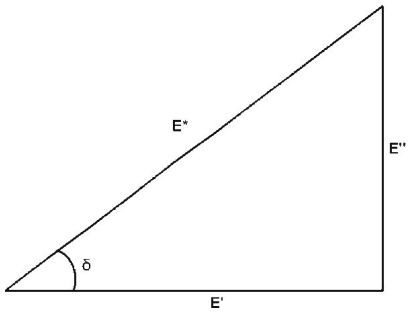

FIGURE 1.5: Schematic representation of the correlation between the dynamic modulus (E^{*}), the storage modulus ($E^{'}$), the loss modulus ($E^{''}$) and the phase angle (δ) [41].

Like many matrix components, collagen is synthesized by the chondrocytes. They play an active role in collagen deposition and the assembly of matrix components. They regulate the amino acid sequence and influence matrix formation through the vectorial discharge of packaged monomers into the extracellular space [42].

The collagen molecules are susceptible to enzymatic degradation and capable of growth, longitudinally and in the radial direction. From development through adulthood, collagen structures are constantly being remodeled [43] and it has been known for a long time, that processes involved in collagen remodeling are influenced by external forces. The matrix is therefore capable of adaption, for example, in order to more efficiently carry the applied loads [44]. Collagen fibers tend to realign, in response to extrinsic loading, in the direction of the applied force. This adaptability is one of the properties that make collagen such a successful component for connective tissue.

The exact mechanisms behind the mechanotransduction in ECM, are not completely clear. Most investigations focus on the genetic and proteomic responses of fibroblastic cells (e.g. chondrocytes in the case of cartilage). Thus, fibripositor-mediated assembly and remodeling of collagen have generally become the standard model to explain the production of highly anisotropic, load-bearing collagenous arrays [45]. This fibripositor model implies that cells, like chondrocytes, direct the production and placement of collagen fibrils. This model implies that fibroblastic cells must individually 'weave' the complex structures, required to support the massive loads, that are produced in the mechanically disadvantaged musculoskeletal system (MS) of vertebrate animals.

In 2005, Ruberti & Hallab came with a whole new theory regarding collagen network adaptability. They suggested that mechanotransduction events, leading to ECM load adaption, may not only occur at the level of the cells, but also directly at the level of the matrix molecules [46]. They based their new theory on two earlier studies ([47, 48]) and described that instead of being solely directed by resident cells, load-bearing collagenous matrices are inherently "smart". This theory states, that collagen fibrils within the matrix that are "in use" (strained) are protected from enzymatic degradation as opposed to fibrils that aren't. Not only could such a strain-stabilization mechanism have the potential to explain why collagen is the molecule of choice for load-bearing, adaptive extracellular matrices. It could also provide very useful theoretical information concerning embryogenesis, remodeling, repair, and disease.

Ruberti & Hallab's statement led to a lot of further research on the subject of

collagen mechanochemistry. Prior to this thesis, a systematic literature study has been conducted to review the current understandings of the mechanochemical effects in collagen structures and the potential cell-independent mechanisms, that are encoded in the helices of collagen molecules [49]. This study found that strain state can serve as either a protecting ([46–48, 50–61]) or accelerating ([62–66]) factor in the catabolism of collagen. This strain dependency of enzymatic degradation can best be explained by changes in the three dimensional (3D) conformation of amino acid. It is suggested that strain can create an unfolding or an unwinding conformation, resulting in respectively less or more accessibility of the cleavage sites for the metalloproteinases [1][66–75]. Furthermore, recent studies show that also the assembly of collagen can be "controlled" by strain [76–81]. The concept of cooperative collagen molecules is not only important for our view on load-bearing ECM morphogenesis, growth, homeostasis and pathology, it could also help engineers with finding new methods to produce collagenous tissues and scaffolds, without the involvement of biological cells. Its suggested capacity to autonomously form when needed and break down when not, could even form the basis of a whole new class of 'smart' materials that are applicable for many different fields.

In the case of unloaded articular cartilage, the collagen fibrils are pre-stressed by the osmotic swelling pressure. According to the theory described above, this prestress protects the fibrils from enzymatic degradation.

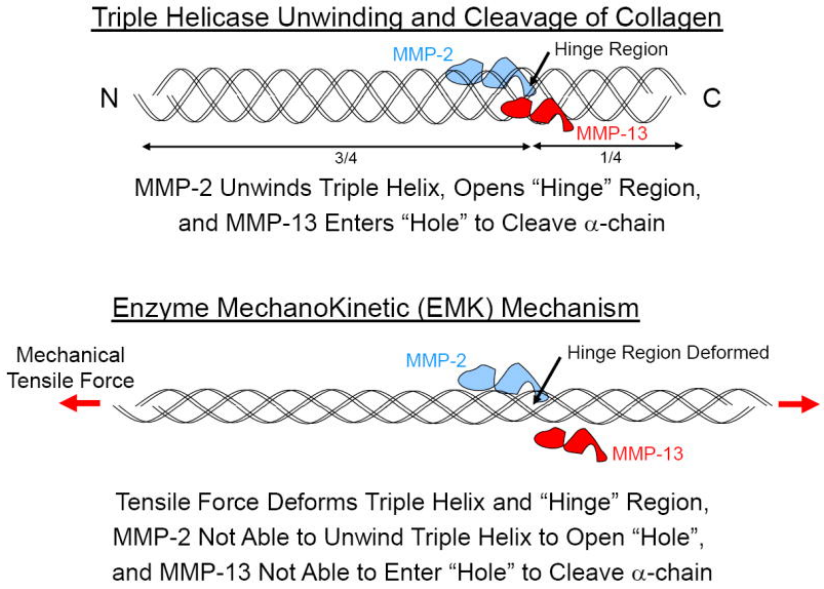

FIGURE 1.6: Triple helicase unwinding and cleavage of collagen (top). MMPs enter the triple helix to cleave the alpha chains. MMP-2 has been shown to aid in the cleavage process by unwinding the alpha chains at the hinge region for easier MMP access. Inhibition of cleavage by enzyme mechanokinetic (EMK) mechanism (bottom). As collagen is stretched it can become resistant to enzyme cleavage from changes in the collagen's molecular conformation induced by the mechanical tensile force [74].

[1]Matrix metalloproteinases (MMPs) comprise a large family of zinc-dependent enzymes, collectively capable of degrading ECM components, like collagen.

1.5 Non-enzymatic glycation

As explained in the previous section, the ECM of articular cartilage is a highly dynamic structure, constantly undergoing a remodeling process where components are deposited and degraded. Another crucial process during the normal aging of articular cartilage is the formation and accumulation of advanced glycation end products (AGEs). These AGEs are formed by non-enzymatic glycation of proteins [82]. Glycation is initiated by the condensation of reducing sugars (glucose, fructose or ribose) with free amino groups on lysine or arginine residues [83]. The formation of AGEs is both spontaneous and relatively slow and it only affects proteins with long half-lives [84]. Fibrillar collagen type II contains lysine and arginine as repeating units in its triple-helix and has a half-live of more than 100 years. Therefore, it is highly susceptible to AGEs. [85–87]. Some AGEs present adducts to the proteins, whereas others form protein-protein cross-links [88, 89]. Once AGEs are formed, they cannot be removed from the tissue and only leave when the protein involved is degraded. Therefore, whilst aging, the collagen matrix in cartilage becomes more and more susceptible to the accumulation of AGEs [90–92].

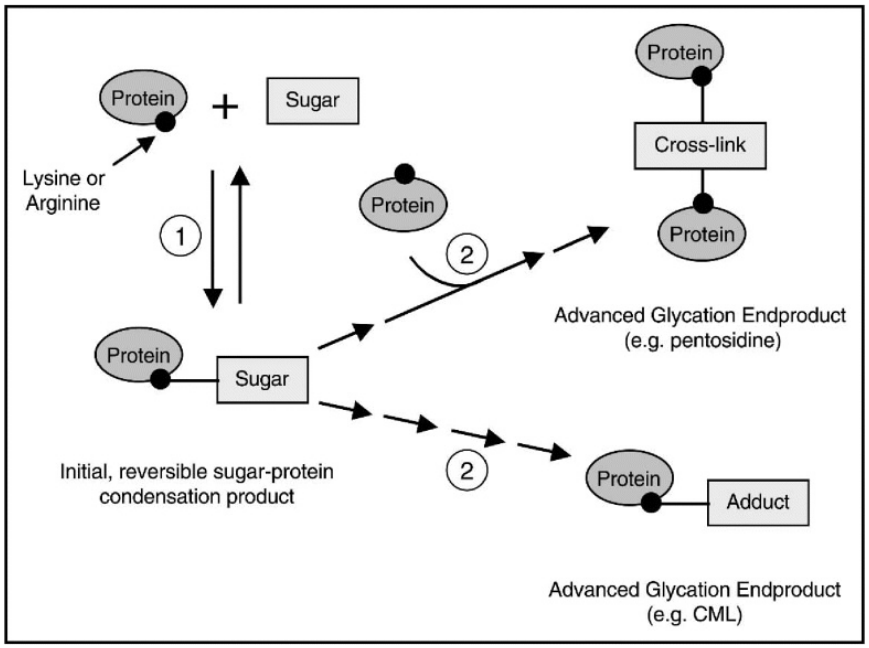

FIGURE 1.7: **Classic view of advanced glycation end product (AGE) formation** Reducing sugars such as glucose or fructose react spontaneously with lysine or arginine residues in proteins. Initially, a reversible adduct (Schiff base [eg, fructose-lysine]) is formed (1). Subsequently, stabilization of the adduct (by Amadori rearrangement) and Maillard browning reactions (2) result in the formation of stable AGEs. Some form protein-protein cross-links whereas others present protein adducts [85].

The accumulation of AGEs in collagen has adverse effects on the biochemical and biomechanical properties of articular cartilage. One the one hand, it interferes with cellular processes and alters molecular recognition, which leads to a decreased turnover of collagen and proteoglycans [93, 94]. On the other hand, it increases the stiffness of the collagen network [92], decreasing its viscoelasticity. An increase

in AGEs makes the cartilage more brittle and thereby more prone to mechanical damage [92, 95].

As mentioned, AGE accumulation is mainly caused by the very low turnover of ECM proteins (like collagen) and is therefore age-dependent. As such, it does not cause disorders like Osteoarthritis (OA) itself. Nevertheless, it is assumed to make the joint more prone to the development and progression of OA [85, 96].

Pentosidine is a member of the AGEs and is one of the most studied [96]. It is found in relatively high abundance in cartilage[97] and is frequently used as a biomarker [91, 98]. Pentosidine is formed in a reaction of the amino acids with the so-called Maillard reaction products of ribose and forms fluorescent cross-links between the arginine and lysine residues in collagen. It has been reported to increase with age in various tissues [99].

1.6 Aim and scope of the thesis

In section 1.4, we explained that enzymatic degradation of collagen is characterized by strain dependency: 3D conformational changes, as a result of mechanical strain, probably lead to changes in the accessibility of the enzymatic cleavage sites, without the involvement of cells.

The cleavage of MMPs shows a lot of similarities with the accumulation of AGEs, produced by non-enzymatic glycation. MMPs recognize a specific site of amino acid residues in the tropocollagen molecule. Its binding opens the triple helix locally, allowing the catalytic domain of the active enzyme to cleave the collagen α-chains sequentially (Figure 1.6). Likewise, the AGEs bind specifically to the amino acid residues of arginine and lysine. This raises the question whether these essential amino acids need a specific 3D conformation as well, to interact with cross-link creating AGEs. In other words: Does strain have an influence on the susceptibility of collagen fibrils to AGEs and therefore on the way they age?

In 2018, Pouran et al. investigated whether collagen cross-linking after exposure to sugars depends on the stretching condition of the collagen fibrils [100]. Healthy equine cartilage specimens were exposed to L-threose sugar and placed in hypo-, iso-, or hyper-osmolar conditions that expanded or shrank the tissue and changed the 3D conformation of collagen fibrils. Amongst others, the cartilage surface color, stiffness (biomechanical) and pentosidine level (biochemical) were measured to investigate the effect of the different osmolarity conditions on the chemical response of collagen fibrils to non-enzymatic glycation. The results indicated that swelling of ECM due to hypo-osmolarity, protects the ECM against glycation or so-called 'artificial aging', whereas shrinkage makes it prone to glycation. This indicates that healthy levels of glycosaminoglycans not solely keep cartilage stiffness at proper levels by swelling and pre-stressed collagen fibrils, but also protect the fibrils from AGEs. Understanding the mechanochemistry of collagen fibrils could be very useful, for example to provide potential aging prohibiting strategies against cartilage deterioration in the future.

In this research, we investigated the effects of mechanical strain on non-enzymatic glycation. The work of this thesis sought to answer the question: does compression have a significant effect on the number of cross-links in the fibrillar collagen type II network of articular cartilage during artificial aging?

During this study, we focused on the potential mechanisms that are encoded in the structure of collagen molecules, regarding cross-linking. Therefore, dead tissue was used and no other cellular or enzymatic mechanisms were involved.

Our primary aim was to investigate the effects of mechanical compression on the number of cross-links in the collagen type II network of articular cartilage. Based on the work of Pouran et al. [100], it was hypothesized that compression would lead to an increase in the number of cross-links, as a result of an increase in the susceptibility of amino acid residues of arginine and lysine.

Taking into account the zonal structure of cartilage (section 1.2.4), our secondary aim was to investigate the difference in cross-linking during compression between the radial and superficial zone. We assumed that the *Poisson effect*[2] will result in the tension of collagen fibrils that are located in the superficial zone, as they are aligned perpendicular to the loading direction. Therefore, it was hypothesized that the increase of cross-links would be less in the superficial zone than in the radial and middle zone.

The first goal was to develop a novel model, that represents an aging knee. A model was designed in which cartilage could be artificially aged while withstanding compression. The second goal was to find methods to assess the effects regarding advanced glycation. The change in cartilage surface color, biomechanical properties (Section 1.3.1) and pentosidine level (Section 1.5), were characterized to determine whether or not mechanical compression enhances the formation of non-enzymatic cross-links in the collagen type II network.

The study consisted of two parts. The first part focused on the effect of static compression and the difference between the radial and superficial layers. The second part focused on the effect of dynamic compression.

[2]Phenomenon in which a material tends to expand in directions perpendicular to the direction of compression [101]

Part I

The Effect of Static Compression

The first part of the study focused on the effect of static compression on the formation of non-enzymatic cross-links in articular cartilage. The experiments of this research were conducted in the research lab of the UMC Utrecht Regenerative Medicine Center at the Hubrecht Institute and in the laboratory of the Department of Pharmaceuticals, University Utrecht.

Chapter 2

Methods

2.1 Tissue Harvest

An equine knee joint was obtained from a mature euthanized Shetland Pony at the Faculty of Veterinary Medicine, Utrecht University. Within 4 hours post-mortem, the joint was stored at -20°C. After thawing, the joint was disarticulated and muscle and tendon were carefully dissected. Osteochondral plugs were subsequently extracted from the visually intact femoral condyles, using a custom-made drill bit (Tubular Chisel 8.5 mm, Smith and Nephew). To prevent the tissue from overheating, the drilling site was constantly being sprayed on with phosphate buffered saline (PBS) (Gibco, UK). Post-extraction, the plugs were stored at -20°C until the day of the experiment. After thawing, the full cartilage layer was carefully removed from the bone using a large scalpel, after which it was split into four quarter disks (i.e. the samples). As the plugs were extracted from the condyles, the bone layers were slightly curved. As a result, half of the quarter disk had a deviating thickness. We took this into account when selecting the test and control samples. Each sample was equilibrated in PBS containing protease inhibitors (complete, Roche, Mannheim, Germany) and 5 mM Ethylenediaminetetraacetic acid (EDTA), to prevent enzymatic degradation. In the following of this report, this solution of PBS with enzyme inhibitors will be referred to as *PBS solution*.

2.2 Mechanical conditioning

2.2.1 Bioreactor design

Before the start of the experiment, a device had to be designed and developed, able to achieve the application of an adjustable, axial, uniform and unconfined compressive strain to the samples. Such a *bioreactor* should be able to compress the sample while being submerged in a cross-link inducing sugar solution. The bioreactor had to comply with the following design requirements:

TABLE 2.1: Design requirements of bioreactor.

	Design criteria
1.	Contains sample, lbh: ∼5x5x3 mm
2.	Fits into 2mL snap-cap vial (Eppendorf), together with 1 mL of solution
3.	Allows sufficient fluid flow to the sample
4.	Supports application of 0-30% strain
	Design wishes
1.	Supports application of strain with one hand
2.	Quantifies/visualizes amount of applied strain

A 3D model for the bioreactor was generated using SOLIDWORKS (EDUCATION EDITION 2017-2018). The final design with functional features is presented in Figure 2.1. Technical drawings can be found in Appendix A. The bioreactor consists of 2 components that were printed from ABS[1] (3DM-ABS resin) in a stereolithography apparatus (DLP station 5, Autumn). A digital caliper was used to validate its accuracy when used to apply deformations with a certain magnitude.

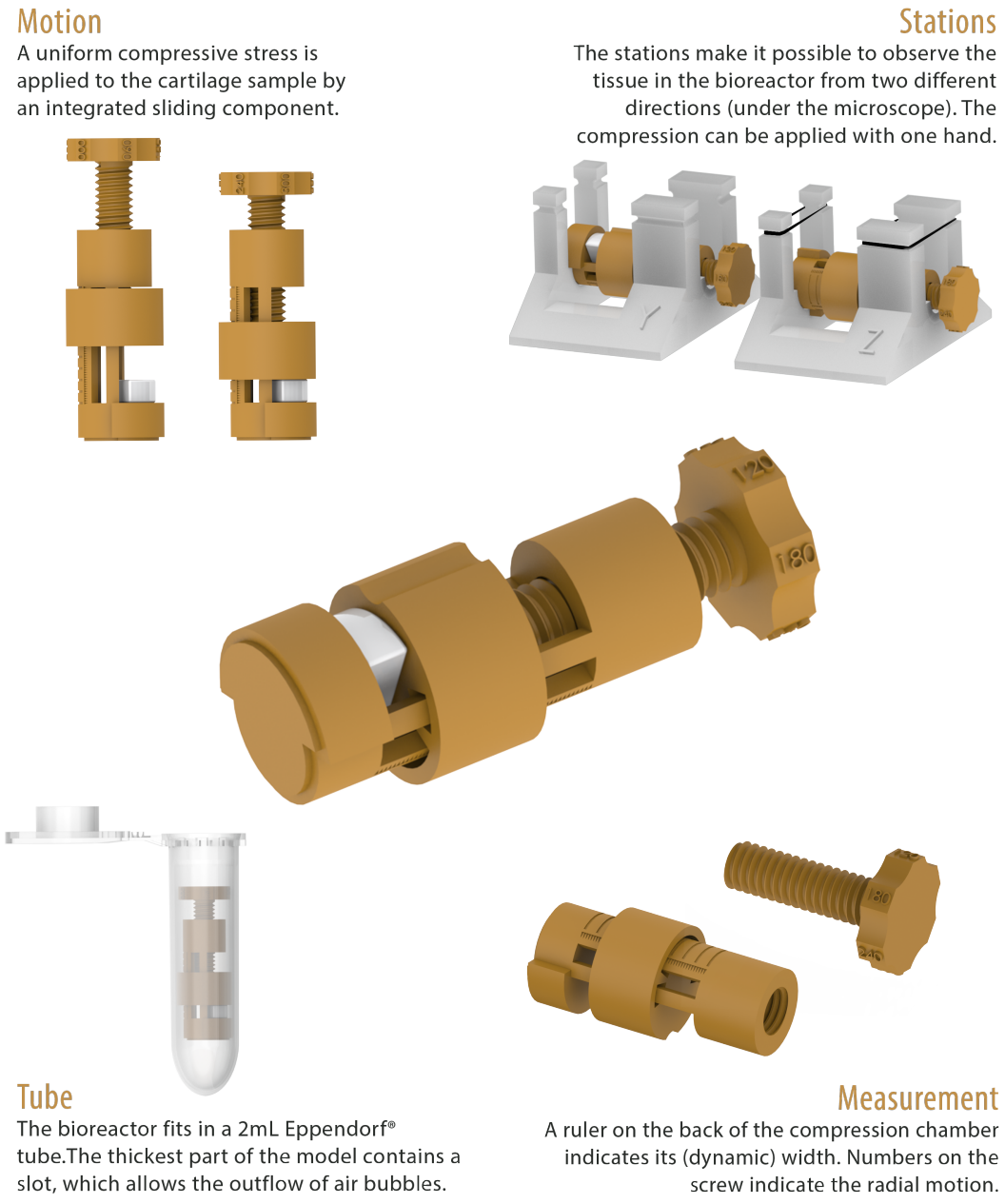

FIGURE 2.1: Bioreactor final design.

[1]Acrylonitrile butadiene styrene (ABS) is a common thermoplastic polymer with a relatively high Young's modulus of 1.5-3.5 GPa (CES EduPack 2013), which is a factor of about 1,000 higher than that of cartilage. Therefore, the deformation of ABS during the compression of cartilage was neglected.

2.2.2 Compression treatment

Two quarter disks of each plug were treated by mechanical conditioning. These samples were compressed with a 15% strain during incubation, while the other two functioned as control samples. Regardless, all samples were placed in a bioreactor during incubation. Prior to placement in the bioreactor, the sample thickness was measured using a digital caliper. Once a sample was placed in the compression chamber of the bioreactor, the screw was turned until first contact was made between the sliding component and the sample. Treatment samples underwent a deformation by turning their screws further, until a 15% strain (n = 16) was applied. For the control group, no further deformations were applied (n = 16). The right amount of deformation was achieved by turning the screw of the bioreactor a pre-calculated amount of degrees. The deformation was simultaneously checked with the digital caliper.

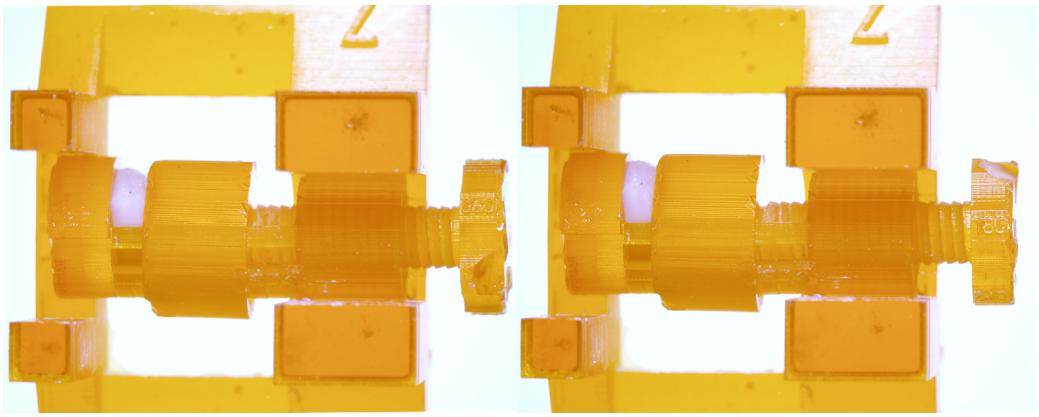

FIGURE 2.2: Applying compression to sample using the bioreactor.
Image captured with stereo microscope.

2.3 Cross-linking

In order to induce cross-linking during the treatment, the samples were incubated in the following way: all bioreactors were placed in a 2 mL snap-cap vial, filled with 1 mL of a solution of 40 mM L-Threose (Sigma, T7642) in PBS (Gibco, UK). L-Threose, a 4-carbon sugar, forms a number of characteristic AGEs [92]. It is able to mimic the age-related increase in cross-link concentration and it can therefore be used to "artificially age" articular cartilage. The solution also contained protease inhibitors (Complete, Roche, Mannheim, Germany) and 5 mM EDTA, to prevent enzymatic degradation. The vials were subsequently placed in empty 50 mL Falcon tubes, wrapped in aluminum foil, to prevent any light passing. These tubes were then placed on a tube roller mixer and stored at 37°C for 96 hours. In the following of this report, this procedure of artificial aging will be referred to as the *incubation* and the solution as *threose solution*.

2.4 Surface Color Analysis

The AGEs that are formed during non-enzymatic glycation form brown pigment [102]. Depending on the intensity of cross-linking, the color of cartilage changes

from white to brown. This change in color can be used as an indicator for the quantity of the cross-links as a result of the incubation with L-threose [100].

Before and after treatment, all samples were placed side by side on a glass dish and analyzed under a light microscope. Images of the cartilage surface were captured with a stereo microscope (SZX7, Olympus, Tokyo, Japan) and photo program software (Cell^F, Olympus, Tokyo, Japan). It was of utmost importance that all image acquisition was performed with identical settings and in the absence of ambient light. The captured background functioned as a reference framework and was configured as white (light intensity: 255 AU). The resulting images were converted to 32-bit images and the average pixel intensity was calculated with Fiji (ImageJ). The color of both the top and bottom surface of the samples was analyzed. After the second color analysis was performed, the samples were washed and stored in PBS solution for 12 hours at 4°C before biomechanical testing started.

2.5 Biomechanical Analysis

Biomechanical testing was carried out before and after incubation to obtain the change in Young's modulus of each sample. Stress-relaxation tests were performed uniaxially by a macroscopic indentation device. The setup consisted of a Lloyd LR5K testing machine (Lloyd Instruments, Bognor Regis, UK) with an extension resolution of less than 1 micron. The machine was equipped with a stainless-steel, spherical-ended indenter head with a radius (r) of 1 mm, a Young's modulus of 200 GPa and a Poisson's ratio of 0.30. To ensure biosafety, the whole set-up had to be wrapped in transparent plastic foil.

The experimental method that was used for this test, was mainly based on earlier work of Jurvelin et al. [103, 104]. Prior to the measurement, the sample was allowed to equilibrate in PBS solution for an hour at room temperature (20°C). Then it was placed in a petri dish with the superficial layer facing upwards and with enough PBS solution to keep it moist, but not too much to prevent it from floating. Before each measurement, the indenter was lowered with a displacement rate of 1 μm/s until a preload of 0.015 N was registered by the load cell, to ensure contact between the indenter and sample. After the preload was reached, the indenter was directly moved up again until the registered load dropped to 0 again. The extension of the machine was tared at this level, as this was the starting point for indentation. Subsequently, we fully submerged the sample in PBS solution and waited until equilibrium was reached, before starting the loading protocol.

The following displacement-controlled protocol was defined in Ondio software (Chatillon Fore Measurement, Largo, FL, USA). It started with a fast ramp compression with a displacement rate of 0.1 mm/s to a depth of 0.2 mm, to reach a strain level of approximately 10%. This deformation was kept constant for 130 seconds while the resulting load was monitored. Unloading followed with the same displacement rate. Indentation was done twice per sample to reveal possible failures in the test system. The sample was allowed to recover for at least an hour between both indentations. Similar load curves confirmed the validity of the measurement.

Application of the ramp displacement started the measurement and data acquisition by the computer. Load and position were recorded every 0.1 seconds by the load cell. As a response to deformation, articular cartilage showed an instant stress response. This instant response was followed by a relaxation to equilibrium stress, visualized in a typical stress-relaxation curve.

The data that were acquired during stress relaxation were used to calculate the stiffness of the sample. The stiffness measurement was based on the quantitation of the force by which the tissue resists instantaneous indentation of a constant depth. The peak load that resulted from the initial ramp compression represents the instantaneous stress while the stress-relaxation measured at t = 125 was set as the equilibrium stress, as can be seen in Figure 2.3.

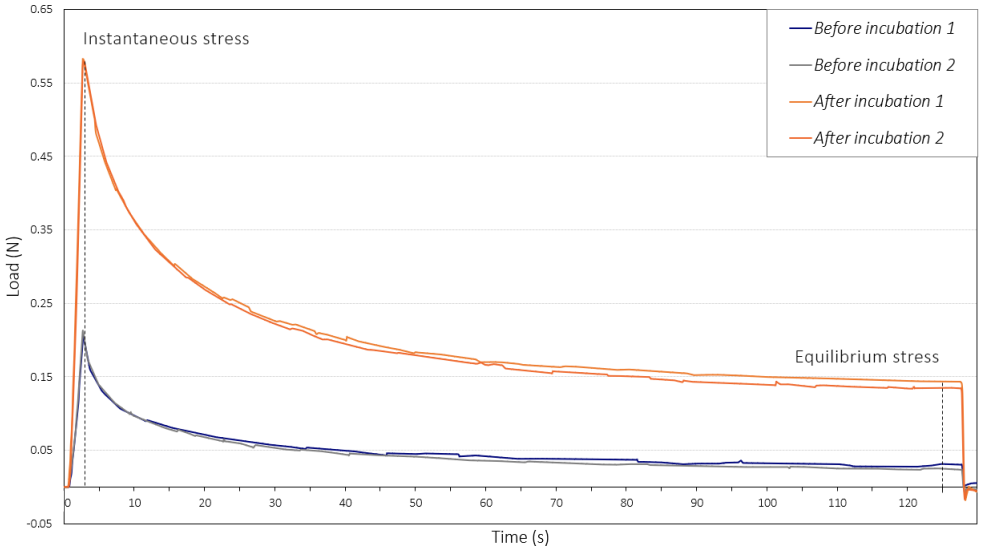

FIGURE 2.3: Example of plots from stress relaxation data, acquired from 1 cartilage quarter disk. The peak load at approximately t=2 is the result of the tissues instant response to the step displacement and is directly proportional with the instantaneous stress. The measured load at t = 125 s is directly proportional to the tissues equilibrium stress

The Hertz model is often used in the case of spherical indenters to analyze the indentation data. The load (P) in this model is expressed as:

$$P = \frac{4}{3} E_{eff} R^{1/2} h^{3/2} \tag{2.1}$$

Where R is the radius of the indenter tip, h is the penetration depth and E_{eff} denotes the reduced contact modulus between the tip and the sample. E_{eff} is related to the cartilage stiffness as follows:

$$\frac{1}{E_{eff}} = \frac{1-\nu^2}{E} + \frac{1-\nu'^2}{E'} \tag{2.2}$$

Where E′ and ν' refer to the indenter's modulus and Poisson's ratio respectively and the other terms to those of the cartilage tissue. During ramp loading, Poisson's ratio value of 0.5 was used in calculation of the instantaneous modulus (E_i). Poisson's ratio of 0.15 was applied for calculation of the equilibrium modulus (E_{eq}) [105]. In the case of soft materials, where $E' \gg E$, this equation can be simplified as follows:

$$\frac{1}{E_{eff}} \approx \frac{1-\nu^2}{E} \tag{2.3}$$

Since stress-relaxation consists of measuring the load relaxation over time in response to a constant step indentation input (h_0), the modulus can be expressed as:

$$E = \frac{3(1-\nu^2)P}{4R^{1/2}h^{3/2}} \tag{2.4}$$

2.6 Pentosidine and Collagen Measurements

The pentosidine and collagen level of the sample were determined using high performance liquid chromatography (HPLC). This is a form of column chromatography, generally used in biochemistry to separate, identify and quantify sample compounds. A full description of this technique can be found in Appendix A.

2.6.1 Sample preparation for HPLC

After micro indentation, the samples were prepared for biochemical analysis. In order to research the difference in the number of cross-links between the superficial zone and the rest of the tissue, half of the samples were cut in two pieces (n = 16). We tried to cut off 20% of its thickness, using the bioreactor as a clamping device and a digital caliper to check the thickness. The samples that resulted from this splitting, will hereinafter be referred to as the *radial* and *superficial* layer. The wet weight of all samples was measured, after which they were stored at -80°C for 10 minutes. A lyopholization of 18 hours in a freeze dryer followed, to remove all the water from the tissue. After dry weight was measured with a microbalance (Mettler Toledo UMX2 Ultra-microbalance), the samples were cut into small pieces. Then they were hydrolyzed in 6 M hydrogen chloride (HCl) in an oven at 110°C for 22 hours to break down the macromolecules in the tissue into individual amino acids. The liquid phase of the digested samples was allowed to completely evaporate at 60°C under a fume hood. This step was repeated after adding 800 μL of purified (MQ) water to remove as much HCl as possible. The residues were dissolved in an internal standard solution as described in the following section. Both HPLC assays that were performed, are based on the method, proposed in 1996 by Bank et al.[106].

2.6.2 Pentosidine Level

In this subsection, we describe the quantification of pentosidine in a reversed-phase HPLC run. Because of its fluorescence, pentosidine can be detected relatively easy. The hydrolyzed sample was diluted in 0.5% (v/v) heptafluorobutyric acid (HFBA) in 10% acetonitrile (ACN). An internal standard of pyridoxine (10 μM) was used to improve the accuracy in the quantification of pentosidine. A volume of 100 μL sample was injected into the system.

The HPLC system consisted of an Alliance 2695 Separations module (Waters Corporation, Milford, MA, USA) in series with an Alliance 2475 Multi Fluorescence detector (Waters Corporation, Milford, MA, USA). For pentosidine measurement, excitation and emission wavelengths were set at 297 nm and 395 nm respectively. For pyridoxine measurement, excitation and emission wavelengths were set at 295 nm and 400 nm respectively. Reversed-phase chromatography was performed using a Tosoh TSKgel ODS-80-TM column (4.6 mm internal diameter x 15.0 cm) packed with C18 coated silica particles. Waters Empower 3 Chromatography Data Software was used for data acquisition and processing. The analysis was performed at 30°C, using a tailored gradient run of 50 minutes with a constant 1.0 mL/min flow rate.

2.6.3 Collagen level

The amount of pentosidine in a sample was normalized by its collagen content to account for sample-to-sample variation. Collagen triple-helix with ∼300 repetitive sequences of Gly-X-Y (where X is often proline (Pro) and Y is hydroxyproline (Hyp)), is usually identified from nucleotide sequences. In this experiment, the amino acid Hyp was quantified to determine the collagen level in the sample, assuming that every 300 Hyp residues represent 1 collagen molecule. Measurements were performed with the same HPLC set-up and a similar column, as was used for the pentosidine measurements (Section 2.6.2). Excitation and emission wavelengths were set at 254 nm and 630 nm respectively.

For Hyp analysis, an aliquot of the above diluted sample (Section 2.6.2) was diluted another 50 times with 0.1 M sodium borate buffer pH 8.0 (dilution factor: 250). To enable the detection of amino acids with the fluorescence detector, 200 μL of the dilution was derivatized with 9-fluorenylmethyl chloroformate (FMOC). Derivation was followed by two pentane extractions to remove the excess FMOC. An internal standard of homoarginine (24 μM) was used to improve the accuracy in the quantification of hydroxyproline. A volume of 50 μL sample was injected in the system.

Mobile phases A and B were citrate solutions with different pH values and mobile phase C consisted of 100% ACN. A solution of 10% methanol (MeOH) was used as a needle wash between each injection. The column was washed and stored in mobile phase C. The analysis was performed at 30°C using a tailored gradient run of 40 minutes with a constant 1.4 mL/min flow rate. A calibration curve was obtained using external standards. The external standards contained hydroxyproline (Sigma H-7279) at concentrations varying from 0 to 60 μM.

The protocol of the HPLC measurements is presented in Appendix C , complete with chemical preparations and machine conditions.

2.7 Statistical Analysis

Statistical analyses were performed using GraphPad, Prism 8. The normality of data distribution was tested using Shapiro-Wilk tests. For data passing the normality test, One-way ANOVA was used, followed by a post-hoc Tukey's range test. For data not passing the normality test, Kruskal–Wallis was used, followed by a post-hoc Dunn's test. The level for statistical significance in all tests was set to p = 0.05. correlations are examined by the Pearson correlation coefficient r. Non-parametrical Mann-Whitney U-test and Spearman's rank correlation coefficient ρ were applied if a data set did not pass the normality test.

Chapter 3

Results

3.1 Surface Color

The non-enzymatic reaction of the collagen network with the threose solution (glycation), caused a change in surface color of the articular cartilage. It was clearly visible that the initial white color of the samples had turned to brown (Figure 3.1).

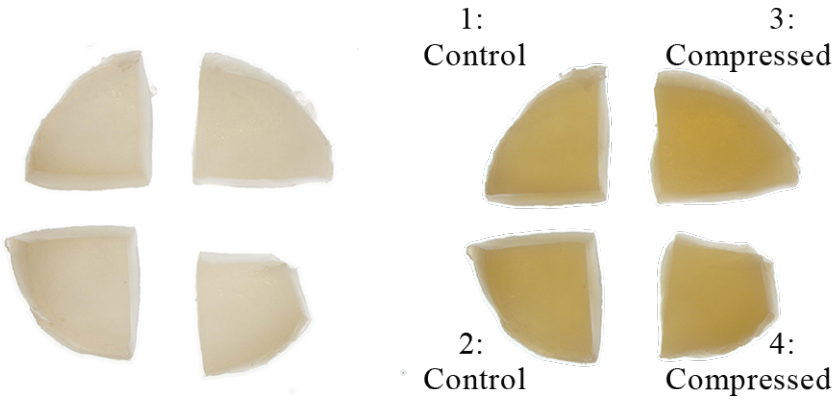

FIGURE 3.1: Changes in the top (or bottom) surface color of equine cartilage for compressed and uncompressed specimens after 96 hours of incubation. These images were obtained with a stereo microscope.

The cartilage surface color analysis allowed us to quantify the differences in the intensity of the color before and after incubation and between the compressed and uncompressed samples. The intensity of the color is used as an indicator of the efficacy of the cross-linking process. The mean magnitude of the average pixel intensity for all samples was 167.24 ± 17.11 AU (n = 32) before incubation and 123.24 ± 19.80 AU (n = 32) after incubation. Figure 3.2 shows the mean values of the average pixel intensity of both the top and bottom surface for the control and treatment group.

Since the Shapiro-Wilk test showed that the data for the average pixel intensity was not normally distributed, a Kruskal-Wallis test was conducted to examine the differences per group, followed by a post-hoc Dunn's test. The test showed that both test groups significantly changed in color ($P < 0.0024$), due to the incubation. However, no differences were measured between the control and treated samples.

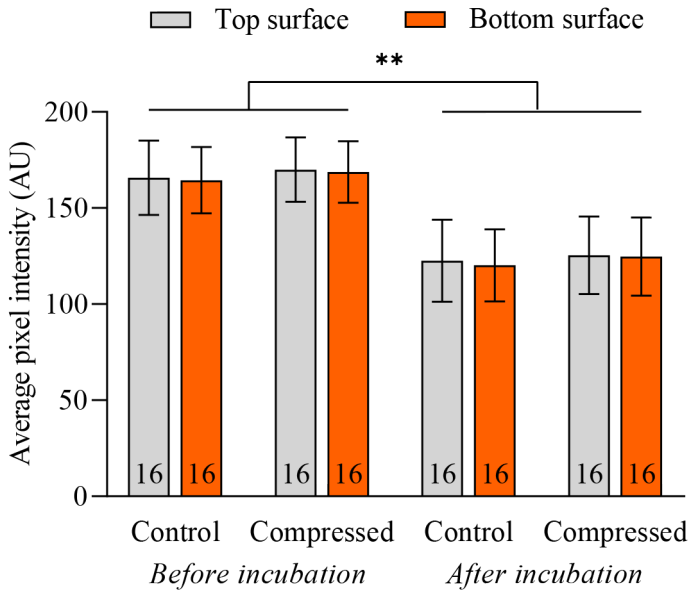

FIGURE 3.2: Average *average pixel intensity* per treatment group, obtained with Fiji (ImageJ). ** represents P < 0.001. The number at the bottom of each bar represents the number of replicates averaged for that bar value and Error bars showing the standard deviation.

3.2 Biomechanical Properties

The stiffness of the samples was measured through indentation experiments. Every sample was indented twice and from every indentation a load-time curve was obtained, representing a typical stress-relaxation. The instantaneous and equilibrium moduli of each sample before and after incubation were calculated, based on the data from the stress relaxations. The mean value of instantaneous modulus, calculated from all samples, was 1.46 ± 0.38 MPa (n = 16) before incubation and 3.79 ± 1.43 MPa after (n = 31) incubation. The mean value of equilibrium modulus was 0.51 ± 0.20 MPa (n = 16) before incubation and 1.87 ± 1.02 MPa (n = 31) after incubation. Figure 3.3a shows the mean values of both moduli for the control and treatment group. The normally distributed data for both moduli (Shapiro-Wilk) were reviewed with a one-way independent ANOVA, followed by a post-hoc Tukey's range test. No significant differences between the control and treatment group were observed. The analysis showed that for both groups the instantaneous and equilibrium had significantly increased due to the incubation ($P < 0.001$).

Since indentation was performed both before and after incubation, we were able to calculate the change in stiffness per sample. Reviewing the change rate per sample could potentially exclude stiffness differences as a result of variation in sample shape and thickness. Nevertheless, these results still varied a lot as the error bars, representing the standard deviation, show in Figure 3.3b. One-way independent ANOVA showed no significant difference in the increase between the control and treated group or between the instantaneous and equilibrium modulus [$F(3,28) = 1.174$, $P = 0.3373$]. Nonetheless, with respect to this percentage change, it seems that the equilibrium modulus has increased more during incubation than the instantaneous modulus.

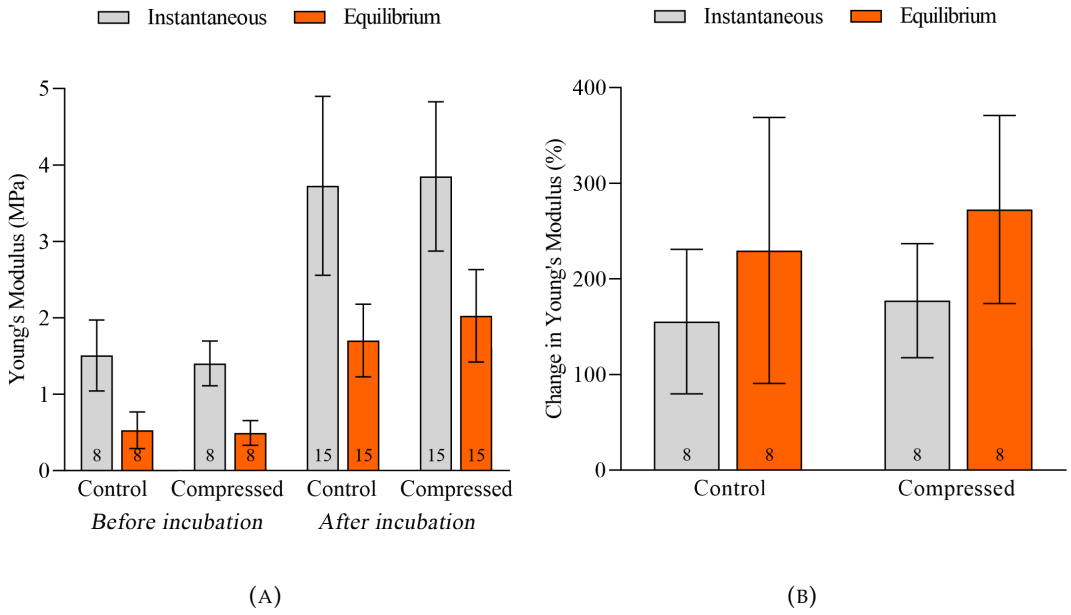

FIGURE 3.3: Instantaneous and equilibrium modulus obtained by indentation. A) Average moduli per group before and after incubation. B) Average percentage change in Young's moduli per treatment group. The number at the bottom of each bar represents the number of replicates averaged for that bar value and the error bars show the standard deviation.

3.3 Pentosidine and Collagen levels

Fluorescence measurements with HPLC were used to obtain the level of the cross-link Pent and the amino acid Hyp in the cartilage samples. All calibration curves, created with external standards (0-50 nM Pent. & 0-60 μM Hyp.), were characterized by a high correlation coefficient ($R^2 > 0.999$). Appendix D provides the following additional information, regarding the performed HPLC measurements: Examples of the chromatograms for pentosidine, pyridoxine and hydroxyproline, the retention times of these compounds and the equations of the calibration curves. Assuming that every 300 Hyp residues represent 1 collagen molecule, the pentosidine per collagen levels could be determined.

The mean pentosidine per collagen level was 0.12 ± 0.018 mol/mol (n = 31). Figure 3.4 shows the mean values for the radial zone, superficial zone and full quarter disks per treatment group.

A Shapiro-Wilk test showed that the distribution of the data for each group followed a normal distribution. Therefore, the pentosidine per collagen level values were statistically assessed using one-way independent ANOVA. One-way independent ANOVA showed no significant difference between the groups [F(5,57) = 0,7898, P = 0.5614]. Nevertheless, a higher pentosidine per collagen level can be seen for radial zones that were assayed in the control group as compared to the ones in the treated group.

In addition to these results, scatter plots are made of the amount of pentosidine per collagen molecules versus the instantaneous and equilibrium modulus (Figure

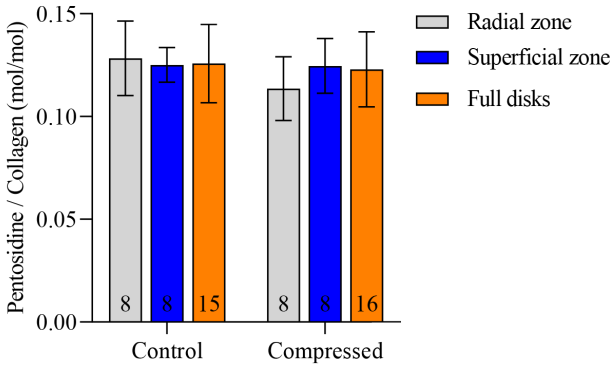

FIGURE 3.4: Pentosidine per collagen level obtained by HPLC. The number at the bottom of each bar represents the number of replicates averaged for that bar value and the error bars show the standard deviation.

3.5). A Pearson correlation coefficient was computed to assess the relationship between these variables. In the case of instantaneous stress, there was a positive correlation between the relative number of crosslinks and the instantaneous modulus (r = 0.5258, P = 0.0024).

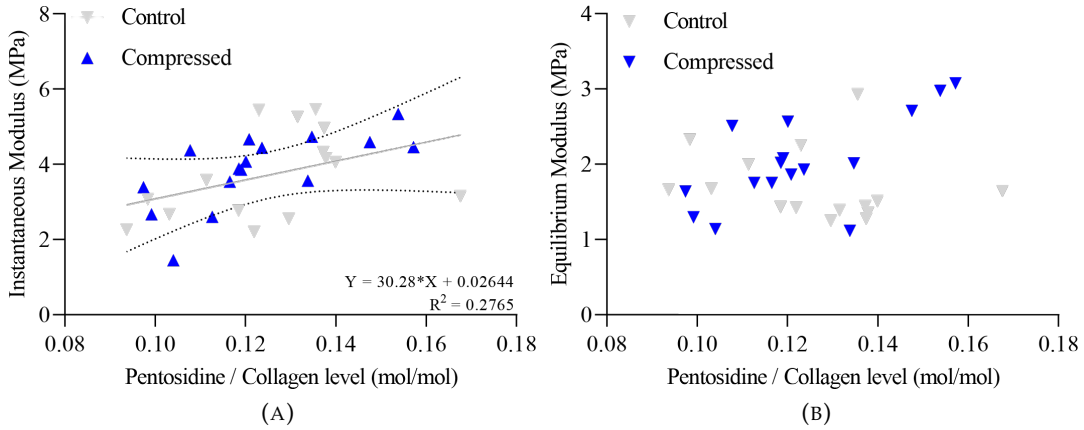

FIGURE 3.5: Instantaneous (A) and equilibrium (B) modulus versus pentosidine per collagen molecules for every sample. A) Linear regression of the instantaneous equilibrium moduli of samples versus their pentosidine per collagen level.

3.4 Conclusion

The first part of the study focused on the effect of static mechanical compression, experienced by the collagen type II fibril network in articular cartilage on its chemical response to non-enzymatic cross-linking, leading to pentosidine cross-links. In short, we observed no increase in the number of cross-links in response to the application of a 15% compressive strain. Together, all findings of this experiment confirmed that the used treatment did not influence the formation of advanced glycation end-products. Moreover, we observed no differences in cross-linking between the superficial and radial zone of articular cartilage. These findings are further discussed in the Discussion (Section 6).

Part II

The Effect of Dynamic Compression

The second part of the study focused on the effect of dynamic compression on the formation of non-enzymatic cross-links in articular cartilage. The experiments of this research were conducted in the Molecular Bioelectrostatics & Drug Delivery Laboratory, Northeastern University, Boston; under the supervision of prof. A.G. Bajpayee.

Chapter 4

Methods

4.1 Tissue Harvest

Cartilage explants were extracted from an immature (2-3 weeks old) bovine knee joint, obtained from a local slaughterhouse (Research 87, Boylston, USA). Cylindrical plugs were initially extracted from the femoropatellar groove using a 3 mm biopsy punch. The plugs were then sliced to obtain 1 mm thick cartilage disks containing the superficial, middle and deep zone of cartilage. Sterile technique was used, because the samples were also harvested for other purposes (culture experiments). Upon harvest, the disks were washed and equilibrated in 1x PBS for up to 1 hour to maintain hydration. Cartilage disks were stored in PBS supplemented with protease inhibitors at -20°C until the day of the experiment.

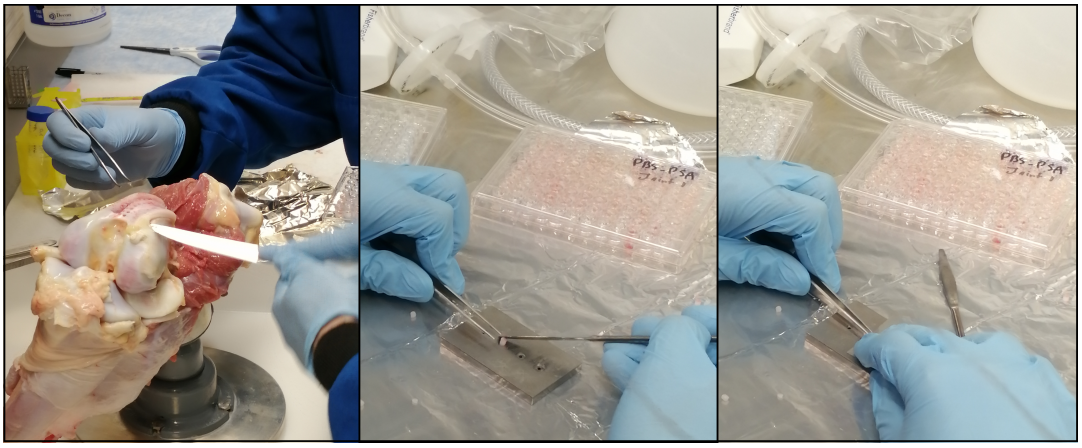

FIGURE 4.1: Tissue harvest. The technique that is used in combination with the custom made tools resulted in the acquirement of cartilage samples with almost identical dimensions.

4.2 Cross-linking

After thawing, the explants were kept in 1x PBS for at least 2 hours to equilibrate. In order to induce cross-linking, the explants were incubated (at 37°C) in a solution (2 mL) of 40 mM L-Threose (Sigma, T7642) in 1x Dulbecco's Phosphate Buffered Saline (ThermoFisher Scientific, Waltham, MA) for 96 hours, while the negative control was incubated in PBS without L-Threose. Both solutions contained protease inhibitors (Roche Life Sciences, Indianapolis, USA) and 5 mM Ethylenediaminetetraacetic acid

(EDTA), to prevent enzymatic degradation. The PBS, used during the whole experiment, did not contain Ca^{2+} or Mg^{2+}. Osmolarity differences between the threose and PBS solution were corrected by adding the required amount of sodium chloride (NaCl) [1]. In the following of this report, these solutions of PBS with enzyme inhibitors will be referred to as *PBS solution* and *threose solution*.

4.3 Mechanical conditioning

Samples were taken out of the incubation solution 8 times to be dynamically compressed. This mechanical conditioning served as the treatment of the experiment. A cycle of unconfined compression steps was performed using a Dynamic Mechanical Analyzer (DMA) (ElectroForce 5500, TA Instruments), equipped with a 250 N load cell.

Before compression, the sample thickness was measured using a digital caliper. A thin layer of glue was carefully applied to fix the disk on the unconfined compression chamber, with the superficial layer facing upward. For compression under hydrated conditions, the explants were submerged in 400 μL PBS [2].

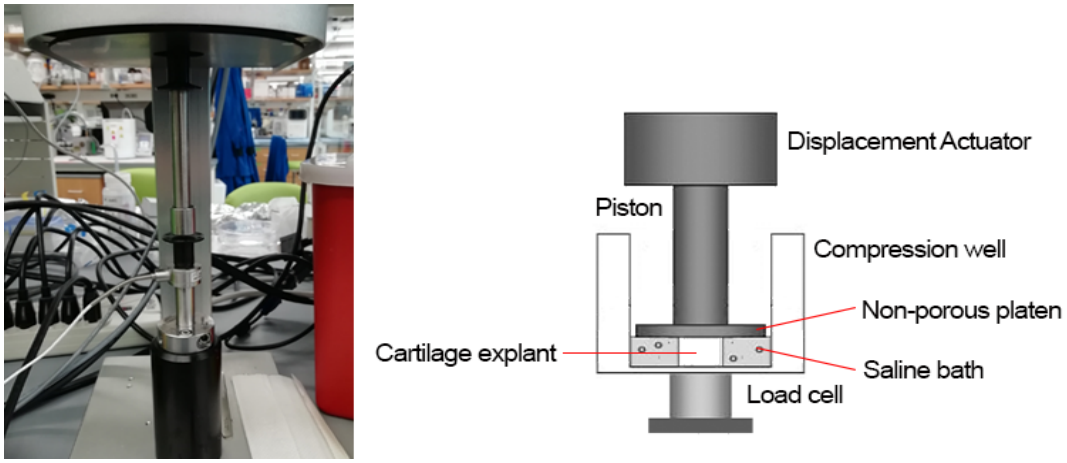

FIGURE 4.2: Experimental set-up for mechanical treatment and measurements. Left) Photo of DMA set-up. Right) Schematic of the set-up. The cartilage explant disk is mounted in radially unconfined axial compression in a PBS bath. The load cell is installed underneath the compression well.

The following displacement-controlled protocol was defined in ElectroForce WinTest^{TM} DMA 7.1 software. Load and piston position were recorded every 0.05

[1] In 2018, Pouran et al. showed that cross-linking of collagen type II fibrils is tuned via an osmolality switch. Since we solely wanted to see the effect of compression in our experiment, we had to make sure that the osmolarity of all incubation solutions is the same.

[2] In the ideal test set-up, the sample would obviously be compressed while being submerged in threose solution, instead of PBS. However, L-Threose could not be used inside the compression chamber. Amongst others, because leftover threose, which is a relatively expensive compound, would go to waste every cycle by sticking to the chamber and piston. On the other hand, if the solution was saved and reused for multiple cycles it would be impossible to completely control the solution's composition and (os)molarity, as there will always be some minor evaporation, contamination and mixing with the glue. Therefore, we had decided to use PBS during compression cycles

seconds by the load cell. First, a preload of 0.1 N was automatically applied to ensure uniform contact between the articular surface and machine piston, after which the protocol started. The sample was allowed to equilibrate in the testing solution first for 600 seconds (step 1). Then, it was initially subjected to a 4% compressive strain with a displacement rate of 0.0001 mm/s (step 2). Such a strain step is indicated as a *ramp*. Again, the sample was allowed to relax and equilibrate at this strain level for 600 seconds before dynamic compression started (step 3). Relaxation steps are indicated as *dwells*.

Dynamic compression consisted of 3 hours of sinusoidal dynamic compression of 1% amplitude superimposed on the 4% static offset strain (step 4). This dynamic compression functions as the actual treatment of this experiment and the frequency differed per treatment group (Section 4.3.1). After dynamic compression, a 600-second dwell followed at the strain level of 4% (step 5).

Directly after the cycle ended, the sample was placed in its incubation solution again. The sample was incubated 4 hours before the first cycle, 4 hours after the last cycle and 8 hours between each cycle.

For measurement reasons, 2 additional strain steps of 2% each were applied to the sample with a displacement rate of 0.0001 mm/s, resulting in a final compression of 8% (step 6 & 8). Both strain steps were followed by a 600-second dwell step (step 7 & 9), after which the piston was suddenly raised to start conditions with a displacement rate of 0.1 mm per second (step 10).

4.3.1 Treatment groups

During this experiment, we focused on the effect of dynamic compression on non-enzymatic glycation in cartilage. The treatment groups differed in the frequency at which compression was applied. The treating frequency of 1 Hz is a typical gait frequency and represents approximate physiologic walking, while the slower (0.01 Hz) frequency represents sitting/office work activities [107, 108]. Treatment started every 12 hours. A treated sample underwent a total of 8 loading cycles, each including a 3 hour long dynamic loading step. Thus, samples were treated 24 hours during the 96-hour experiment.

As described in Section 4.2, artificial aging was induced by L-Threose. Negative control groups were added to the experiment, in which no response was expected, to exclude any effects that are not cross-link related. The samples in these control groups were incubated in PBS solution. The treatment groups are summarized in Table 4.1.

TABLE 4.1: Treatment groups with related test factors and function.

Treatment group	Incubation in	Frequency	Function
A (n = 3)	Threose	no compression	Positive control
B (n = 3)	Threose	0.01 Hz	
C (n = 3)	Threose	1 Hz	
D (n = 3)	PBS	no compression	Negative control
E (n = 1)	PBS	1 Hz	Negative control

4.4 Mechanical Analysis

Once the final incubation period was completed, the sample was washed in PBS for 24 hours at 4°C, with a change of the solution after 8 hours. To obtain the final mechanical properties of each sample, an additional unconfined compression test was performed. For this final measurement, the same displacement-controlled apparatus and set-up were used as for the dynamic compression cycles (Section 4.3) and the same preparations were carried out before starting the loading protocol. Mechanical testing consisted of unconfined compression in stress-relaxation followed by harmonic loading, to determine respectively the equilibrium and dynamic stiffness of the cartilage explants. The following displacement-controlled protocol was defined in ElectroForce WinTest™ DMA 7.1 software. Load and position were recorded every 0.05 seconds by the load cell.

4.4.1 Loading protocol

After achieving a contact preload of 0.1 N, the cycle started with a dwell of 600 seconds, allowing the sample to equilibrate. Preliminary tests revealed that a 600-second relaxation period was sufficient to allow the specimen to fully equilibrate. The preload was based on the signal-to-noise ratio of the apparatus and was used to ensure contact between the sample and the piston. Ramp-stress relaxation testing was performed, where a series of 3 consecutive ramps was applied to compress the sample in the following order: 4%, 6% and 8% of its initial thickness with a displacement rate of 0.0001 mm/s. Each ramp was followed by a dwell of 600 seconds, resulting in 3 typical stress-relaxations.

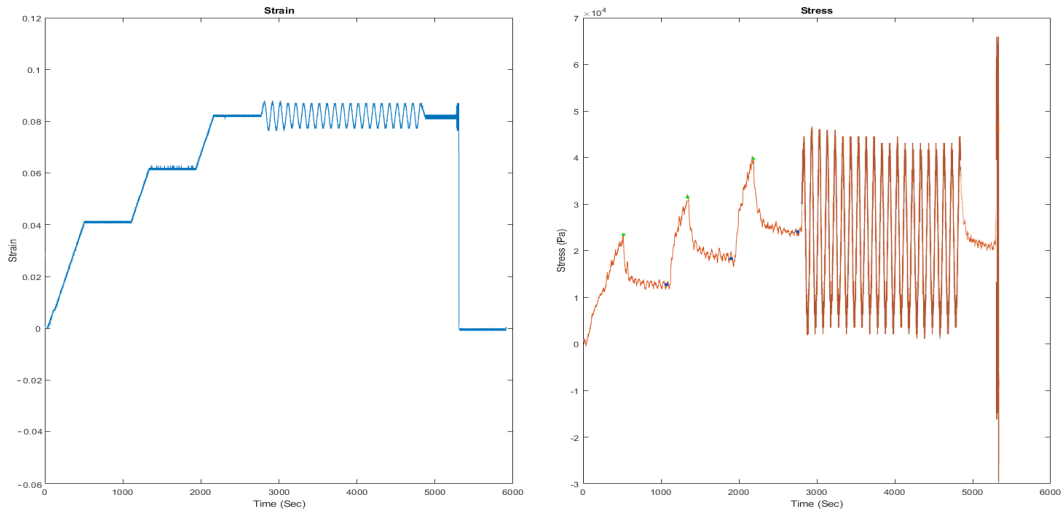

FIGURE 4.3: Plots of the loading cycle. Left) Applied strain in percentile. Right) Resulting stress in Pascal. The 10 loading steps of the cycle can clearly be identified

The 3 stress-relaxations were followed by harmonic loading, to determine the dynamic stiffness of the sample. After the last dwell, a 1% amplitude sinusoidal strain was superimposed on the 8% strain at a frequency of 0.01 Hz for 20 cycles. A 600-second dwell followed to let the specimen recover. Subsequently, a second sinusoidal strain was applied with a 1% amplitude at a frequency of 1 Hz for 30 cycles,

after which the piston was suddenly raised to start conditions with a speed of 0.1 mm per second. The piston displacement and corresponding loads were recorded and stored for analysis.

4.4.2 Data processing

To acquire the mechanical properties, the raw data from the loading cycle were processed with MATLAB (MathWorks, version R2016b). By means of a custom-made MATLAB script (Appendix E) all peaks and equilibrium forces were identified, data was smoothened and calculations were performed (See Figure 4.3).

The magnitude of the equilibrium stress of each strain increment was calculated, by dividing the measured forces by the sample cross-sectional area. The equilibrium modulus was determined from the slope of the best linear fit of the equilibrium stress, plotted against the applied strain.

The dynamic modulus (E*) and phase angle (δ) were determined from a dynamic analysis of the measured stress and strain responses. E* is defined as the ratio of maximum stress to maximum strain and provides a measure of the total resistance to deformation of the sample when subjected to loading. The fundamental component of load was normalized to original area and the fundamental component of position was normalized to current thickness (considering the 8 percent compression offset). By dividing these two components, the dynamic modulus was obtained.

The phase angle is a measure of the viscoelastic balance of the sample behavior. If δ equals 90° then the sample can be considered to be purely viscous in nature, whereas δ of 0° corresponds to purely elastic behavior. Between these two extremes, the material behavior can be considered to be viscoelastic in nature with a combination of viscous and elastic responses.

4.5 Pentosidine and Collagen Measurements

At the conclusion of the experiment, the wet weight of the sample was measured. The sample was digested overnight at 57°C in 1 mL solution of the broad-spectrum enzyme proteinase K (0.5 mg/L) in Tris (UltraPure^{TM} 1M Tris-HCl, pH 8.0) Buffer (ThermoFisher Scientific, Waltham, USA)).

4.5.1 Pentosidine Level

Pentosidine was quantified based on fluorescence measurement. The fluorescence intensity of 100 μL digest samples was measured using a Synergy H1 Microplate Reader (Biotek). The emission signal was monitored at 328 nm upon excitation at 378 nm. Fluorescence values were correlated to Pentosidine concentrations using a calibration curve equation. The calibration curve was obtained using external standards. The external standards contained Pentosidine (Cayman 10010254) at concentrations varying from 0 to 10 μM.

4.5.2 Collagen level

The amount of pentosidine in a sample was normalized by its collagen content to account for sample-to-sample variation. The measurement of hydroxyproline concentration was used to determine the collagen content in the samples. The hydroxyproline concentration was determined by the reaction of oxidized hydroxyproline with 4-(dimethylamino)benzaldehyde (DMAB), resulting in a colorimetric product,

proportional to the hydroxyproline present. The protocol for the hydroxyproline assay can be found in Appendix F. Absorbance measurements were used to quantify hydroxyproline content, using a Synergy H1 Microplate reader (Biotek). The absorbance signal was monitored at 560 nm. Absorbance values were correlated to hydroxyproline concentrations using a calibration curve equation. The calibration curve was obtained using external standards. The external standards contained hydroxyproline (Sigma H-7279) at concentrations varying from 0 to 60 μM.

All values in the results from the plate reader represent the mean value of two measured injections of the same sample.

4.6 Statistical Analysis

Statistical analyses were performed using GraphPad, Prism 8. The normality of data distribution was tested using Shapiro-Wilk tests. For data passing the normality test, One-way ANOVA was used, followed by a post-hoc Tukey's range test. For data not passing the normality test, Kruskal–Wallis was used, followed by a post-hoc Dunn's test. The level for statistical significance in all tests was set to p = 0.05. correlations are examined by the Pearson correlation coefficient r. Non-parametrical Mann-Whitney U-test and Spearman's rank correlation coefficient ρ were applied if a data set did not pass the normality test.

Chapter 5

Results

In this experiment, bovine femoral cartilage was studied to evaluate the effects of dynamic unconfined compression on non-enzymatic glycation of articular cartilage. The first part of this experiment aimed at the assessment of the biomechanical properties of the samples. The second part focused on the quantification of advanced glycation end products. All the data are presented as mean ± standard deviation.

5.1 Biomechanical Properties

5.1.1 Equilibrium properties

The final equilibrium modulus of each sample was calculated, based on the data from the three stress relaxations. The mean magnitude of equilibrium modulus for all the samples was 0.22 ± 0.09 MPa (n = 13).

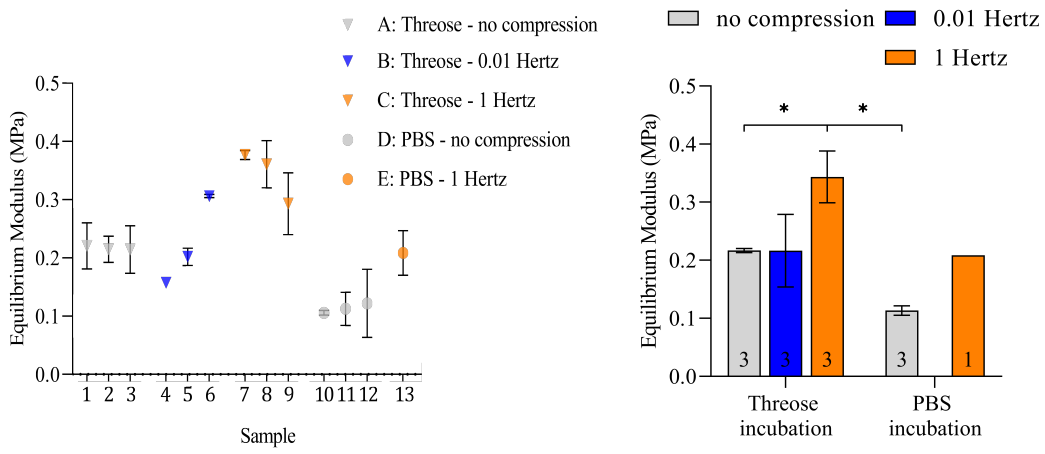

(A) (B)

FIGURE 5.1: Equilibrium modulus obtained by unconfined compression. A) Individual modulus per sample. Error bars showing the mean and standard deviation from individual measurements (strain increments). Distinction is made between each treatment group. B) Average equilibrium modulus per treatment group. The number at the bottom of each bar represents the number of replicates averaged for that bar value and the error bars show the standard deviation. * represents $P < 0.05$.

Figure 5.1 shows the individual values per sample and mean values per treatment group. All equilibrium moduli were calculated with the data from three stress

relaxations. Therefore, error bars are also added in Figure 5.1b, representing the standard deviations of the calculated moduli per strain increment.

Dynamic compression with a frequency of 1 Hz "during" incubation seems to increase the tissue's equilibrium modulus, compared to treatment with 0.01 Hz compression or no compression at all. However, since the same phenomenon can be seen for the in PBS incubated (negative control) groups, it is not clear if this increase is cross-link related.

According to the Shapiro-Wilk test, the data of all treatment groups were normally distributed. Therefore, the calculated mean equilibrium moduli were statistically assessed using a one-way independent ANOVA, followed by a post-hoc Tukey's range test. The one-way independent ANOVA showed that there was a significant difference in equilibrium modulus between the 5 treatment groups [$F(4,8) = 10.12$, $P = 0.0032$]. Samples that were compressed with a 1 Hz frequency during incubation (treatment group C) showed a significant higher equilibrium modulus compared to those that were not compressed during threose incubation (treatment group A) ($P = 0.0473$) or incubated in PBS (treatment group D) ($P = 0.0015$).

5.1.2 Dynamic properties

The dynamic modulus of the samples at both frequencies is presented in Figure 5.2. The mean magnitude of dynamic modulus for all the samples was 4.11 ± 1.63 MPa (n = 13) at 0.01 Hz and 7.08 ± 2.90 (n = 13) at 1 Hz. When comparing the results of the dynamic moduli at the 2 frequencies, one can immediately recognize a very similar trend.

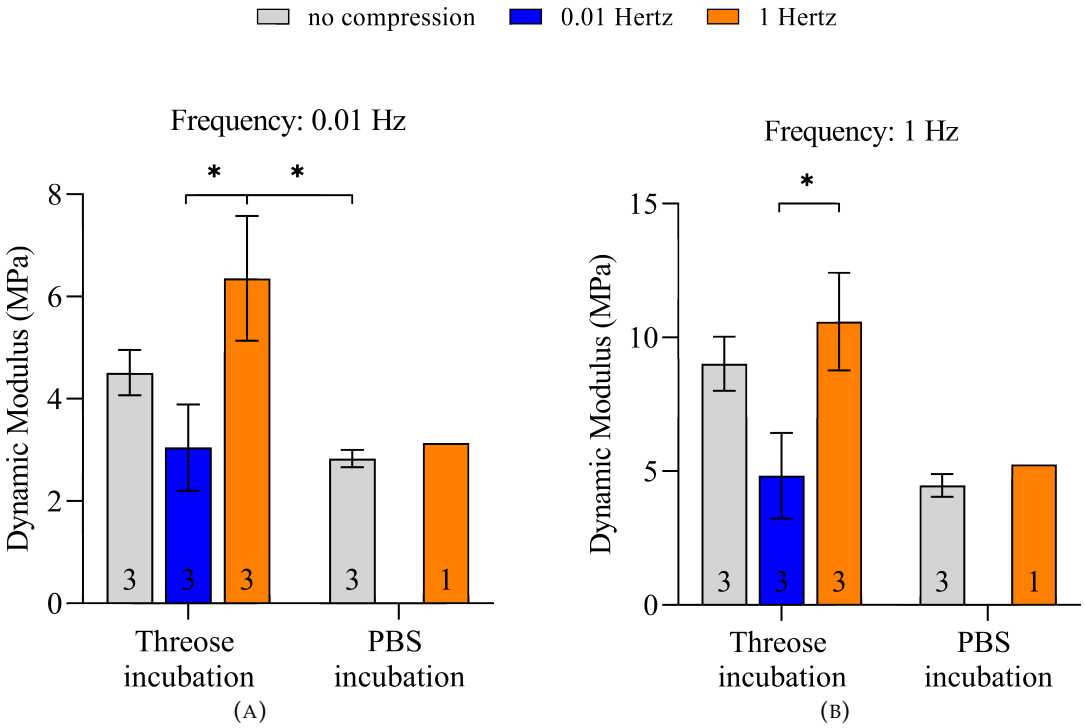

FIGURE 5.2: Average dynamic modulus per treatment group, obtained by unconfined dynamic compression at a frequency of A) 0.01 Hz. B) 1 Hz. The number at the bottom of each bar represents the number of replicates averaged for that bar value and the error bars show the standard deviation. * represents $P < 0.05$.

According to the assessed one-way independent ANOVA, there were statistically significant differences between the treatment groups in dynamic modulus at 0.01 Hz [F(4,8) = 6.994, P = 0.0101]. The dynamic modulus at 0.01 Hz of the samples of treatment group C was significantly higher compared to those of treatment group B (P = 0.0163) and D (P = 0.0114).

Since the Shapiro-Wilk test showed that the data for dynamic compression at 1 Hz were not normally distributed, a Kruskal-Wallis test was conducted to examine the differences in dynamic modulus between treatment groups, followed by a post-hoc Dunn's test. A significant difference was found between treatment groups B and C (P = 0.0211). Additionally, samples of treatment group D showed a significantly lower dynamic modulus at 1 Hz compared to both treatment group A (P= 0.0464) and treatment group B (P = 0.0119). This is not shown in the graph. It seems that the treatment with a 1 Hz compression during incubation increases the tissue's dynamic modulus significantly more than treatment with a 0.01 Hz compression, regardless of whether you measure the modulus at a frequency of 1 Hz or 0.01 Hz.

The phase shift of the samples at both frequencies is presented in Figure 5.3. The mean magnitude of phase shift for all samples was 39.3 $\pm$ 5.53 degrees (n=13) at 0.01 Hz and 8.87 $\pm$ 2.84 (n = 13) at 1 Hz.

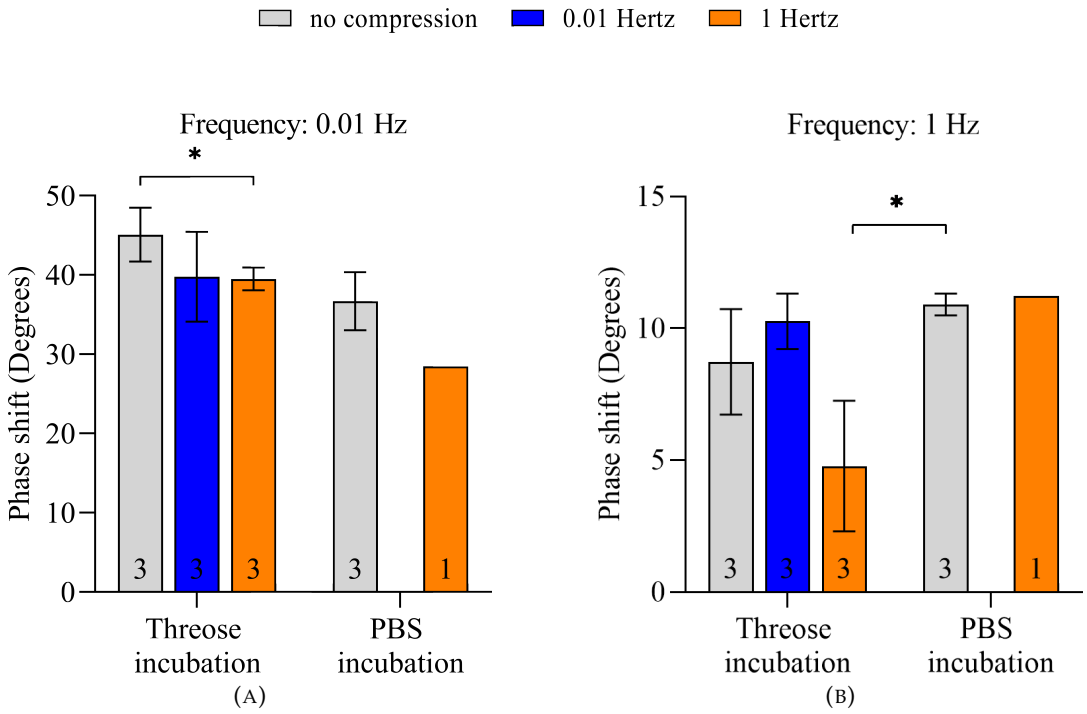

FIGURE 5.3: Average phase shift per treatment group, obtained by unconfined dynamic compression at a frequency of A) 0.01 Hz. B) 1 Hz. The number at the bottom of each bar represents the number of replicates averaged for that bar value and the error bars show the standard deviation. * represents P < 0.05.

The normally distributed data for phase shift were again reviewed with a one-way independent ANOVA, which showed a significant difference between the different treatment groups for both frequencies; 0.01 Hz [F(4, 8) = 3.716, P = 0.0540], 1 Hz [F(4, 8) = 6.073, P = 0.0151]. Regarding dynamic compression at 0.01 Hz, a post hoc test shows a significant difference in phase shift between the samples of treatment group A and treatment group C (P = 0.0418).

In the case of dynamic compression at 1 Hz, the test shows that the samples of treatment group C have a significant lower phase shift (viscosity) than those of treatment group D.

5.1.3 Stiffness over time

As briefly mentioned in the *Methods* (Section 4.3), two additional loading steps were added to each treatment loading cycle (step 6-9). Based on the obtained data, an attempt was made to determine the equilibrium stiffness of the treated samples after each cycle, by reviewing the stress response of the explant to these additional compression steps. Unfortunately, the data that we retrieved from these intermediate stress relaxations, gave us very conflicting and unusable results. A possible explanation for this, may have to do with the fact that the tissue was not recovered from the 3-hour cyclic loading [78]. Therefore, these findings were excluded from the study.

5.2 Pentosidine and Collagen levels

A fluorescence measurement with a plate reader was used to determine the pentosidine level of the samples, as an indicator for the number of cross-links. The calibration curve, that was created with 8 standards (0-10 μM), was characterized by a high correlation coefficient ($R^2 > 0.999$). The mean pentosidine level was 0.24 ± 0.03 μmol (n = 9) for samples that were incubated in threose solution and 73 ± 5.3 pmol (n = 4) for samples that were incubated in PBS solution. Figure 5.4 shows the mean values per treatment group.

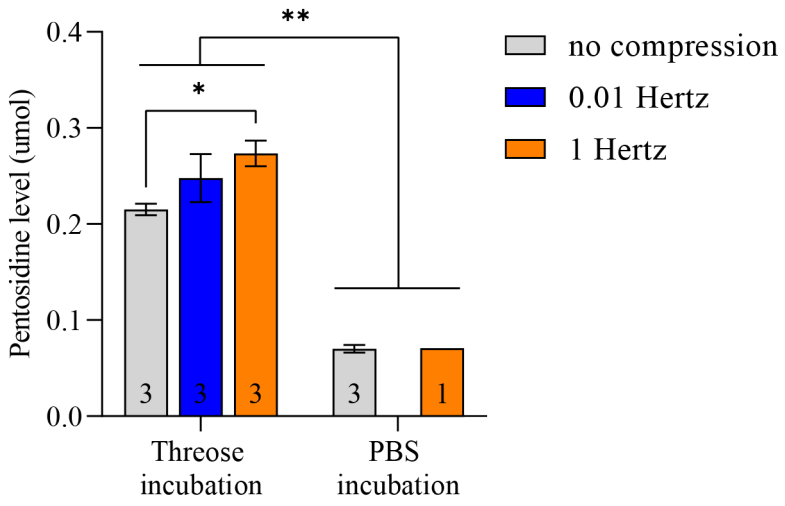

FIGURE 5.4: Average pentosidine level per treatment group, obtained by fluorescence measurement. The number at the bottom of each bar represents the number of replicates averaged for that bar value and the error bars show the standard deviation. * represents $P < 0.05$ and ** represents $P < 0.001$.

A Shapiro-Wilk test showed that the distribution of the data for each treatment group followed a normal distribution. Therefore, the pentosidine level values were statistically assessed using a one-way independent ANOVA, followed by a post-hoc Tukey's range test. A one-way independent ANOVA showed a significant difference

between the treatment groups [F(4,8) = 84.25, P < 0.0001]. Samples of all treatment groups, incubated in threose (A, B and C) showed significant higher pentosidine levels compared to those incubated in PBS solution (P < 0.001). Moreover, samples of treatment group C showed a significant higher pentosidine level compared to the samples of treatment group A (P = 0.0217).

The level of hydroxyproline was measured with the use of absorbance measurements, to determine the collagen level per sample. The calibration curve for this assay, created with 9 standards (0-60 μM), was characterized by a high correlation coefficient ($R^2 > 0.999$). By means of these values, the collagen levels could be calculated. The mean collagen level for all samples was 4.90 $\pm$ 0.96 μmol (n = 13). The amount of pentosidine per collagen molecules (mol/mol) is presented in Figure 5.5a.

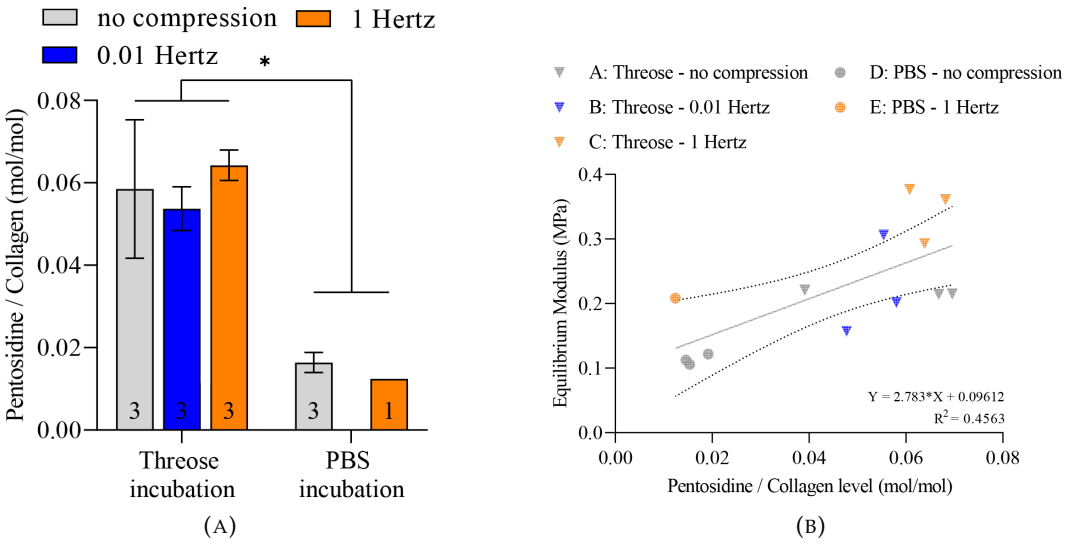

FIGURE 5.5: A) Average molecular amount of pentosidine per collagen (mol/mol) per treatment group. The number at the bottom of each bar represents the number of replicates averaged for that bar value and the error bars show the standard deviation. B) Linear regression of the individual equilibrium moduli of samples versus their pentosidine per collagen level.

The trend that we observed earlier with the absolute pentosidine levels of the samples had changed after normalization to collagen content. For the treatment group that was treated with no compression, it meant a relative increase in mean cross-link level with a high standard deviation. A one-way independent ANOVA showed no significant difference anymore between the treatment groups that were incubated in threose. The groups that were incubated in PBS still showed significantly lower cross-link levels than those that were incubated in threose (P < 0.05).

A Pearson correlation coefficient was computed to assess the relationship between the pentosidine per collagen level and the equilibrium modulus. As expected, there was a positive correlation between the two variables (r = 0.7006, P = 0.0077). A scatter plot summarizes these results (Figure 5.5b).

Chapter 6

Discussion

The first part of the study focused on the effects of static mechanical compression, experienced by the collagen type II fibril network in articular cartilage on its chemical response to non-enzymatic cross-linking, leading to pentosidine cross-links. We observed no increase in the number of cross-links in response to the application of a 15% compressive strain. Together, all findings of this experiment confirmed that the used treatment had no influence on the formation of AGE cross-links. Moreover, we observed no differences in cross-linking between the superficial and radial zone of articular cartilage.

The results are not in accordance with findings reported by Pouran et al., that suggested that shrinkage makes cartilage tissue more prone to glycation. It was shown that shrinkage of less than 3%, induced by exposure to hyper-osmolality, affected the cross-link efficiency significantly [100]. The main difference between both studies is the direction of deformation. The treatment in our study consisted of uniaxial compression, which is different from strain in all directions (like shrinkage). Pouran et al. have explained that shrinkage of the tissue can result in a denser collagen fibril network, which potentially alters the spatial conformation of the lysine and arginine, the amino-acids responsible for non-enzymatic cross-linking. The compression in our experiment was unconfined, which may have resulted in a less dense network in which fibrils can more easily recover, preventing them from conformational changes.

A biomechanical and biochemical analysis was performed to assess cross-linking efficiency. The mechanical properties were obtained by indentation experiments. Incubation of articular cartilage with threose clearly resulted in an increase in stiffness, but no differences in stiffness were observed between the different treatment groups. The smallest available indenter for our experiments was a spherical indenter with a radius of 1 mm. Therefore, the indentation tests were applied at a homogenized-scale [109]. The elastic response was analyzed using the Hertzian contact model, which focuses on the loading portion of the load-displacement curve; instead of the classical unloading portion, like in the Oliver-Pharr model. The Hertzian model is more suitable for soft biological tissues, according to literature [110]. The mean values of the instantaneous and equilibrium modulus calculated from all samples before incubation was 1.46 ± 0.38 MPa (n = 16) and 0.51 ± 0.20 MPa (n = 16) respectively. Since the methods and tissues in literature vary and we not have based our method completely on an existing study, it was hard to determine whether our results were in the expected range. The study with the most comparative test method found an average equilibrium modulus of 0.47 ± 0.15 MPa (n = 9) for bovine femoral cartilage, using a spherical indenter with a radius of 1.5 mm [111]. An instantaneous and equilibrium modulus of 1.79 ± 0.59 and 0.45 ± 0.26 Mpa (n=7) respectively, were measured for bovine patellae, using a flat-ended cylindrical indenter with a radius of 4 mm [112]. These results correlate with ours. Though, for future experiments, it

is advised to use a reference material (like rubber) with predefined mechanical properties, to use as a standard for this protocol. This way the method can be validated before starting the measurement.

An apparent limitation of the indentation method was the detection of the surface. This was done by manually lowering the indenter until pre-stress was observed. Because cartilage is a soft and viscoelastic material, it will relax as soon as load is applied to it; making it hard to determine the right starting position. Additionally, the samples were not fixed to the petri dish, making it hard to keep them fixed when applying pre-stress. In many other studies, the bone substrate is being glued to the petri dish before loading [12, 113–115]. This was not possible in our case, as the cartilage layer was removed from the bone and glue seemed to damage the samples in a preliminary study when directly applied.

HPLC was performed to determine the pentosidine and collagen content of the samples. No clear differences in the relative amount of pentosidine were observed between the different treatment groups. Half of the samples were cut into two pieces before HPLC preparations started, to compare the pentosidine per collagen levels between the radial and superficial zone. The average value for the radial zone of compressed samples was slightly lower than the rest, indicating that fewer cross-links have been formed in this deeper zone. The mean value of the level pentosidine per collagen molecule, measured for all samples with HPLC, was 0.12 ± 0.018 mol/mol (n = 31). Considering the differences in incubation time and sugar concentration, this result ties well with previous studies in which pieces of cartilage were incubated in threose [100, 116]. As expected, also a strong correlation was found between the collagen content and the dry weight ($r = 0.964$, $p < 0.0001$). HPLC seemed to be an accurate method for the separation and quantification of the analytes.

Since only one strain magnitude was used to investigate the effects of static compression, an additional experiment has been conducted (see Appendix G). Compression with multiple different strain magnitudes were investigated for their effect on cross-link formation. No significant differences were observed between the treatment groups with regard to pentosidine level. Therefore, we conclude that static compression does not influence non-enzymatic glycation in articular cartilage.

In the second part of this exploratory study, we have investigated the effects of dynamic mechanical compression on enzymatic glycation, leading to pentosidine cross-links. The findings reported here demonstrate that dynamic compression at the physiological magnitude and frequency of walking can lead to increased non-enzymatic cross-linking. Biomechanical and biochemical variations were observed between treatments with different frequencies. The highest stimulation of cross-linking was observed at a frequency of 1 Hz. These findings show an interesting trend, which indicates that dynamic mechanical stress *in vivo*, may regulate the accumulation of AGEs and thereby may influence cartilage aging and deterioration.

In this study, biomechanical properties of the bovine cartilage samples were determined only after the incubation period, by analyzing the tissue response during unconfined compression. The biomechanical properties (stiffness) of the samples were hypothesized to be correlated with the level of cross-links in the collagen type II network [92, 117]. To quantify the biomechanical properties, the samples were characterized by an equilibrium modulus (elastic properties) and two dynamic moduli, together with two corresponding phase shifts (viscoelastic properties). The biomechanical data together indicated that incubation with L-threose as reducing sugar results in a stiffened collagen matrix, which is consistent with a previous study [92].

The biomechanical analysis that was used in this experiment is a widely used measuring technique within the lab. It is assumed to be an accurate way of measuring the biomechanical properties of cartilage explants. Moreover, the average equilibrium modulus of immature femoral bovine cartilage, that was obtained from the samples that were incubated in PBS without any treatment, agrees with the findings of another study (0.1 MPa [118]). Yet, (despite some minor variation in used sample dimensions and methods) different values have been published too, e.g. (0.7 MPa [119]).

Our data, regarding the equilibrium modulus, illustrate that alternating the L-threose incubation with dynamic loading cycles with a frequency of 1 Hz, enhances the formation of cross-links compared to treatment with a frequency of 0.01 Hz or no compression at all. However, the negative control groups, the treatment groups that were incubated in the absence of a cross-link inducing sugar, show a similar difference. The negative control samples that were treated with 1 Hz show a much higher equilibrium modulus than the "no compression" group. This unexpected value cannot be caused by AGEs. As this group only consisted of one sample, it is hard to tell whether this high value is caused by its treatment or by an anomaly.

Furthermore, the effect of the treatment on the dynamic moduli was analyzed. The dynamic loading protocol for these measurements consisted of a sinusoidal loading at a frequency of 0.01 and 1 Hz (not to be confused with the treatment frequencies). For the dynamic moduli, a similar pattern of results was obtained as for the equilibrium modulus. Again, the results suggest that alternating the L-threose incubation with dynamic loading cycles with a frequency of 1 Hz, increases the stiffness of the tissue, supposedly by enhancing the formation of cross-links. The dynamic moduli for samples that had been treated with a 0.01 Hz compression were remarkably low.

Lastly, also the phase shift could be determined from the sinusoidal loading. The phase shift is a measure of the tissue's viscoelasticity. The values for phase shift at a low frequency (0.01 Hz) were substantially higher than those at a higher frequency (1 Hz). During low-frequency loading, the interstitial fluid can flow more freely through the cartilage matrix. This way, a relatively large amount of energy can be dissipated, resulting in highly viscoelastic behavior. As frequency increases, the flow of the interstitial fluid is more restricted. Fluid pressurization and fiber tension take over its role, resulting in a more elastic behavior [120]. When comparing the data between the treatment groups, a similar trend was recognized for treatment at the high frequency as before. The group that has been treated with dynamic loading at 1 Hz had a visibly lower phase shift compared to the other groups, indicating a higher stiffness. On the other hand, at the low frequency, we see that this trend has changed. If we relate stiffness directly to cross-links, this would indicate that in our experiment, cross- links influenced the tissue's elastic behavior, without influencing its viscoelastic behavior. This could mean that cross-links, which are relatively small molecules, have less influence on the attraction of fluid by proteoglycans and the tissue's permeability. Unfortunately, no literature could be found on this matter.

The observations regarding the biomechanical properties were partly substantiated by the results of the biochemical analysis. The absolute pentosidine levels, that were measured with the plate reader, show a similar trend and thereby confirm our previous findings to some extent. Again, samples that were treated with 1 Hz dynamic loading showed to have a higher level of pentosidine than the other treatment groups. However, only significant difference was found between treatment at 1Hz and no compression at all. The bovine explants that were used during this experiment were considered to have similar initial properties and structures,

as they were harvested from the "unloaded" patellofemoral groove of an immature calf. Nonetheless, the absolute pentosidine levels were normalized to collagen content, to exclude potential irregularities in sample dimensions or composition. After normalization with collagen content, the difference between the 0.01 Hz and 1 Hz treated groups was still visible. Though, the data of the untreated group (threose - no compression) showed a very high standard deviation.

Plotting the amounts of pentosidine per collagen molecules versus equilibrium modulus revealed an increasing trend as expected [92]. Overall, the findings of this study show a trend that is in line with previous research by Pouran et al. [100]. It has been shown that shrinkage of the ECM, as a result of an osmolarity difference, makes it more prone to glycation. Such shrinkage seems comparable with our dynamic compression. We can indirectly relate this to previous research, that revealed intrinsic strain dependency of collagen fibrils to enzymatic degradation [46–48, 50–81]. Sufficient compressive strain of the ECM has been shown to decrease the elastic pre-stress developed in the collagen network. By affecting the molecular conformation of the fibrils, this results in a higher susceptibility for enzymatic degradation [121]. We observed no increased glycation for compression at 0.01 Hz. We speculate that this might be due to the fact that the tissue does have time to recover its original shape during intermittent compression at such a low frequency, due to the viscoelastic (rate-dependent) mechanical properties of articular cartilage [122].

Although our study provided insight into the biomechanical and biochemical effects of compression during aging of articular cartilage, it had some significant limitations that should be considered. First, samples were dynamically compressed in PBS, instead of threose solution as described in Section 4.3. This was a limiting factor, as the goal of this study was to examine the direct effect of compression on the formation of cross-links. Accumulation during compression was also inhibited by the temperature, as the loading cycles were performed at room temperature. These adaptations resulted in an aging model in which the samples were incubated for roughly 64 hours. Second, the sample size was limited. The time frame of the treatment was chosen to be 96 hours in total. Treatment consisted of two loading cycles a day with 8 hours of incubation in between. Consequently, only one sample could be treated at a time. The sample size could be increased to enhance the power of the study. Nevertheless, the aim was to create an experimental setup.

We have found a trend in which dynamic mechanical compression with a frequency of 1 Hz increases the glycation efficiency in collagen fibrils. We believe that this is due to conformational changes in the collagen molecules. These findings suggest that walking could negatively influence the aging of articular cartilage. What could be the biological reason for this cell-independent mechanism? Several studies have shown that the accumulation of collagen cross-links increase resistance to collagenolytic digestion [80, 92, 123, 124]. The increased susceptibility for AGEs might be a protection mechanism of the fibrils against the increased susceptibility for enzymes. During this study, we have not investigated the potential depletion of proteoglycan. Collagen cross-linking may protect the matrix from proteoglycan loss, by creating a denser collagen mesh. However, no existing literature could be found on this matter.

Future research should include analysis of PG loss. For a follow-up study we recommend using dynamic mechanical analysis and HPLC for respectively biomechanical and biochemical analysis of the samples after treatment, because these methods

are both more accurate than their alternatives, described in this report. For the treatment, we advise designing a test set-up in which one or more samples can be compressed in threose solution for a longer period of time at 37°C. The compression chamber could be covered with parafilm to minimize the evaporation of the test liquid over the course of the experiment and a pump could be inserted to accomplish re-circulation [125]. The primary goal of a follow-up study is to increase sample size with the same frequencies. If the trend is confirmed, a similar study could be conducted on whole knee joints from cadavers with a specially designed loading and connecting device [126].

Chapter 7

Conclusion

In conclusion, our results suggest that non-enzymatic cross-linking of collagen fibrils in articular cartilage is enhanced by dynamic loading in the physiological frequency of walking, which we applied in unconfined conditions using a dynamic mechanical analyzer. We have created two different aging knee models to investigate the effect of both static and dynamic compression. We tested and compared different methods to measure the biomechanical and biochemical properties of the treated samples. Our micro-indentation data, dynamic mechanical analysis and pentosidine level measurements indicate that 1 Hertz compression accelerates advanced glycation and the "aging" of articular cartilage. On the contrary, static compression with a 5, 10 and 15% strain and dynamic compression at a frequency of 0.01 Hz showed no effect. Altogether these findings contribute to a better understanding of how external mechanical factors influence the chemical reactions of collagen fibrils on the micro-scale. They provide insight into the cell independent mechanisms that are potentially encoded in the molecular structure of collagen. Moreover, this study builds on previous work, investigating the mechanochemistry in collagen networks, that revealed strain dependency of the enzymatic degradation. A better understanding of the intrinsic properties of collagen fibrils is necessary to develop future strategies against cartilage aging and deterioration.

Bibliography

[1] Alexander P Spence and Elliott B Mason. *Human anatomy and physiology*. Benjamin-Cummings Publishing Company, 1987.

[2] Bozidar Potocnik et al. "A Patient-specific Knee Joint Computer Model Using MRI Data and 'in vivo' Compressive Load from the Optical Force Measuring System." In: July 2014 (2008). DOI: 10.2498/cit.1001126.

[3] Jawad F Abulhasan and Michael J Grey. "Anatomy and Physiology of Knee Stability". In: (2017). DOI: 10.3390/jfmk2040034.

[4] Cheng-kung Cheng. "Weight bearing influence on knee joint bony contact movements : an in vivo video-fluoroscopy study". In: February 1997 (2014).

[5] Johannah Sanchez-adams et al. "The Mechanobiology of Articular Cartilage: Bearing the Burden of Osteoarthritis". In: 16.10 (2015), pp. 1–15. DOI: 10.1007/s11926-014-0451-6.The.

[6] Gerard A Ateshian and Huiqun Wang. "A Theoretical Contact Solution for the Frictionless Rolling of Cylindrical Cartilage Layers". In: 28.Ii (1995), pp. 1341–1355.

[7] HJ Helminen et al. "Joint loading effects on articular cartilage: a historical review". In: *Joint loading: biology and health of articular structures* (1987), pp. 1–46.

[8] VC Mow and GA Ateshian. "Lubrication and wear of diarthrodial joints". In: *Basic orthopaedic biomechanics* 2 (1997), pp. 275–315.

[9] AJ Bollet and JL Nance. "Biochemical Findings in Normal and Osteoarthritic Articular Cartilage . II . Chondroitin Sulfate Concentration and Chain Length , Water , and Ash Content *". In: 45.7 (1966).

[10] RS Gilmore and AJ Palfrey. "Chondrocyte distribution in the articular cartilage of human femoral condyles". In: 4 (1988), pp. 23–31.

[11] AJ Sophia Fox, A Bedi, and SA Rodeo. "The Basic Science of Articular Cartilage: Structure, Composition, and Function". In: 1.6 (2009), pp. 461–468. DOI: 10.1177/1941738109350438.

[12] V. C. Mow et al. "Biphasic Creep and Stress Relaxation of Articular Cartilage in Compression: Theory and Experiments". In: *Journal of Biomechanical Engineering* (1980). ISSN: 01480731. DOI: 10.1115/1.3138202.

[13] Gidon Ofek and Kyriacos Athanasiou. "Micromechanical properties of chondrocytes and chondrons: relevance to articular cartilage tissue engineering". In: *Journal of Mechanics of Materials and Structures* 2.6 (2007), pp. 1059–1086.

[14] Helen Muir. "The chondrocyte, architect of cartilage. Biomechanics, structure, function and molecular biology of cartilage matrix macromolecules". In: *Bioessays* 17.12 (1995), pp. 1039–1048.

[15] Margareta Nordin and Victor Hirsch Frankel. *Basic biomechanics of the musculoskeletal system*. Lippincott Williams & Wilkins, 2001.

[16] Qin Zhang et al. “Preparation of collagen scaffolds with controlled pore structures and improved mechanical property for cartilage tissue engineering”. In: *Journal of Bioactive and Compatible Polymers* (2013). ISSN: 08839115. DOI: 10.1177/0883911513494620.

[17] Jouni Uitto, Barbara A. Booth, and Kathy L. Polak. “Collagen biosynthesis by human skin fibroblasts II. Isolation and further characterization of type I and type III procollagens synthesized in culture”. In: *Biochimica et Biophysica Acta (BBA) - Protein Structure* (2003). ISSN: 00052795. DOI: 10.1016/0005-2795(80)90095-1.

[18] Van C. Mow, Anthony Ratcliffe, and A. Robin Poole. “Cartilage and diarthrodial joints as paradigms for hierarchical materials and structures”. In: *Biomaterials* 13.2 (1992), pp. 67–97. ISSN: 01429612. DOI: 10.1016/0142-9612(92)90001-5.

[19] W. Wilson et al. “A fibril-reinforced poroviscoelastic swelling model for articular cartilage”. In: *Journal of Biomechanics* 38.6 (2005), pp. 1195–1204. ISSN: 00219290. DOI: 10.1016/j.jbiomech.2004.07.003.

[20] Silvia P. Canelón and Joseph M. Wallace. “β-Aminopropionitrile-induced reduction in enzymatic crosslinking causes in vitro changes in collagen morphology and molecular composition”. In: *PLoS ONE* (2016). ISSN: 19326203. DOI: 10.1371/journal.pone.0166392.

[21] Wayne D Comper. *Extracellular matrix*. Vol. 1. Crc Press, 1996.

[22] D. D.N. Sun and K. W. Leong. “Functional Engineering of Load-supporting Soft Tissues”. In: *Comprehensive Structural Integrity*. Vol. 9. Elsevier Ltd, July 2007, pp. 97–130. ISBN: 9780080437491. DOI: 10.1016/B0-08-043749-4/09013-3.

[23] Frederick George Donnan. “The theory of membrane equilibria.” In: *Chemical Reviews* 1.1 (1924), pp. 73–90.

[24] A Maroudas. “Balance between swelling pressure and collagen tension in normal and degenerate cartilage”. In: *Nature* 260.5554 (1976), p. 808.

[25] M. Parsons et al. “Mechanical load enhances procollagen processing in dermal fibroblasts by regulating levels of procollagen C-proteinase”. In: *Experimental Cell Research* 252.2 (1999), pp. 319–331. DOI: 10.1006/excr.1999.4618.

[26] A Maroudas et al. “Factors involved in the nutrition of the human lumbar intervertebral disc: cellularity and diffusion of glucose in vitro.” In: *Journal of anatomy* 120.Pt 1 (1975), p. 113.

[27] Jasmine Seror et al. “Normal and shear interactions between hyaluronan–aggrecan complexes mimicking possible boundary lubricants in articular cartilage in synovial joints”. In: *Biomacromolecules* 13.11 (2012), pp. 3823–3832.

[28] Joseph A. Buckwalter, Peter J. Roughley, and Lawrence C. Rosenberg. “Age-Related changes in cartilage proteoglycans: Quantitative electron microscopic studies”. In: *Microscopy Research and Technique* 28.5 (1994), pp. 398–408. ISSN: 10970029. DOI: 10.1002/jemt.1070280506.

[29] R. Shirazi and A. Shirazi-Adl. “Deep vertical collagen fibrils play a significant role in mechanics of articular cartilage”. In: *Journal of Orthopaedic Research* 26.5 (2008), pp. 608–615. ISSN: 07360266. DOI: 10.1002/jor.20537.

[30] Van C Mow, W Michael Lai, and Irving Redler. "Some surface characteristics of articular cartilage—I. A scanning electron microscopy study and a theoretical model for the dynamic interaction of synovial fluid and articular cartilage". In: *Journal of Biomechanics* 7.5 (1974), pp. 449–456.

[31] Jessica C Mansfield et al. "Collagen reorganization in cartilage under strain probed by polarization sensitive second harmonic generation microscopy". In: *Journal of the Royal Society Interface* 16.150 (2019), p. 20180611.

[32] Irving Redler and Marilyn L Zimny. "Scanning electron microscopy of normal and abnormal articular cartilage and synovium". In: *JBJS* 52.7 (1970), pp. 1395–1404.

[33] Joseph Borrelli Jr et al. "Cartilage tolerates single impact loads of as much as half the joint fracture threshold". In: *Clinical Orthopaedics and Related Research®* 426 (2004), pp. 266–273.

[34] Sven Knecht, Benedicte Vanwanseele, and Edgar Stüssi. "A review on the mechanical quality of articular cartilage–implications for the diagnosis of osteoarthritis". In: *Clinical biomechanics* 21.10 (2006), pp. 999–1012.

[35] Evelyne M Hasler et al. "Articular cartilage biomechanics: theoretical models, material properties, and biosynthetic response." In: *Critical reviews in biomedical engineering* 27.6 (1999), pp. 415–488.

[36] Nathaniel P Cohen, Robert J Foster, and Van C Mow. "Composition and dynamics of articular cartilage: structure, function, and maintaining healthy state". In: *Journal of Orthopaedic & Sports Physical Therapy* 28.4 (1998), pp. 203–215.

[37] S Park, CT Hung, and GA Ateshian. "Mechanical response of bovine articular cartilage under dynamic unconfined compression loading at physiological stress levels". In: *Osteoarthritis and cartilage* 12.1 (2004), pp. 65–73.

[38] WC Hayes et al. "A mathematical analysis for indentation tests of articular cartilage". In: *Journal of biomechanics* 5.5 (1972), pp. 541–551.

[39] Michael A Soltz and Gerard A Ateshian. "Interstitial fluid pressurization during confined compression cyclical loading of articular cartilage". In: *Annals of biomedical engineering* 28.2 (2000), pp. 150–159.

[40] DavidáW L Hukins, JohannaáC Leahy, and KatharineáJ Mathias. "Biomaterials: defining the mechanical properties of natural tissues and selection of replacement materials". In: *Journal of Materials Chemistry* 9.3 (1999), pp. 629–636.

[41] S Ronken et al. "A comparison of healthy human and swine articular cartilage dynamic indentation mechanics". In: *Biomechanics and modeling in mechanobiology* 11.5 (2012), pp. 631–639.

[42] R. L. Trelstad, D. E. Birk, and F. H. Silver. "Collagen fibrillogenesis in tissues, in solution and from modeling: A synthesis". In: *Journal of Investigative Dermatology* 79.Suppl. 1 (1982), pp. 109–112. ISSN: 0022202X. DOI: 10.1038/jid.1982.21.

[43] G.J. Laurent. "Dynamic state of collagen : pathways of collagen degradation in vivo and their possible role in regulation of collagen mass". In: *Cell Physiology* 252.1 (1987), pp. C1–C9. ISSN: 0002-9513. DOI: 10.1152/ajpcell.1987.252.1.C1.

[44] M. Eastwood, D. A. McGrouther, and R. A. Brown. "Fibroblast responses to mechanical forces". In: *Proceedings of the Institution of Mechanical Engineers, Part H: Journal of Engineering in Medicine* 212.2 (1998), pp. 85–92. ISSN: 09544119. DOI: 10.1243/0954411981533854.

[45] E.D. Hay. *Cell Biology of Extracellular Matrix*. Second edi. Boston: Plenum Press, 1991, p. 468. ISBN: ISBN 978-1-4615-3770-0. DOI: 10.1007/978-1-4615-3770-0.

[46] Jeffrey W. J.W. Ruberti and Nadim J. N.J. Hallab. "Strain-controlled enzymatic cleavage of collagen in loaded matrix". In: *Biochemical and Biophysical Research Communications* 336.2 (2005), pp. 483–489. ISSN: 0006291X. DOI: 10.1016/j.bbrc.2005.08.128.

[47] C. Huang and I.V. Yannas. "Mechanochemical studies of enzymatic degradation of insoluble collagen fibers". In: *Journal of Biomedical Materials Research* 11.1 (1977), pp. 137–154. DOI: 10.1002/jbm.820110113.

[48] Y. Nabeshima et al. "Uniaxial tension inhibits tendon collagen degradation by collagenase in vitro". In: *Journal of Orthopaedic Research* 14.1 (1996), pp. 123–130. DOI: 10.1002/jor.1100140120.

[49] Jaap Lagrand. "The Effect of Mechanical Strain on the Cell Independent Mechanisms in Collagen Structures: A Literature Review". In: (2019).

[50] J.C. Jeffrey C. Lotz et al. "Anulus fibrosus tension inhibits degenerative structural changes in lamellar collagen". In: *European Spine Journal* 17.9 (2008), pp. 1149–1159. ISSN: 09406719. DOI: 10.1007/s00586-008-0721-y.

[51] A.P. P. Amit P. Bhole et al. "Mechanical strain enhances survivability of collagen micronetworks in the presence of collagenase: implications for load-bearing matrix growth and stability". In: *Philosophical Transactions of the Royal Society A: Mathematical, Physical and Engineering Sciences* 367.1902 (2009), pp. 3339–3362. ISSN: 1364503X. DOI: 10.1098/rsta.2009.0093. URL: http://rsta.royalsocietypublishing.org/cgi/doi/10.1098/rsta.2009.0093.

[52] K.E.-K. Wyatt, J.W. Bourne, and P.A. Torzilli. "Deformation-dependent enzyme mechanokinetic cleavage of type I collagen". In: *Journal of Biomechanical Engineering* 131.5 (2009). DOI: 10.1115/1.3078177.

[53] Brendan P. B.P. Flynn et al. "Mechanical strain stabilizes reconstituted collagen fibrils against enzymatic degradation by mammalian collagenase matrix metalloproteinase 8 (MMP-8)". In: *PLoS ONE* 5.8 (2010), pp. 21–23. ISSN: 19326203. DOI: 10.1371/journal.pone.0012337.

[54] Ramin Zareian et al. "Probing collagen/enzyme mechanochemistry in native tissue with dynamic, enzyme-induced creep". In: *Langmuir* 26.12 (2010), pp. 9917–9926. ISSN: 07437463. DOI: 10.1021/la100384e.

[55] R.J. Robert J. Camp et al. "Molecular mechanochemistry: Low force switch slows enzymatic cleavage of human type I collagen monomer". In: *Journal of the American Chemical Society* 133.11 (2011), pp. 4073–4078. ISSN: 00027863. DOI: 10.1021/ja110098b.

[56] Michael C. Robitaille et al. "Small-angle light scattering to detect strain-directed collagen degradation in native tissue". In: *Interface Focus* 1.5 (2011), pp. 767–776. ISSN: 20428901. DOI: 10.1098/rsfs.2011.0039.

[57] Brendan P. B.P. Flynn, Graham E. G.E. Tilburey, and Jeffrey W. J.W. Ruberti. "Highly sensitive single-fibril erosion assay demonstrates mechanochemical switch in native collagen fibrils". In: *Biomechanics and Modeling in Mechanobiology* 12.2 (2013), pp. 291–300. ISSN: 16177959. DOI: 10.1007/s10237-012-0399-2.

[58] S. Ghazanfari et al. "Modulation of collagen fiber orientation by strain-controlled enzymatic degradation". In: *Acta Biomaterialia* 35 (2016), pp. 118–126. ISSN: 18787568. DOI: 10.1016/j.actbio.2016.02.033.

[59] Eunice Yi et al. "Mechanical forces accelerate collagen digestion by bacterial collagenase in lung tissue strips". In: *Frontiers in Physiology* 7.JUL (2016). ISSN: 1664042X. DOI: 10.3389/fphys.2016.00287.

[60] R.T. Gaul et al. "Strain mediated enzymatic degradation of arterial tissue: Insights into the role of the non-collagenous tissue matrix and collagen crimp". In: *Acta Biomaterialia* 77 (2018), pp. 301–310. DOI: 10.1016/j.actbio.2018.06.037.

[61] R.T. T. Gaul, D.R. R. Nolan, and C. Lally. "The use of small angle light scattering in assessing strain induced collagen degradation in arterial tissue ex vivo". In: *Journal of Biomechanics* 81 (2018), pp. 155–160. ISSN: 18732380. DOI: 10.1016/j.jbiomech.2018.10.006.

[62] A.S. Arjun S. Adhikari, Jack Chai, and A.R. Alexander R. Dunn. "Mechanical load induces a 100-fold increase in the rate of collagen proteolysis by MMP-1". In: *Journal of the American Chemical Society* 133.6 (2011), pp. 1686–1689. ISSN: 00027863. DOI: 10.1021/ja109972p.

[63] A.S. Arjun S. Adhikari, Emerson Glassey, and A.R. Alexander R. Dunn. "Conformational dynamics accompanying the proteolytic degradation of trimeric collagen I by collagenases". In: *Journal of the American Chemical Society* 134.32 (2012), pp. 13259–13265. ISSN: 00027863. DOI: 10.1021/ja212170b.

[64] James C. Ellsmere, Rajesh A. Khanna, and J. Michael Lee. "Mechanical loading of bovine pericardium accelerates enzymatic degradation". In: *Biomaterials* (1999). ISSN: 01429612. DOI: 10.1016/S0142-9612(99)00013-7.

[65] Siyao Huang and H.-Y.S. Hsiao Ying Shadow Huang. "Biaxial stress relaxation of semilunar heart valve leaflets during simulated collagen catabolism: Effects of collagenase concentration and equibiaxial strain state". In: *Proceedings of the Institution of Mechanical Engineers, Part H: Journal of Engineering in Medicine* 229.10 (2015), pp. 721–731. ISSN: 20413033. DOI: 10.1177/0954411915604336.

[66] Jonathan W. J.W. Bourne and Peter A. P.A. Torzilli. "Molecular simulations predict novel collagen conformations during cross-link loading". In: *Matrix Biology* 30.5-6 (2011), pp. 356–360. ISSN: 0945053X. DOI: 10.1016/j.matbio.2011.03.010.

[67] M.F. F. Hadi et al. "Simulated remodeling of loaded collagen networks via strain-dependent enzymatic degradation and constant-rate fiber growth". In: *Mechanics of Materials* 44 (2012), pp. 72–82. ISSN: 01676636. DOI: 10.1016/j.mechmat.2011.07.003.

[68] William J. W.J. Richardson et al. "Potential strain-dependent mechanisms defining matrix alignment in healing tendons". In: *Biomechanics and Modeling in Mechanobiology* 17.6 (2018), pp. 1569–1580. ISSN: 16177940. DOI: 10.1007/s10237-018-1044-5.

[69] Krishnakumar M Ravikumar, Jay D Humphrey, and Wonmuk Hwang. *Mechanics of Materials and Structures spontaneous unwinding of a labile domain in a collagen triple helix*. Tech. rep. 6. 2007.

[70] Krishnakumar M. K.M. Ravikumar and Wonmuk Hwang. "Region-specific role of water in collagen unwinding and assembly". In: *Proteins: Structure, Function and Genetics* 72.4 (2008), pp. 1320–1332. ISSN: 08873585. DOI: 10.1002/prot.22026.

[71] Xiaojing Teng and Wonmuk Hwang. "Chain registry and load-dependent conformational dynamics of collagen". In: *Biomacromolecules* 15.8 (2014), pp. 3019–3029. ISSN: 15264602. DOI: 10.1021/bm500641f.

[72] Thomas L. T.L. Willett, Rosalind S. Labow, and J.M. Michael Lee. "Mechanical overload decreases the thermal stability of collagen in an in vitro tensile overload tendon model". In: *Journal of Orthopaedic Research* 26.12 (2008), pp. 1605–1610. ISSN: 07360266. DOI: 10.1002/jor.20672.

[73] S.-W. Shu Wei Chang and M.J. Markus J. Buehler. *Molecular biomechanics of collagen molecules*. 2014. DOI: 10.1016/j.mattod.2014.01.019.

[74] Peter A. P.A. Torzilli et al. *A new paradigm for mechanobiological mechanisms in tumor metastasis*. 2012. DOI: 10.1016/j.semcancer.2012.05.002.

[75] Andrew Dittmore et al. "Internal strain drives spontaneous periodic buckling in collagen and regulates remodeling". In: 113.30 (2016), pp. 8436–8441. ISSN: 0027-8424. DOI: 10.1073/pnas.1523228113.

[76] Frank Baaijens, Carlijn Bouten, and Niels Driessen. "Modeling collagen remodeling". In: *Journal of Biomechanics* 43.1 (2010), pp. 166–175. ISSN: 00219290. DOI: 10.1016/j.jbiomech.2009.09.022.

[77] N.J.B. Niels J. B. Driessen et al. "Improved Prediction of the Collagen Fiber Architecture in the Aortic Heart Valve". In: *Journal of Biomechanical Engineering* 127.2 (2005), pp. 329–336. ISSN: 01480731. DOI: 10.1115/1.1865187.

[78] Monica E. M.E. Susilo et al. "Collagen network strengthening following cyclic tensile loading". In: *Interface Focus* 6.1 (2016). ISSN: 20428901. DOI: 10.1098/rsfs.2015.0088.

[79] Michelle L. M.L. Chen, Jeffrey W. J.W. Ruberti, and Thao D. T.D. Nguyen. "Increased stiffness of collagen fibrils following cyclic tensile loading". In: *Journal of the Mechanical Behavior of Biomedical Materials* 82.January (2018), pp. 345–354. ISSN: 18780180. DOI: 10.1016/j.jmbbm.2018.03.027.

[80] Samaneh Ghazanfari, Ali Khademhosseini, and T.H. Theodoor H. Smit. *Mechanisms of lamellar collagen formation in connective tissues*. 2016. DOI: 10.1016/j.biomaterials.2016.04.028.

[81] Nima Saeidi et al. "Molecular crowding of collagen: A pathway to produce highly-organized collagenous structures". In: *Biomaterials* 33.30 (2012), pp. 7366–7374. ISSN: 01429612. DOI: 10.1016/j.biomaterials.2012.06.041.

[82] Sharanya Reddy et al. "N. epsilon.-(Carboxymethyl) lysine is a dominant advanced glycation end product (AGE) antigen in tissue proteins". In: *Biochemistry* 34.34 (1995), pp. 10872–10878.

[83] Martin Lotz and Richard F Loeser. "Effects of aging on articular cartilage homeostasis". In: *Bone* 51.2 (2012), pp. 241–248.

[84] Sho-ichi Yamagishi. "Role of advanced glycation end products (AGEs) and receptor for AGEs (RAGE) in vascular damage in diabetes". In: *Experimental gerontology* 46.4 (2011), pp. 217–224.

[85] Nicole Verzijl et al. "AGEing and osteoarthritis: a different perspective". In: *Current opinion in rheumatology* 15.5 (2003), pp. 616–622.

[86] Jeroen DeGroot et al. "Accumulation of advanced glycation end products as a molecular mechanism for aging as a risk factor in osteoarthritis". In: *Arthritis & Rheumatism: Official Journal of the American College of Rheumatology* 50.4 (2004), pp. 1207–1215.

[87] Alfonso Gautieri et al. "Advanced glycation end-products: Mechanics of aged collagen from molecule to tissue". In: *Matrix Biology* 59 (2017), pp. 95–108. ISSN: 15691802. DOI: 10.1016/j.matbio.2016.09.001. URL: http://dx.doi.org/10.1016/j.matbio.2016.09.001.

[88] Karen M Reiser. "Nonenzymatic glycation of collagen in aging and diabetes". In: *Proceedings of the Society for Experimental Biology and Medicine* 196.1 (1991), pp. 17–29.

[89] John W Baynes and Suzanne R Thorpe. "Role of oxidative stress in diabetic complications: a new perspective on an old paradigm." In: *Diabetes* 48.1 (1999), pp. 1–9.

[90] Nicole Verzijl et al. "Age-related accumulation of Maillard reaction products in human articular cartilage collagen". In: *Biochemical Journal* 350.2 (2000), pp. 381–387.

[91] Nicole Verzijl et al. "Effect of collagen turnover on the accumulation of advanced glycation end products". In: *Journal of Biological Chemistry* 275.50 (2000), pp. 39027–39031.

[92] Nicole Verzijl et al. "Crosslinking by advanced glycation end products increases the stiffness of the collagen network in human articular cartilage: a possible mechanism through which age is a risk factor for osteoarthritis". In: *Arthritis & Rheumatism* 46.1 (2002), pp. 114–123.

[93] Jeroen DeGroot et al. "Age-related decrease in proteoglycan synthesis of human articular chondrocytes: the role of nonenzymatic glycation". In: *Arthritis & Rheumatism: Official Journal of the American College of Rheumatology* 42.5 (1999), pp. 1003–1009.

[94] Jeroen DeGroot et al. "Age-related decrease in susceptibility of human articular cartilage to matrix metalloproteinase–mediated degradation: The role of advanced glycation end products". In: *Arthritis & Rheumatism* 44.11 (2001), pp. 2562–2571.

[95] Albert C Chen et al. "Induction of advanced glycation end products and alterations of the tensile properties of articular cartilage". In: *Arthritis & Rheumatism* 46.12 (2002), pp. 3212–3217.

[96] Deborah M Saudek and Jonathan Kay. "Advanced glycation endproducts and osteoarthritis". In: *Current rheumatology reports* 5.1 (2003), pp. 33–40.

[97] David R Sell and Vincent M Monnier. "End-stage renal disease and diabetes catalyze the formation of a pentose-derived crosslink from aging human collagen." In: *The Journal of clinical investigation* 85.2 (1990), pp. 380–384.

[98] Michael T BAYLISS et al. "Ageing and zonal variation in post-translational modification of collagen in normal human articular cartilage: the age-related increase in non-enzymatic glycation affects biomechanical properties of cartilage". In: *Biochemical Journal* 330.1 (1998), pp. 345–351.

[99] Vincent M Monnier. "Nonenzymatic glycosylation, the Maillard reaction and the aging process". In: *Journal of Gerontology* 45.4 (1990), B105–B111.

[100] Behdad Pouran et al. "Non-enzymatic cross-linking of collagen type II fibrils is tuned via osmolality switch". In: *Journal of Orthopaedic Research* 36.7 (2018), pp. 1–8. ISSN: 1554527X. DOI: 10.1002/jor.23857.

[101] SD Poisson. "Traite de Mecanique, I, II". In: *Paris: Courcier Pub* (1811).

[102] Vincent M Monnier, Robert R Kohn, and Anthony Cerami. "Accelerated age-related browning of human collagen in diabetes mellitus". In: *Proceedings of the National Academy of Sciences* 81.2 (1984), pp. 583–587.

[103] J Jurvelin et al. "Indentation stiffness of young canine knee articular cartilage—influence of strenuous joint loading". In: *Journal of biomechanics* 23.12 (1990), pp. 1239–1246.

[104] P Kiviranta et al. "Indentation diagnostics of cartilage degeneration". In: *Osteoarthritis and Cartilage* 16.7 (2008), pp. 796–804.

[105] Petro Julkunen et al. "Comparison of single-phase isotropic elastic and fibril-reinforced poroelastic models for indentation of rabbit articular cartilage". In: *Journal of biomechanics* 42.5 (2009), pp. 652–656.

[106] Ruud A Bank et al. "Amino acid analysis by reverse-phase high-performance liquid chromatography: improved derivatization and detection conditions with 9-fluorenylmethyl chloroformate". In: *Analytical biochemistry analytical biochemistry* 240.2 (1996), pp. 167–176.

[107] Hamid Sadeghi, DET Shepherd, and DM Espino. "Effect of the variation of loading frequency on surface failure of bovine articular cartilage". In: *Osteoarthritis and cartilage* 23.12 (2015), pp. 2252–2258.

[108] John J Costi et al. "Frequency-dependent behavior of the intervertebral disc in response to each of six degree of freedom dynamic loading: solid phase and fluid phase contributions". In: *Spine* 33.16 (2008), p. 1731.

[109] P Rahnamay Moshtagh. "Mechanobiology of articular cartilage: Consequences of physical activity and advanced glycation". PhD thesis. Utrecht University, 2017.

[110] Optics11 B.V. "White paper: Measuring micro-mechanical properties of (bio)materials by nano-indentation". In: (2017).

[111] RK Korhonen et al. "Comparison of the equilibrium response of articular cartilage in unconfined compression, confined compression and indentation". In: *Journal of biomechanics* 35.7 (2002), pp. 903–909.

[112] Hui Jin and Jack L Lewis. "Determination of Poisson's ratio of articular cartilage in indentation test using different sized indenters". In: *Bioengineering Conference, June*. 2003, pp. 25–29.

[113] S.R. Moore et al. "Translating periosteum's regenerative power: Insights from quantitative analysis of tissue genesis with a periosteum substitute implant". In: *Stem Cells Translational Medicine* 5.12 (2016), pp. 1739–1749. DOI: 10.5966/sctm.2016-0004.

[114] CG Armstrong and VC Mow. "Variations in the intrinsic mechanical properties of human articular cartilage with age, degeneration, and water content." In: *The Journal of bone and joint surgery. American volume* 64.1 (1982), pp. 88–94.

[115] DH Hoch et al. "Early changes in material properties of rabbit articular cartilage after meniscectomy". In: *Journal of Orthopaedic Research* 1.1 (1983), pp. 4–12.

[116] Jussi Kinnunen et al. "Nondestructive fluorescence-based quantification of threose-induced collagen cross-linking in bovine articular cartilage". In: *Journal of biomedical optics* 17.9 (2012), p. 097003.

[117] Fereshteh Mirahmadi et al. "Mechanical stiffness of TMJ condylar cartilage increases after artificial aging by ribose". In: *Archives of oral biology* 87 (2018), pp. 102–109.

[118] Liming Bian et al. "Influence of chondroitin sulfate on the biochemical, mechanical and frictional properties of cartilage explants in long-term culture". In: *Journal of biomechanics* 42.3 (2009), pp. 286–290.

[119] Seonghun Park and Gerard A Ateshian. "Dynamic response of immature bovine articular cartilage in tension and compression, and nonlinear viscoelastic modeling of the tensile response". In: *Journal of biomechanical engineering* 128.4 (2006), pp. 623–630.

[120] Bernard M Lawless et al. "Viscoelasticity of articular cartilage: analysing the effect of induced stress and the restraint of bone in a dynamic environment". In: *Journal of the mechanical behavior of biomedical materials* 75 (2017), pp. 293–301.

[121] P.J. Basser et al. "Mechanical properties of the collagen network in human articular cartilage as measured by osmotic stress technique". In: *Archives of Biochemistry and Biophysics* 351.2 (1998), pp. 207–219. DOI: 10.1006/abbi.1997.0507.

[122] Beverley Fermor et al. "The effects of static and intermittent compression on nitric oxide production in articular cartilage explants". In: *Journal of Orthopaedic Research* 19.4 (2001), pp. 729–737.

[123] J. DeGroot et al. "Accumulation of advanced glycation endproducts reduces chondrocyte-mediated extracellular matrix turnover in human articular cartilage". In: *Osteoarthritis and Cartilage* 9.8 (2001), pp. 720–726. ISSN: 10634584. DOI: 10.1053/joca.2001.0469.

[124] David C Paik et al. "Nitrite-induced cross-linking alters remodeling and mechanical properties of collagenous engineered tissues". In: *Connective tissue research* 47.3 (2006), pp. 163–176.

[125] Whitney Terese Young. "Cartilage stress relaxation induced by intra-tissue transport of cationic nanoparticles: implications for post-traumatic osteoarthritis drug delivery". PhD thesis. Massachusetts Institute of Technology, 2016.

[126] Jianping Wang et al. "Modelling and analysis on biomechanical dynamic characteristics of knee flexion movement under squatting". In: *The Scientific World Journal* 2014 (2014).

[127] Rishabha Malviya et al. "High performance liquid chromatography: a short review". In: *Journal of global pharma technology* 2.5 (2010), pp. 22–26.

Appendix A

Bioreactor Design

This section presents the technical drawings of the bioreactor components. These drawings were generated using SOLIDWORKS (EDUCATION EDITION 2017-2018). The scales have been adjusted to fit on the page (scale = 0.75).

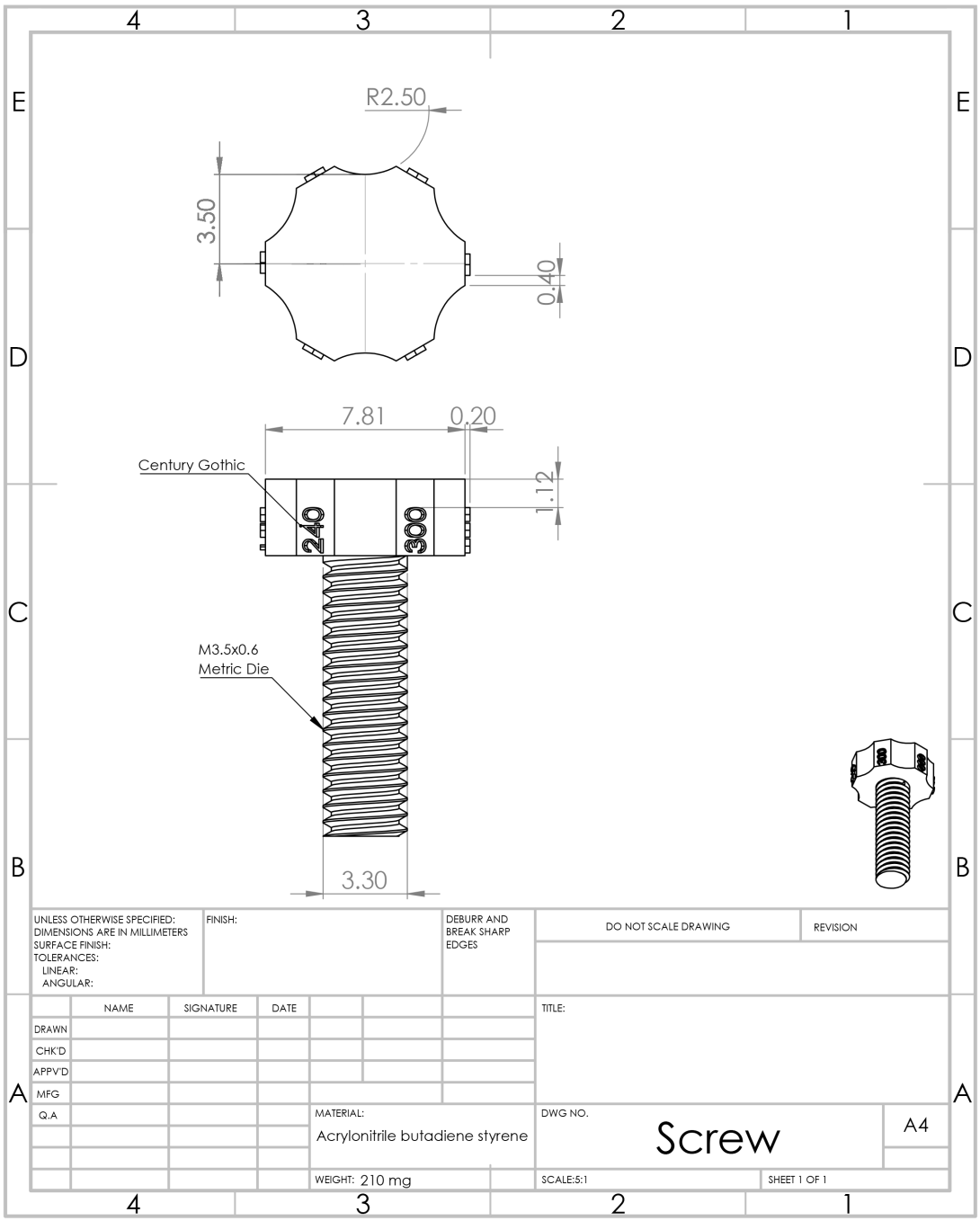

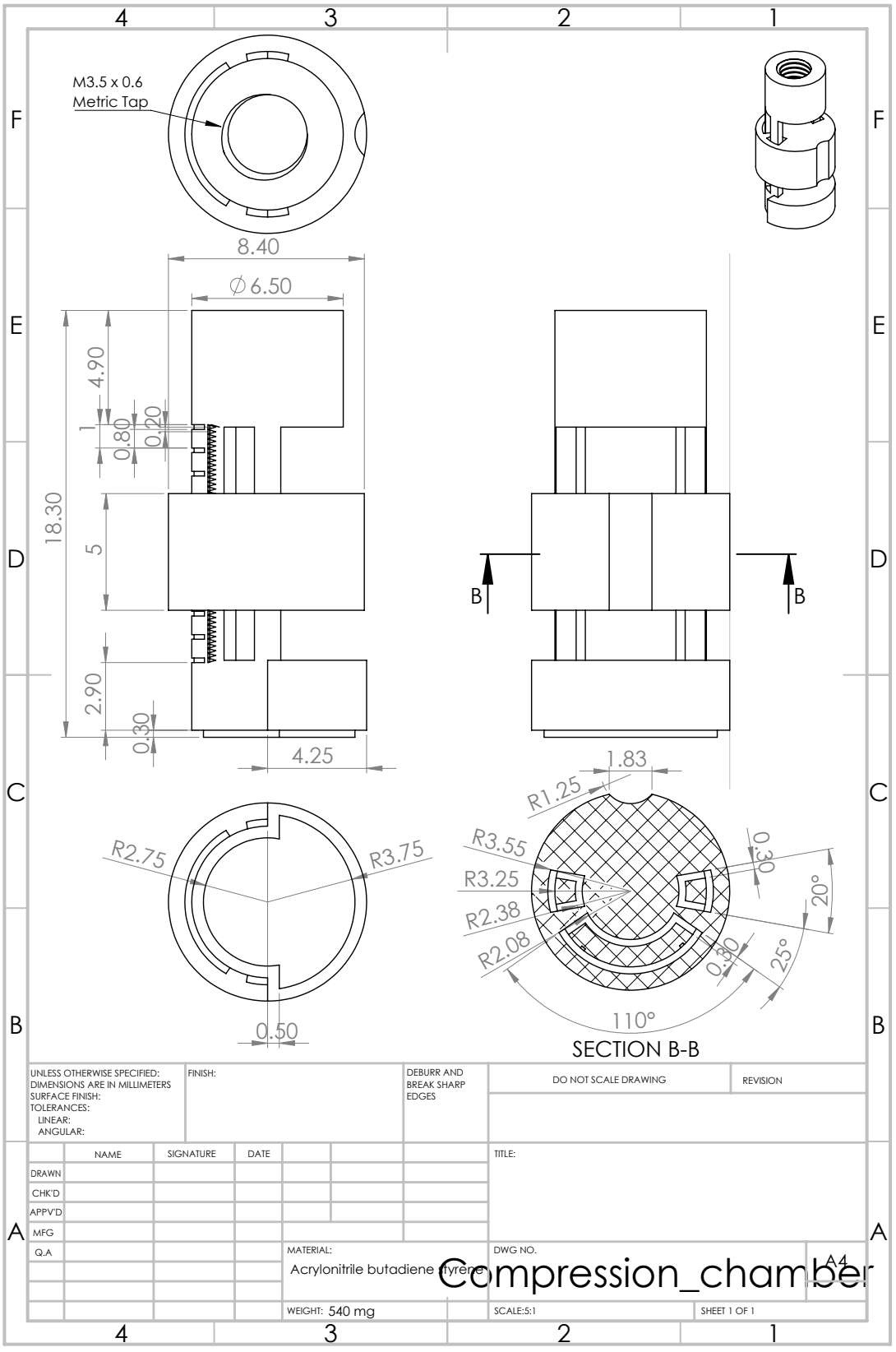
M3.5 x 0.6
Metric Tap
8.40
∅6.50
4.90
1
0.80
0.20
18.30
5
2.90
0.30
4.25
B
B
1.83
R1.25
R3.55
R3.25
R2.38
R2.08
0.30
20°
0.80
25°
110°
R2.75
R3.75
0.50
SECTION B-B
UNLESS OTHERWISE SPECIFIED:
DIMENSIONS ARE IN MILLIMETERS
SURFACE FINISH:
TOLERANCES:
LINEAR:
ANGULAR:
FINISH:
DEBURR AND BREAK SHARP EDGES
DO NOT SCALE DRAWING
REVISION
NAME
SIGNATURE
DATE
DRAWN
CHK'D
APPV'D
MFG
Q.A
TITLE:
MATERIAL:
Acrylonitrile butadiene styrene
DWG NO.
Compression_chamber
A4
WEIGHT: 540 mg
SCALE:5:1
SHEET 1 OF 1

Appendix B

Explanation HPLC

This section presents a full description of the liquid chromatography technique, used in section 2.6.

High Performance Liquid Chromatography (HPLC) is a form of column chromatography, generally used in biochemistry to separate, identify and quantify sample compounds. HPLC typically utilizes a pump that moves one or more liquid mobile phases (eluents) through a column that holds packing material, known as the stationary phase. A detector at the end of the cycle shows the retention time of the different molecules. The retention time depends on the interaction between the stationary phase, the analyte and the mobile phase(s). The sample with analyte is introduced in a small volume to the stream of the mobile phase and is retarded by specific chemical or physical interactions with the stationary phase.

Analytes within the sample are separated based on their specific affinity for the stationary and mobile phase(s), often due to different polarities for example. Therefore, analytes that have a relatively high interaction with the mobile phase and low interaction with the stationary phase, will move faster through the column. Molecules of the same compound will generally move in groups, seperating the compounds into distinct bands within the column. The components of a basic HPLC system are shown in the diagram in Figure B.1.

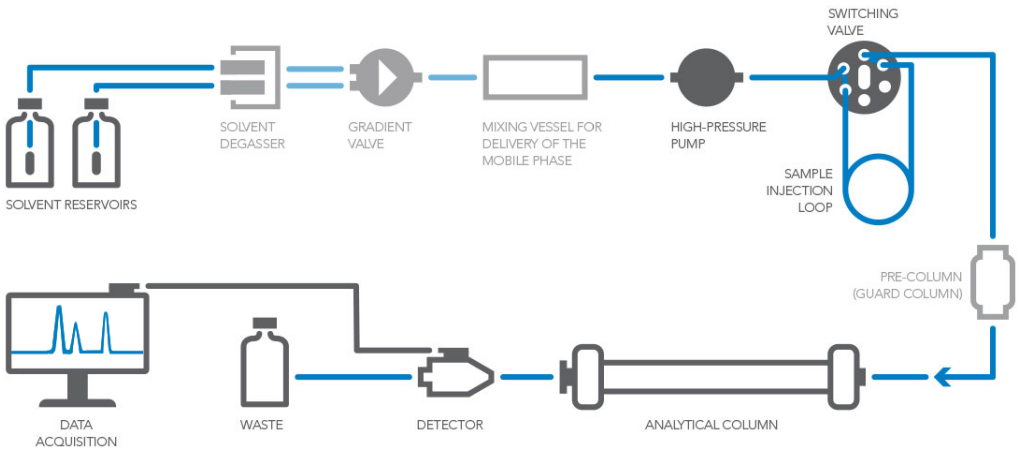

FIGURE B.1: Schematic set-up of an HPLC system with components
[*courtesy: https://www.idex-hs.com/ literature-tools/ educational-materials /hplc-center/*]

Reversed phase HPLC (RPC) is characterized by a non-polar stationary phase and an aqueous, polar mobile phase. The underlying principle common to RPC is that it operates through hydrophobic interactions, as a result from the repulsive forces between a polar eluent, moderatly non-polar analyte and non-polar stationary phase. The hydrophobic molecules in the mobile phase tend to adsorb to the hydrophobic stationary phase, while the hydrophilic molecules in the mobile phase pass through the column and are eluted first [127].

The chemical separation that occurs, is visualized in a chromatogram. A chromatogram shows a time axis with a series of peaks rising from the baseline. Each peak represents the detector's response to a certain compound. The area under the peak curve is considered as a measure of component concentration. All detectors for HPLC respond to some physico-chemical property of the analyte. Two popular ones are UV absorbance and fluorescence. These detectors often contain flow cells, that function as detecting components (Figure B.2). The resulting chromatogram is a plot of the absorbance or fluorescence signal as a function of elution time. A fluorescence detector provides additional selectivity because only a few of a sample's components are fluorescent.

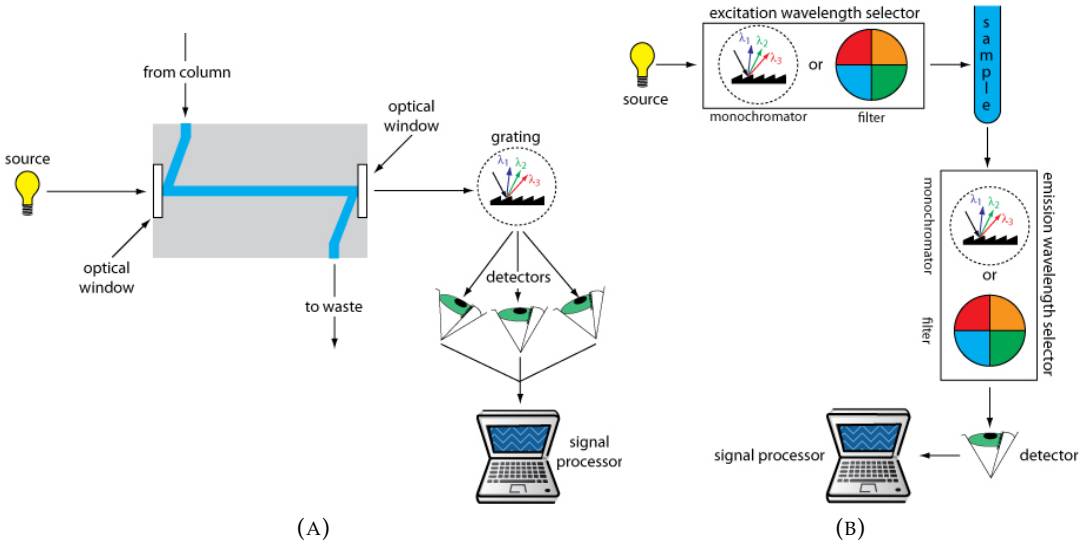

FIGURE B.2: HPLC detectors - basic instruments for measuring A) absorbance & B) fluorescence [*courtesy: https:// community.asdlib.org /imageandvideoexchangeforum/2013 /08/02/absorbance - and-fluorescence-detection -for-hplc-separations/*]

Appendix C

HPLC protocol

This section presents the protocol that has been used for the HPLC measurements. It includes the preparation of samples and standards, as well as the apparatuses and settings.

Preparation for amino acid and cross-link analysis

Reagents

- Acetonitrile, HPLC (Biosolve 012007)
- Acetone (Merck 100014)
- Heptafluorobutyric acid (HFBA) 99% GC (Sigma 77429)
- Pyridoxine hydrochloride ≥ 98%, HPLC (Sigma P9755)
- Pentosidine (Cayman Chemical ; 10010254-1; MW 378,4)
- L-homoarginine (Sigma H1007)

Preparation of Internal Standard (IS)

A1. A Stock solution pyridoxine (10 mM): Dissolve 0.2056 gram pyridoxine monohydrochloride in exactly 100 ml Milli-Q water. Store at -20˚C in 15 mL tubes. Vortex rigorously for use.

A2. Internal standard solution (10 µM pyridoxine 2,4 mM homoarginine): Dilute 200 µl stock solution pyridoxine to exactly 200 ml with Milli-Q water; dissolve in this solution 0.1078 g homoarginine. The concentration of pyridoxine is 10 µM and the concentration homoarginine is 2,40 mM. Store at -20˚C (for 1 year) in 15 mL tubes or at 4 ˚C for a month. Vortex rigorously for use.

Preparation of External Standards (ES)

B1. 1% (v/v) HFBA in 10% (v/v) acetonitrile: 89 ml Milli-Q water + 1 ml heptaflurobutyric acid + 10 ml acetonitrile. Store at room temperature; prepare freshly every 2-3 weeks.

B2. 26,4 µM Pentosidine solution: Dissolve 1 mg of pentosidine in 1 mL and subsequently add to another 99 mL of Milli-Q water. Store at -20^{0}C in 15 mL tubes.

B3. 50 nM Pentosidine in 1% (v/v) HFBA in 10% (v/v) acetonitrile: Mix 200 mL 1% (v/v) HFBA in 10% (v/v) acetonitrile with 378 µL 26,4 µM Pentosidine solution. Store at -20^0 in 15 mL tubes.

B4. 2 mM Pyridoxine solution: Dilute 20 mL of 10 mM pyridoxine stock with 80 mL Milli-Q water to make a 2 mM Pyridoxine solution. Store at -20˚C in 50 mL tubes.

B5. 50 nM Pentosidine 2 µM Pyridoxine in 1% (v/v) HFBA in 10% (v/v) acetonitrile: Mix 200 mL 50 nM Pentosidine in 1% (v/v) HFBA in 10% (v/v) acetonitrile with 200 µL 2 mM pyridoxine solution.

B6. 2 µM Pyridoxine in 1% (v/v) HFBA in 10% (v/v) acetonitrile: Mix 200 mL 1% (v/v) HFBA in 10% (v/v) acetonitrile with 200 µL 2 mM pyridoxine solution.

B7. Pentosidine standards 2 mM Pyridoxine in 0,1 M boric acid buffer pH 8,0: Mix *Reagent B5.* and *B6.* as indicated to make hydroxyproline standards with the right concentrations. Store at -20˚C in 15 mL tubes.

	50nM Pent. 2mM Pyr.	*25nM Pent. 2mM Pyr.*	*10nM Pent. 2mM Pyr.*	*5nM Pent. 2mM Pyr.*	*2,5nM Pent. 2mM Pyr.*	*0nM Pent. 2mM Pyr.*
B5.	15 mL	7,5 mL	3 mL	1,5 mL	0,75 mL	0 mL
B6.	0 mL	7,5 mL	12 mL	13,5 mL	14,25 mL	15 mL

Preparation of samples

C1. Dilute 100 µl supernatant with 400 µl 0.5% (v/v) HFBA in 10% (v/v) acetonitrile. By doing so, the supernatant is diluted with a factor 5. Bring 150 µl in an HPLC insert; inject 100 µl on the reversed-phase HPLC column for crosslink analysis with the protocol as described below.

HPLC analysis of cross-links

Apparatus:

- Waters 2795 Separation Module
- Column: TosoHaas TSKgel ODS-80-TM, 4.6 mm ID x 15 cm
- Waters 2475 HPLC Multi Fluorescence detector (excitation 254 nm, emission 630 nm)
- Waters Empower 3 Chromatography Data software programme for data analysis

Machine settings:

- Analysis time: 0:50:00
- Injection volume: 150 µl
- Column temperature: 30°C
- Sample environment temperature: 20°C.
- Initial system pressure before sample injection (150µl) was 1790 psi with a steady pressure ripple between 15-20 psi.
- Flow rate of 1 ml/min.
- The injection needle was washed after every injection with 10% methanol.
- After measurements, the column is washed and stored in 100% acetonitrile.

Chromatographic gradient conditions for HPLC analysis of cross-links

Time (min)	% eluent A	% eluent B	% eluent C	remarks
0	100	0	0	elution of HP and LP
17	0	100	0	elution of pentosidine
30	0	0	100	cleaning of the column
40	100	0	0	back to start conditions
50	100	0	0	equilibration of the column

0-20 min: excitation 295 nm, emission 400 nm (wavelengths for pyridoxine, HP and LP)
20-30 min: excitation 328 nm, emission 378 nm (wavelengths for pentosidine)

Preparation of eluents:

D1. Eluent A: 0.09%-0.16% (v/v) HFBA in 24% (v/v) methanol
240 ml methanol + 0.9 to 1.6 ml HFBA; bring the volume to 1000 ml with Milli-Q water. The amount of added HFBA depends on the quality of the column (with eluent A the cross-links HP and LP are separated) and should be determined by trial and error (start with 0.09%).

D2. Eluent B: 0.07% (v/v) HFBA in 40% (v/v) methanol
400 methanol + 0.7 ml HFBA; bring the volume to 1000 ml with Milli-Q water.

D3. Eluent C: 0.15% (v/v) HFBA in 75% acetonitrile
750 ml acetonitrile + 1.5 ml HFBA; bring the volume to 1000 ml with Milli-Q water.

HPLC analysis of FMOC derivatized amino acids

Reagents

- L-homoarginine (Sigma H1007)
- Boric acid (Sigma B0252)
- Pentane > 95% (Interchema 601-006-00-1)
- Tri-sodiumcitrate-dihydrate (Merck 1.06448)
- Citric acid monohydrate (Sigma 251275)
- Tetramethylammonium chloride (Sigma T19526)
- Sodium azide (Sigma S2002)
- Phosphoric acid 85%wt (Acros Organics)
- Acetonitrile (Biosolve HPLC grade)
- Methanol absolute, HPLC (Biosolve, 136806)
- Acetone (Merck 100014)
- Sodium hydroxide (Sigma S8045)
- FMOC-L-Hydroxyproline ≥ 98%, HPLC (Sigma 47686)
- 9-fluorenylmethyl chloroformate (Sigma 8.18203)
- 5 M NaOH: dissolve 6 g NaOH in 30 ml MilliQ water.
- 0.1 M borate buffer: dissolve 6.183 g boric acid in ± 900 ml MilliQ water. Bring the pH to 8.0 with 5 M NaOH; add Milli-Q water to 1000 ml. Store at 4 ºC; check before use the clarity of the solution (it should be clear).
- 6 mM FMOC: dissolve in a stoppered glass tube 15 mg 9-fluorenylmethyl chloroformate in 10 ml acetone. Prepare freshly every day; avoid attraction of water from the air by closing the glass tube. With 10 ml about 40-45 samples can be derivatized.
- 25% (v/v) acetonitrile in 0.1 M borate buffer pH 8.0: Add 125 ml acetonitrile to 375 ml 0.1 M borate buffer pH 8.0. Store at 4 ºC.

Preparation of External Standards (ES)

E1. 60 µM FMOC-Hyp in 0,1 M boric acid buffer pH 8,0: Dissolve 21,2 mg FMOC-Hyp-OH to 1 L 0,1 M borate buffer pH 8,0. Use a magnetic stirrer for 30 minutes to make sure all is dissolved.

E2. 4,8 mM Homoarginine solution: Dissolve 0,1079 gram homoarginine in 100 ml Milli-Q water to make a 4,8 mM solution. Store at -20˚C in 5 mL tubes.

E3. 60 µM Hyp-Standard 9,6 µM Homoarginine in 0,1 M boric acid buffer pH 8,0: Mix 200 mL FMOC solution *(Reagent E1.)* with 400 µL 4,8 mM Homoarginine solution.

E4. 9,6 µM Homoarginine in 0,1 M boric acid buffer pH 8,0: Mix 200 mL 0,1 M boric acid buffer pH 8,0 with 400 µL 4,8 mM Homoarginine solution.

E5. Hydroxyproline standards 9,6 µM Homoarginine in 0,1 M boric acid buffer pH 8,0: Mix *Reagent E3.* and *E4.* as indicated to make hydroxyproline standards with the right concentrations. Store at -20˚C in 15 mL tubes.

	60 µM Hyp 9,6 µM HA	*30 µM Hyp 9,6 µM HA*	*10 µM Hyp 9,6 µM HA*	*5 µM Hyp 9,6 µM HA*	*2,5 µM Hyp 9,6 µM HA*	*0 µM Hyp 9,6 µM HA*
Reagent c	15 mL	7,5 mL	2,5 mL	1 mL	0,5 mL	0 mL
Reagent d	0 mL	7,5 mL	12,5 mL	11 mL	11,5 mL	15 mL

Preparation of samples

F1. Dilute 20 µl of the above diluted sample subsequently with 980 µl 0.1 M borate buffer pH 8.0. The total dilution factor of the supernatant is now 250. Derivatize 200 µl of this diluted sample with FMOC for amino acid analysis with the protocol described below.

Derivatisation of amino acids with FMOC

Protocol

G1. Add 200 µl sample (dissolved in 0.1 M borate buffer pH 8.0) or 200 µl amino acid standard pH 8.0 in a safe lock Eppendorf tube

G2. Add 200 µl 6 mM FMOC, vortex immediately, allow to stand at room temperature for at least 5 minutes. FMOC gives with amino acids a strong fluorescent signal; the FMOC reacts with both secondary and primary amino acids. A 75-fold excess of FMOC is present

G3. Add 600 µl pentane, vortex rigorously (extraction step!), allow to stand at room temperature for at least 1 minute (in order to allow phase separation), and remove the upper layer (with this extraction step the hydrolysis product of FMOC with water (=FMOC-OH), the excess FMOC and the acetone is removed). Carry the extraction out in a fume hood.

G4. Repeat the extraction step

G5. Add to the remaining lower layer 400 µl 25% (v/v) acetonitrile in 0.1 M borate buffer pH 8.0 and vortex

G6. Add 150 µl of the mixture into HPLC inserts

G7. Inject 50 µl onto the reversed-phase HPLC column for separation of the amino acids.

HPLC analysis of FMOC derivatized amino acids

Apparatus:

- Waters 2795 Separation Module
- Column: TosoHaas TSKgel ODS-80-TM, 4.6 mm ID x 15 cm
- Waters 2475 HPLC Multi Fluorescence detector (excitation 254 nm, emission 630 nm)
- Waters Empower 3 Chromatography Data software programme for data analysis

Machine settings:

- Analysis time: 0:40:00
- Injection volume: 50 µl
- Column temperature: 30°C
- Sample environment temperature: 20°C.
- Initial system pressure before sample injection (50µl) was 1790 psi with a steady pressure ripple between 15-20 psi.
- Flow rate of 1.4ml/min.
- The injection needle was washed after every injection with 10% methanol.
- After measurements, the column is washed and stored in 100% acetonitrile.

Chromatographic gradient conditions for HPLC analysis of FMOC derivatized amino acids

Time (0.1 min)	**% eluent A**	**% eluent B**	**% eluent C**	**flow µl/min.**
	citrate pH 2.85	**citrate pH 4.5**	**Acetonitrile**	
0	75		25	1400
115	60		40	1400
130	60		40	1400
131		64	36	1400
180		62	38	1400
250		30	70	1400
300		25	75	1400
320		25	75	1400
321	75		25	1400
400	75		25	1400

Preparation of eluents:

H1. *solution 1*
8,56 g citric acid
1.10 g tetramethylammonium chloride
200 mg sodium azide
Dissolve in 2000 ml Milli-Q water

H2. *solution 2*
11.17 g tri-sodiumcitrate-dihydrate
1.10 g tetramethylammonium chloride
200 mg sodium azide
Dissolve in 2000 ml Milli-Q water

H3. **Eluent A:** bring 1600 ml solution 1 to pH 2,85 with solution 2 (about 200 ml)

H4. **Eluent B:** bring 1600 ml solution 2 to pH 4.5 with phosphoric acid, add 400 ml methanol

H5. **Eluent C:** acetonitrile

Appendix D

HPLC results

This section presents supplementary information from the HPLC measurements: data of the calibrations, retention times and examples of chromatograms.

Compound	Retention time (min)	Calibration curve	R^2
Pentosidine	22.93	y = 0.0267x - 0.0072	0.9998
Pyridoxine	5.96		
Hydroxyproline	10.19	y = 0.119x - 0.0324	0.9993
Homoarginine	9.20		

TABLE D.1: Data from HPLC measurements

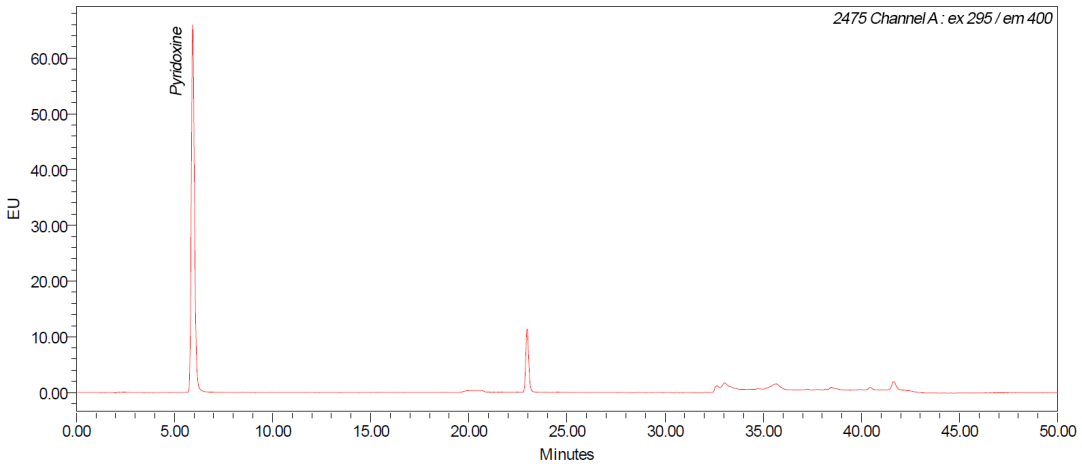

FIGURE D.1: Example of HPLC chromatogram, showing the separation of pyridoxine, the internal standard for pentosidine measurements.

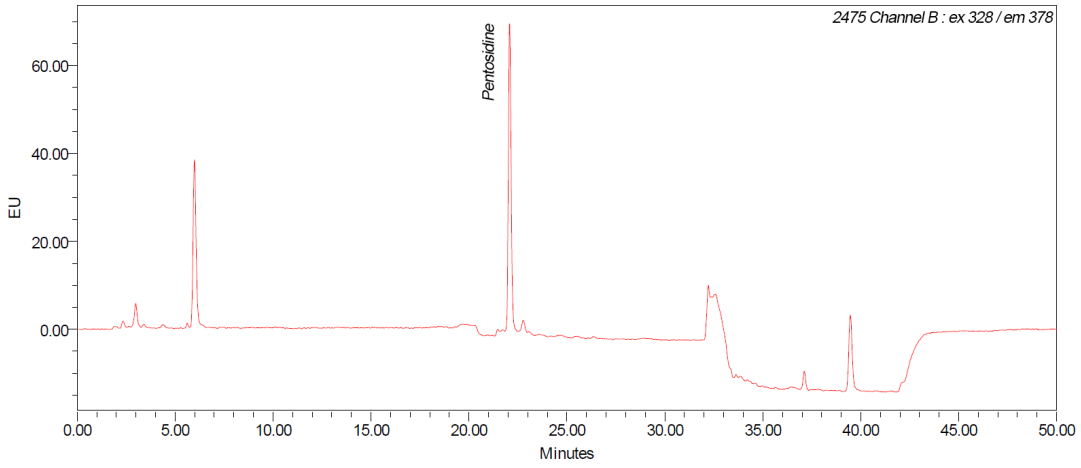

FIGURE D.2: Example of HPLC chromatogram, showing the separation of pentosidine, the analyte representing the amount of cross-links.

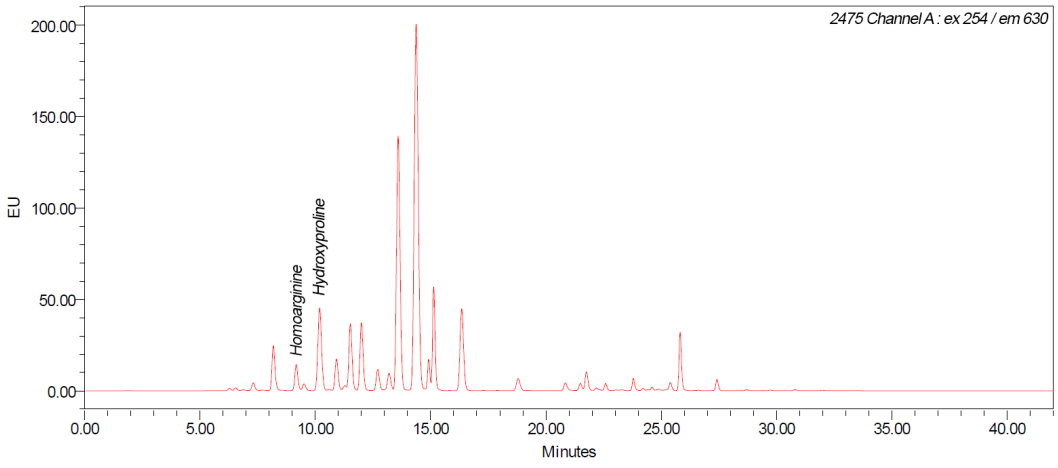

FIGURE D.3: Example of HPLC chromatogram, showing the separation of hydroxyproline, the analyte representing the amount of collagen, and homoarginine, the internal standard.

Appendix E

Matlab code

This section presents the Matlab code that has been used for the analysis of biomechanical data from the Dynamic Mechanical Analyzer. The code involves multiple visual checks, of which the plots are presented here too.

```
clear all;
% Take in data
Data = xlsread('y13_fm_excel');

% Testing Parameters
num_ints = 3; % number of S/R intervals tested
int_strains = [0.04 0.02 0.02]; % strain levels
dwell_time = 600;
dynamic = true;
strain_rate = 0.0001;
radius = 0.0015;% explant radius (m)
height = 1.11;% explant height (mm)
pps = 0.05; % time between data scans

% In raw data set, 1st column = time, 2nd column = displacement,
3rd column = load
time1 = Data(:,1); % Time (s)

SR_cutoff = dwell_time-40; % beginning of first ramp
if dynamic
dyna_cutoff = (length(time1))*pps - 2000 - 600 - 25 -
(height*0.05*pps/0.0001); %switch point from S/R´s to dynamic
loading
else
    dyna_cutoff = length(time1)*0.05;
end
time = time1(SR_cutoff/pps:dyna_cutoff/pps);

strain1 = -1*(Data(:,2)/height); % displacement (mm)
strain = strain1(SR_cutoff/pps:dyna_cutoff/pps)-strain1(1);

load = Data(:,3);
smooth_load = (movmean(load,53)); % smoothed Load (N)

raw1 = -1*smooth_load/(pi*radius*radius); % smoothed stress (Pa)
raw01 = -1*load/(pi*radius*radius); % raw stress (Pa)
raw = raw1(SR_cutoff/pps:dyna_cutoff/pps);

stress = raw-raw(1);

%Predicting time intervals to isolate sections

ramp_time4 = height*0.04/strain_rate;
max_indexes = [height*int_strains(1)/strain_rate];
for i = 2:num_ints
```

```
    max_indexes = [max_indexes (max_indexes(i-
1)+dwell_time+(height*int_strains(i)/strain_rate))];

end
max_indexes = (max_indexes/pps);

min_indexes = [(height*int_strains(1)/strain_rate)+dwell_time];
for j = 2:num_ints

    min_indexes = [min_indexes (min_indexes(j-
1)+dwell_time+(height*int_strains(i)/strain_rate))];

end
min_indexes = (min_indexes/pps);

% Plotting Stress/Relax Data
figure();
subplot(1,2,1);
plot(time, (strain-strain(1)));
xlabel('time');
ylabel('Strain');
title('Controlled Strain over Time');

subplot(1,2,2);
hold on
plot(time,raw,time(min_indexes), raw(min_indexes),  'b*');
plot(time,stress,time(max_indexes), stress(max_indexes),  'g*',
'LineWidth', 1.5);
%movmean(raw-min(raw),53)
hold off
xlabel('time');
ylabel('Stress (Pa)');
title('Smoothed/Tared Stress Data Over Raw');

strain_add = (strain1(151/0.05)-strain1(143/0.05))/height;
```

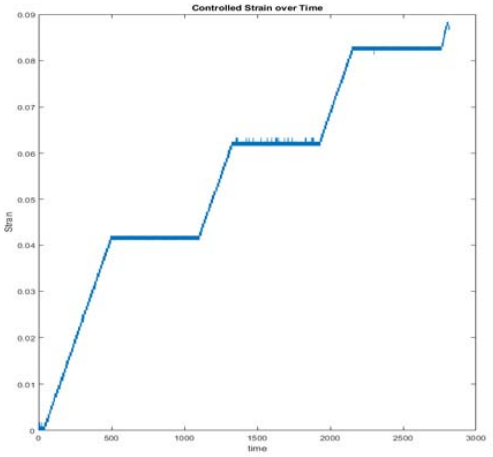

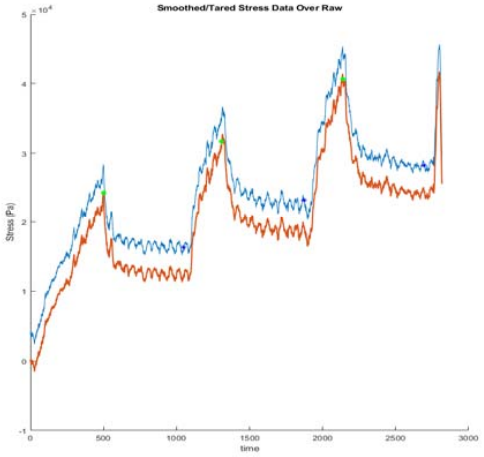


```
%% Visualize whole raw data set

figure();
subplot(1,2,1)
plot(time1, raw01);
```

```
title('Stress')
ylabel('Stress (Pa)');
xlabel('Time (Sec)')

subplot(1,2,2)
plot(time1, strain1-min(strain1));
title('Strain')
ylabel('Strain');
xlabel('Time (Sec)')
```

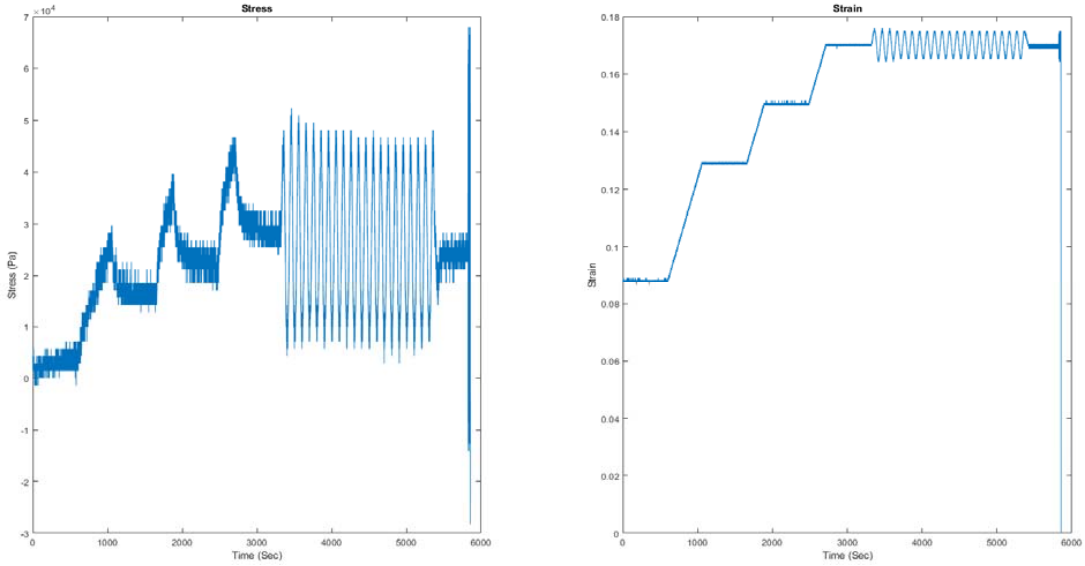


```
%% Isolating and fitting each S/R Interval
figure();
xs = [0 0 0 ];
x0 = [1 1 1];
hybridopts = optimset('MaxFunEvals', 1000000000000, 'MaxIter',
1000000000000);

for p = 1:1:num_ints

%isolate interval to be regressed
    iso_time = time([max_indexes(p):min_indexes(p)]); %
independent (X) variable in the curve fitting tool
    iso_time = iso_time - min(iso_time);
    iso_stress = stress([max_indexes(p):min_indexes(p)]);% change
"RAW" to "STRESS" to regress smoothed data
    r = 5;

    S = @(x,xdata)((x(1)*10^5)+(x(2)*10^r)*exp(-
(xdata)/(x(3)*100)));
%SLV equation format
    x = lsqcurvefit(S,x0,iso_time,iso_stress,[],[],hybridopts);

    subplot(1,num_ints,p)
    hold on
    plot(iso_time, iso_stress);
    plot(iso_time, S(x, iso_time), 'LineWidth', 1.5);
```

```
    hold off
    xlabel('Time');
    ylabel('Stress (Pa)');

    xs = [xs; x];
end
```

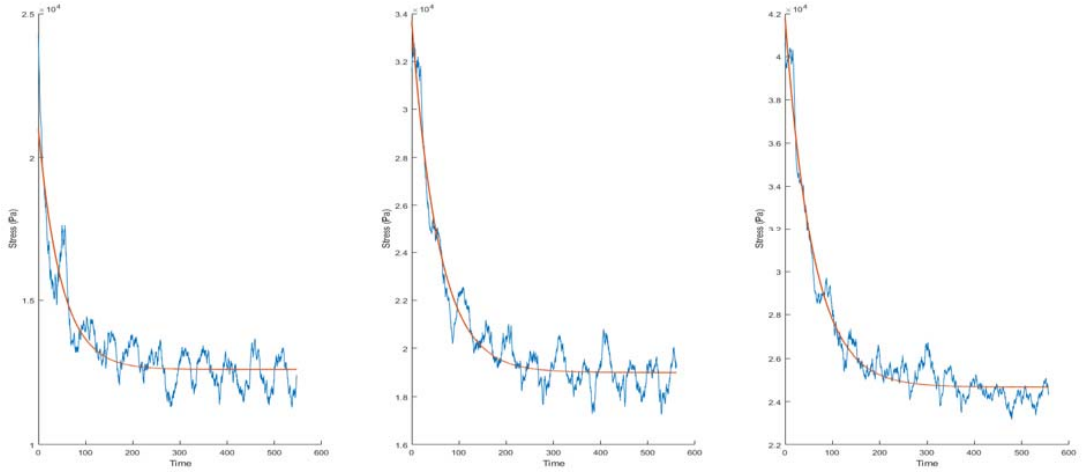


```
%% Linear fit for eq stress vs. dwell strain plot
strains = [0 0.04 0.06 0.08];%+strain_add;
stresses = (xs(:,1)')*10^5;
p = fitlm(strains, stresses);
figure();
plot(p)
```

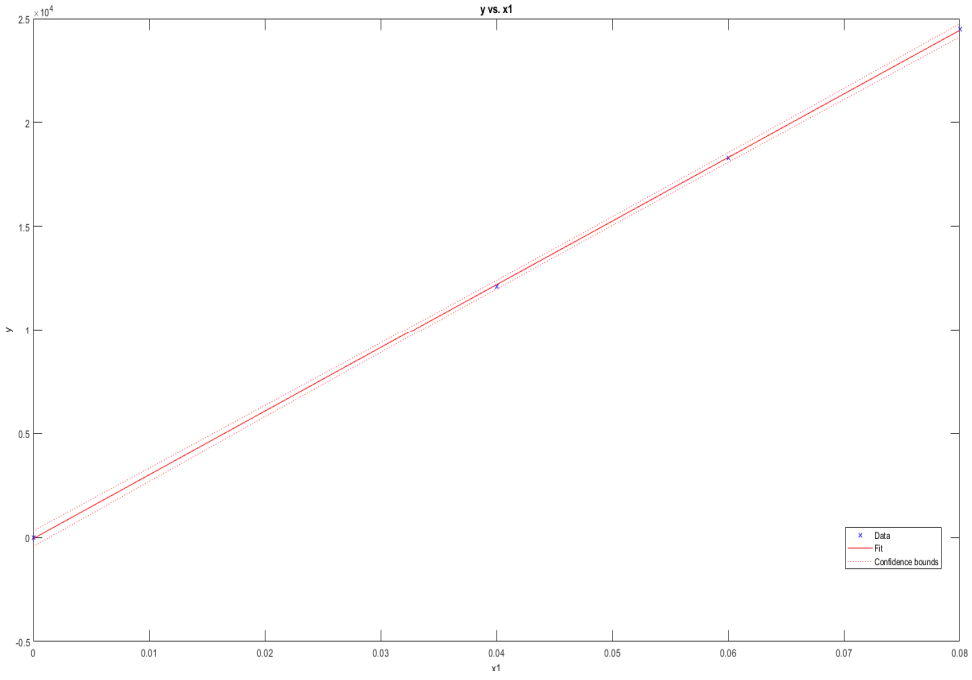

```
%% Dynamic analysis

starts = [dyna_cutoff (length(time1)*0.05)-30];
ends = [dyna_cutoff+2000 (length(time1)*0.05)-5];

fs = [0.01 1]; % frequencies

G_average = [];% dynamic modulus
phi = [];% phase shift

for p = 1:1:2

 disp('new run');

     start = starts(p)/0.05;
     fin = ends(p)/0.05;

f = fs(p);
c = 16;

dynamic_time = time1(start:fin);
dynamic_time = dynamic_time-min(dynamic_time);
dynamic_strain = strain1(start:fin);
dynamic_stress = raw01(start:fin);

stress_maxes = maxes(dynamic_time,dynamic_stress, f);
stress_mins = mins(dynamic_time, dynamic_stress, f);
strain_maxes = maxes(dynamic_time,dynamic_strain, f);
strain_mins = mins(dynamic_time, dynamic_strain, f);

A_stress = (mean(dynamic_stress(stress_maxes(3:c-1)))-
mean(dynamic_stress(stress_mins(3:c-1))))/2;
A_strain = (mean(dynamic_strain(strain_maxes(3:c-1)))-
mean(dynamic_strain(strain_mins(3:c-1))))/2;

y_stress = mean(dynamic_stress(stress_mins(3:c-1)))+(A_stress);
y_strain = mean(dynamic_strain(strain_mins(3:c-1)))+(A_strain);

hybridopts = optimset('MaxFunEvals', 100000, 'MaxIter', 10000);
S3 = @(x3,xdata3)(A_strain*cos((2*pi*f*xdata3)+x3(1)))+y_strain;
x03 = [0];
x3 = lsqcurvefit(S3,x03,dynamic_time, dynamic_strain,[], [],
hybridopts);

S2 = @(x2,xdata2)(A_stress*cos((2*pi*f*xdata2)+x2(1)));
x02 = [0];
x2 = lsqcurvefit(S2,x02,dynamic_time, dynamic_stress,[], [],
hybridopts);

figure();
hold on
plot(dynamic_time,dynamic_stress-y_stress, 'r',
dynamic_time(stress_maxes), dynamic_stress(stress_maxes)-
y_stress, 'b*', dynamic_time(stress_mins),
dynamic_stress(stress_mins)-y_stress, 'r*');
plot(dynamic_time, S2(x2, dynamic_time), 'b', 'LineWidth', 1.5)
```

```
hold off
title('Dynamic Stress, 0.01 Hz')
xlabel('Time')
ylabel('Stress (Pa)');

G_average = [G_average A_stress/A_strain];

phi = [phi ((x3-x2)*-1)*180/pi]
end
figure();
subplot(1,2,1)
plot(fs, G_average, '-o', 'LineWidth', 2);
xlabel('Frequency');
ylabel('Dynamic Modulus');

subplot(1,2,2);
plot(fs, phi, '-o', 'LineWidth', 2);
xlabel('Frequency');
ylabel('Phase Shift');


results = [G_average; phi]
if abs(results(2,1)) > 100
   results(2,1) = results(2,1) + 360;
end
% (1Hz graph will have “0.01Hz” as title too)
```

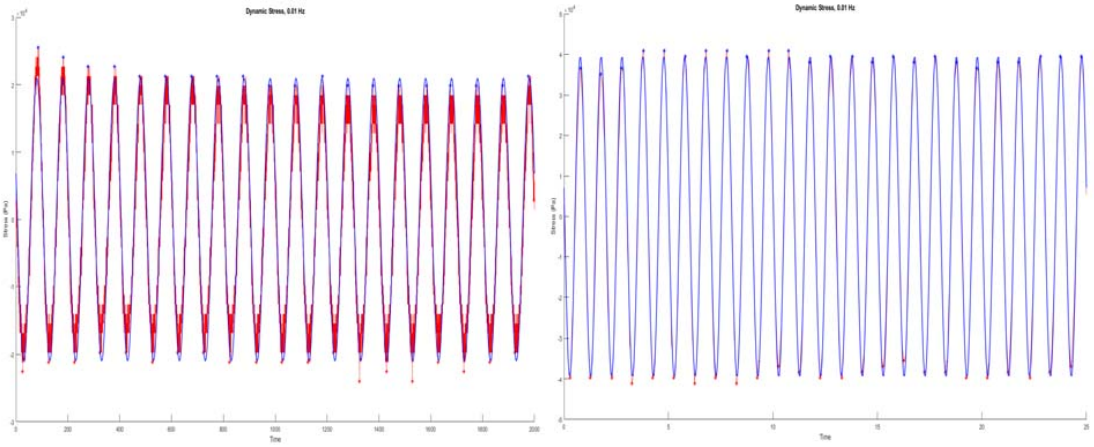

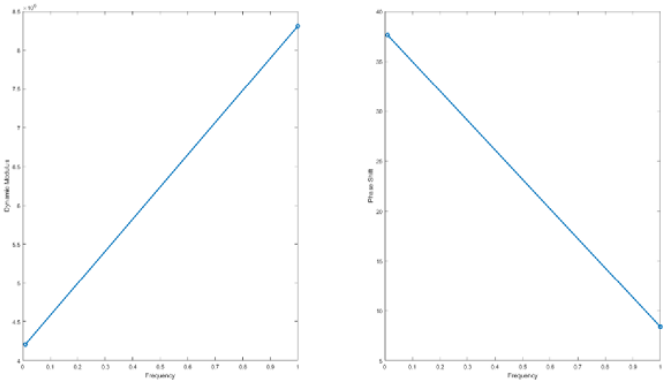

Appendix F

Hydroxyproline assay protocol

Hydroxyproline Assay of Cartilage by Chloramine-T and DMAB

MIT. Grodzinsky's Lab

This assay quantifies the hydroxyproline content of cartilage, and thus can be used as an estimate of collagen content. The assay is based upon the oxidation of hydroxyproline with Chloramine-T and reaction of the products with p-dimethylaminobenzaldehyde (DMAB) to form a color product.

Material:

12N HCl
Acetic acid
Citric acid Monohydrate
Sodium Acetate
Sodium Hydroxide (pellets)
ChloramineT (Sigma #C-9887)
p-dimethylaminobenzaldehyde (Fisher D71-100 or Sigma)
DD H_2O
n-Propanol (isopropanol)
Hydroxyproline (Sigma #H-7279)
60% Perchloric Acid

Special Material:

Fume hood for preparation reagents
Acid evaporator (e.g~50^0 Oven to vacuum in fume hood)
60^0 water bath
Spectrophotometer (96-well plate reader with 560nm filter)
Eppendorf repeater pipette
2.0ml Short bottle (Wheaton #224821)
Cap for 2.0ml bottle (Wheaton(240408)
96 well plate (NUNC)
Foil

Reagent:

1. Hydroxyproline standard stock solution 1mg/ml

Hydroxyproline	10mg
DD H_2O	10ml

Final Concentration: 1mg/ml

2. pH 6 Buffer-100mL (store for 2-4months max)

Citric Acid Monohydrate	5g
Sodium Acetate (Trihydrate)	12g
Nanopure H_2O	54mL
Glacial Acetic Acid	1.2mL
NaOH pellets	3.4g (or add 7mL of 12.5M NaOH solution)
Total	~75mL

*Bring up to 100ml with nanopore water ~25mL

Add in all reagents except for the NaOH pellets into a 250-mL beaker and then bring up the volume to 100mL with nanopore water. Use the pH probe to check pH (should be acidic >6) and slowly add in NaOH pellets continuously checking with probe until pH=6 is reached.

3. Working Assay buffer
   Make working assay buffer by performing a 1/10 dilution of pH6 buffer.
   a. Each sample requires 0.5mL of working assay buffer. Make sure to make an extra 10mL for standard as well as 30mL for Chloramine T reagent.

# samples	***Amt Working Assay Buffer (samples+ 40 mL)***	***pH 6: nanopore ratio***
10 samples	(10 samples/2) +40mL= **45mL**	4.5mL pH6 : 40.5mL nanopure
50 samples	(50 samples/2) + 40mL= **65mL**	6.5mL pH 6: 58.5mL nanopure

4. Chloramine T reagent-50mL (store in a dark bottle at 4^{o} for max of 2 weeks)

*****make at least 24 hours in advance*****

Chloramine T	0.57g
n-propanol	13.00ml
nanopure H2O	10.35ml
10x diluted pH 6 buffer	26.65ml
Total	50.00ml

Each samples needs ~.1mL of sample and the standard needs ~1mL. Thus, 50mL should be enough for about 450 samples and the standard.

5. p-DMAB solution (**DMAB degrades rapidly-Use within 24 hrs of preparation.)

Total Volume	10mL	6.9mL
n-propanol	6.97mL	4.81mL
DMAB	1.74g	1.20g
60% perchloride Acid	3.03mL	2.09mL

(6.9mL of DMAB→90 samples max; 10mL→130 samples max)

Make an ice bath by filling a large beaker with ice. Measure DMAB directly into smaller beaker before adding a stir bar and placing in ice bath. Put ice bath on the stir plate in the fume hood. Add in n-propanol and turn on stir plate. While stirring, slowly add in 60% perchloric Acid in a drop-wise fashion. The solution should turn yellow. Allow to stir in hood for at least 10min after which parafilm the beaker and leave at room temp for max of 24 hrs.

Procedure:

Hydrolysis & Evaporation of samples at 110°C

2. Digest tissue sample with proteinase K or papain. Calculate the amount of tissue digest that contains approximately 6.25ug of Hydroxyproline (Assuming a bovine cartilage explant contains ~20ug hydroxyproline per ul tissue, a standard 3mm 1mm explant contains ~141400 ug of hydroxyproline. If sample is digested in 1000uL of proteinase K, 45uL of sample will be used.

3. Aliquot the calculated amount of sample to correlating glass vial. Bring volume up to 200uL with nanopore H2O if necessary.

4. Add an equal volume of 12N HCl to the sample vial. (So, if each vial contains 200uL of sample (or sample + water), add 200 uL of HCl.)
   The final HCl concentration is 6N.

5. Close the cap tightly and place vials in oven @ 110°C to hydrolyze overnight (16h)

6. Remove caps and allow HCl to evaporate in oven/ hot plate in fume hood set to 60°C

Reconstituting samples

7. Add 375 ul of working assay buffer to each vial pipetting up and down until thoroughly mixed.

Making Standard

8. Make standard as following:
   Perform a 1:5 dilution of hydroxyproline sample to working assay buffer to make a 1mL stock of 200ug/ml hydroxyproline from the original 1mg/ml stock.

Hydroxyproline stock (1mg/mL)	Working Assay Buffer
200 uL	800 uL

9. Add 300uL of diluted stock solution (200ug/mL) and 700uL of nanopure to vial #6. For each consecutive vial, take 500uL form previous and mix with 500uL of nanopure. Vial #0 should have only nanopure.

Make 1ml of each std	OH standard(ug/ml)	200ug/ml of OH(diluted stock)	Nanopure water
6	60	300uL	700uL
5	30	500uL	500uL
4	15	500uL	500uL
3	7.5	500uL	500uL
2	3.75	500uL	500uL
1	1.875	500uL	500uL
0	0	0uL	1000uL

10. Transfer 150 ul of each sample in duplicates into a 96 well plate.

11. Transfer 150ul of each Hydroxyproline standard in duplicates into wells on the same 96 well plate.

12. Add 75ul of Chloramine T reagent to each samples and standards in the 96 well plate.

13. Put foil on the plate and let stand 20 minutes at room temperature

14. Add 75 ul of DMAB to each samples and standards in the 96 well plate. The samples will fizz on addition. After fizzing stops, seal tightly with plate sealers (Costal #3095).

15. Place the plate on the foam rack that has been adjusted to 60^0C water bath, and heat for 15 minutes.

16. Cool sample in cold water until room temperature for about 5 minutes.

17. Blot the plate dry and remove the plate sealer and determine absorbance at 560λnm with 96 well plate reader.

*****Perchloride acid must be handle with extreme care. It is a strong acid and a powerful oxidizing reagent. Contact with flammables, combustibles, organic compounds and other oxidizable material may result in violent and even explosive reactions, especially when heated. Read protocol and MSDS before handling.*******

Appendix G

Experiment 1B

An additional experiment was conducted to research the effects of different strain magnitudes (static compression) on the formation of cross-links in articular cartilage.

G.1 Methods

This experiment was an addition to the experiment in Part 1 of this report. Thus, the used treatment of samples was very similar, except for the fact that we used multiple different strain magnitudes. As this experiment was conducted in the Boston laboratory, the other used methods are very similar to those in Part 2 of this report.

The bioreactors were used to treat bovine cartilage samples with static compression (n = 16). Depending on the treatment group, the samples were compressed with a strain magnitude of : 0%, 5%, 10% or 15%. The bioreactors with samples were incubated in a 40 mM L-Threose solution at 37°C) for 96 hours. At the conclusion of the experiment, after the samples were digested, the pentosidine and hydroxyproline levels were measured using a microplate reader. The obtained values were used for statistical analysis.

G.2 Results

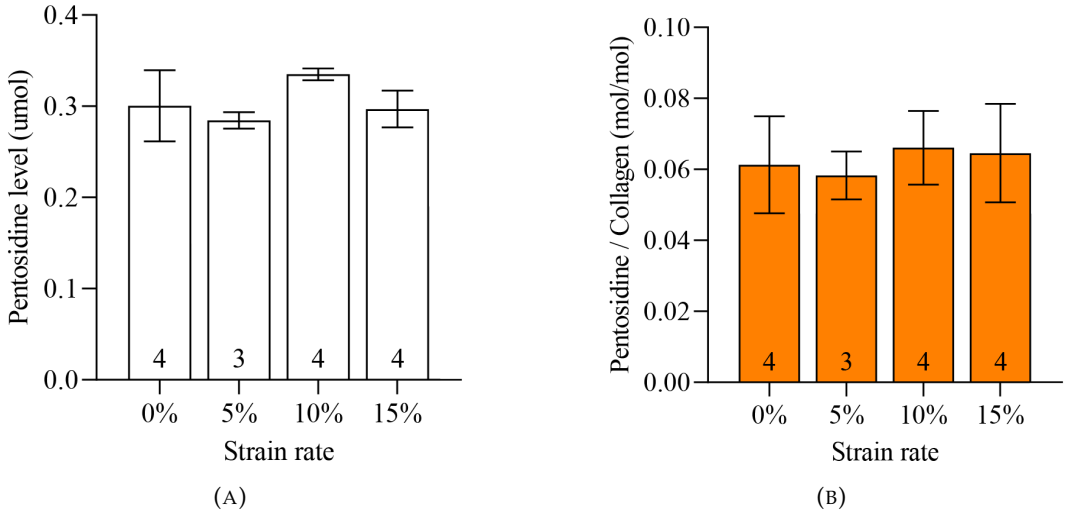

FIGURE G.1: A) Average pentosidine level per treatment group, obtained by fluorescence measurement. B) Average molecular amount of pentosidine per collagen (mol/mol) per treatment group. The number at the bottom of each bar represents the number of replicates averaged for that bar value and the error bars show the standard deviation.

The mean pentosidine level of all samples was 0.31 ± 0.03 μmol (n = 11). The mean collagen level of all samples was 4.97 ± 0.81 μmol (n = 11). Figure G.1 shows the mean values of the absolute and normalized pentosidine level per treatment group. A Shapiro-Wilk test showed that the distribution of the data for each treatment group followed a normal distribution. One-way independent ANOVA showed no significant difference between the treatment groups.

G.3 Discussion

No significant differences were observed between the treatment groups with regard to pentosidine level. Static compression with a strain magnitude of 0, 5, 10 or 15% during incubation seemed to have no influence on the formation of cross links. Despite the fact that the samples that were treated with a 10% strain seemed to have a slightly higher pentosidine level after incubation, no clear trend could be identified. Therefore, we conclude that static compression does not influence non-enzymatic glycation in (bovine) articular cartilage.

Master's thesis
Jaap Lagrand
2019